# Università degli Studi di Ferrara

DOTTORATO DI RICERCA IN
SCIENZE CHIMICHE

CICLO XXIII

COORDINATORE Prof. Bignozzi Alberto

# TOWARDS LABEL-FREE BIOSENSORS BASED ON LOCALIZED SURFACE PLASMON RESONANCE

Settore Scientifico Disciplinare CHIM/03

**Dottorando**
Dott. Cantale Vera

**Tutore**
Prof. Rampi Maria Anita

Anni 2008/2010

# Table of Contents

# Abstract

Medical diagnostics is in constant search of new tools and devices able to provide in short time, accurate and versatile tests performed on patients. Nanotechnology has contributed largely in developing biosensors of smaller size at a lower cost by using a minimal amount of sample. Biosensors aim to monitor and diagnosticate “in situ” the patient status and the diseases caused by alteration of the body metabolism by, for example, the detection of gene mutations, alteration of gene expression or alteration of proteins.

The aim of this work is the development of biosensors that satisfy the requirements which are critical for applications. A biosensor must be i) easy to use, ii) economically convenient, and therefore preferentially label free, iii) highly sensitive, iv) reversible, v) and suitable for *Point of Care Testing*, that is to be used ”in situ” on the patient.

We have focused on biosensors based on the optical properties of nanostructured metals as Au or Ag, in particular by using on Localized Surface Plasmon Resonance (LSPR) spectroscopy.

Nanostructured metals under irradiation of electromagnetic wave (as light) exhibit intense absorption bands as results of the localized electronic charges of the metal surface coming into resonance with the incident energy. According to the Mie’s theory, the LSPR absorption band feature changes when the refractive index of the media surrounding the metal nanostructures is varied.

Of particular interest for our purpose are the possible changes of the LSPR band features taking place under molecular interactions occurring at the nanostructures surfaces: *the shift of LSPR bands is the “transducer” of molecular interactions*. These changes can be easily detected by conventional UV-Vis spectroscopy, in transmittance mode.

While a large number of studies have been carried out on monodisperse nanoparticles suspended in solution, gold nanoparticles (NPs) deposited on a transparent surface open the possibility to fabricate biosensor based on multiplex array platforms. Nonetheless, one of the major problems in using these plasmonic materials for biosensing purpose is related to the stability of the metal NPs in different solvents and in particular in aqueous solutions.

In this study we demonstrate i) the possibility to achieve highly stable NPs by simple thermal evaporation of Au on a substrate commercially available, the Fluorine Tin Oxide (FTO)

(Chapter 2); ii) a reproducible variation of the LSPR bands under formation of organic self-assembled monolayers (SAMs), iii) reversible changes in the features of the LSPR bands, (Chapter 3), iv) a specific and reproducible LSPR band changes under molecular interactions occurring at NPs surfaces, as DNA hybridization (Chapter 4).

This work demonstrates that the plasmonic material based on Au NPs deposited on FTO surfaces represents a convenient platform for biosensors because of i) inexpensive fabrication, ii) stability of this material in various solvent, including water, of, iii) the easy way to detect the molecular interaction, and iv) the good sensitivity to molecular interactions.

# Chapter 1

## 1.1 Biosensors

A biosensor is an analytical device that uses a biodetector (enzymes, antibodies, nucleic acids, microorganisms, or tissues) to perceive a target analyte directly without the need for complex specimen processing. It is assembled by attaching the biodetector to a suitable transducer (solid-state integrated circuit, metal electrode, or optical fiber) that converts the biochemical reaction occurring between the biodetector and target analyte into a quantifiable and processible electrical signal proportional to the concentration of the analyte. The signal is then displayed in a conventional format (Figure 1).

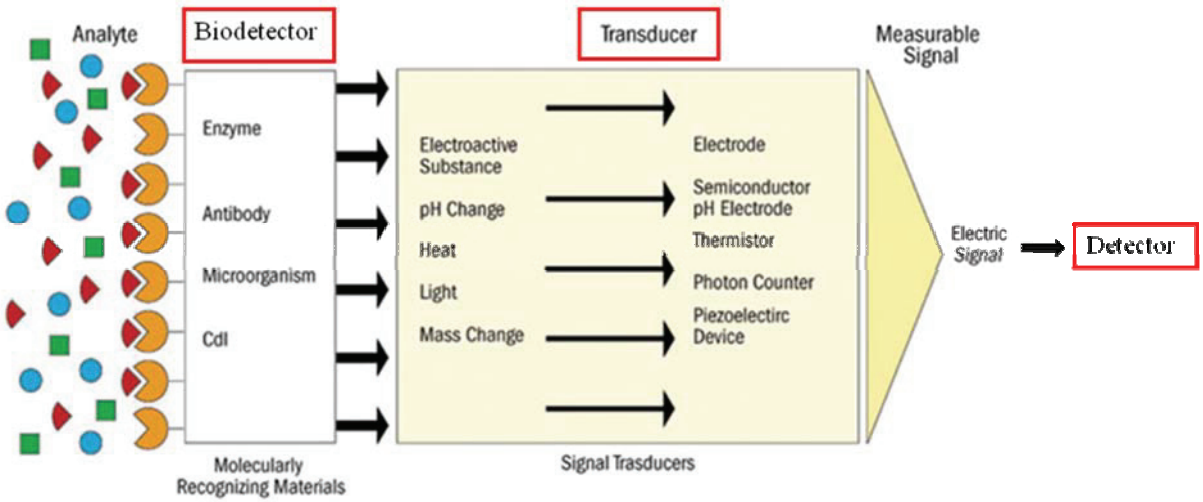


**Figure 1.** Illustrative scheme of different kind of biosensors.

Biosensor nomenclature is based on the type of transduction used. Systems that use metal electrodes, solid-state integrated circuits, or ion-selective electrodes with or without a biodetector (usually an enzyme) are called *electrochemical biosensors*. Those that use optical fibers or waveguide devices are called *optical biosensors*. Units that employ thermistors or diodes are called calorimetric or *thermal biosensors*.

The first biosensor device was developed by Leland C. Clark in 1962 (1). This glucose biosensor relied on a thin layer of Glucose Oxidase (GOx) entrapped over an oxygen electrode (via a semi permeable dialysis membrane), and was monitoring the oxygen consumed by the enzyme-catalyzed reaction. A decrease in the measured oxygen concentration was proportional to the glucose concentration (Figure 1). Updike and Hicks significantly simplified the electrochemical glucose assay by immobilizing and thereby stabilizing GOx in 1967 (2). They immobilized GOx in a polyacrylamide gel on an oxygen electrode for the first time and measured glucose concentration in biological fluids. The first commercially glucose biosensor (1975) using Clark's technology was the Yellow Springs Instrument Company analyzer was based on the amperometric detection of hydrogen peroxide (3-4).

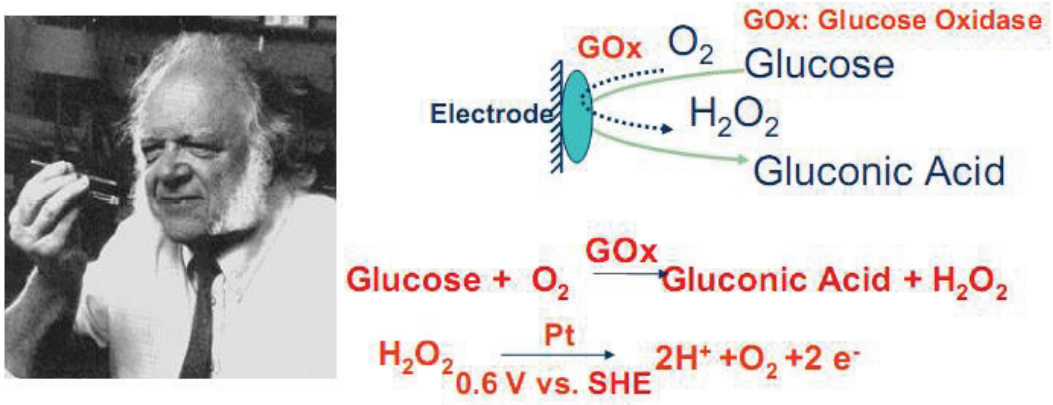


**Figure 1.** Schematic illustration of Clark's glucose sensor working and Leland C. Clark photo.

Later on, was necessary to develop new tools, such as devices and assays, enabling to give a rapid response, highly sensitive and specific. The most known and efficient techniques are the Enzyme-Linked ImmunoSorbent Assay (ELISA) and the Microarray of DNA.

The Enzyme-Linked ImmunoSorbent Assay (ELISA) has been developed at the same time and in independently way by Engvall and Perlmann (5) at Stockholm University in Sweden, and van Weemen and Schuurs (6) in the Netherlands in 1971. The ELISA is a biochemical technique used mainly in immunology (but also as a diagnostic tool in medicine and plant

pathology) to detect the presence of an antibody or an antigen in the sample to analyze. ELISA is typically performed in 96-well polystyrene plates, where an unknown amount of antigen is affixed to a surface, and then a specific antibody is applied over the surface so that it can bind to the antigen. The antibody is linked to an enzyme, which converts the added substance in some detectable signal, most commonly a color change of the chemical substrate (Figure 2).

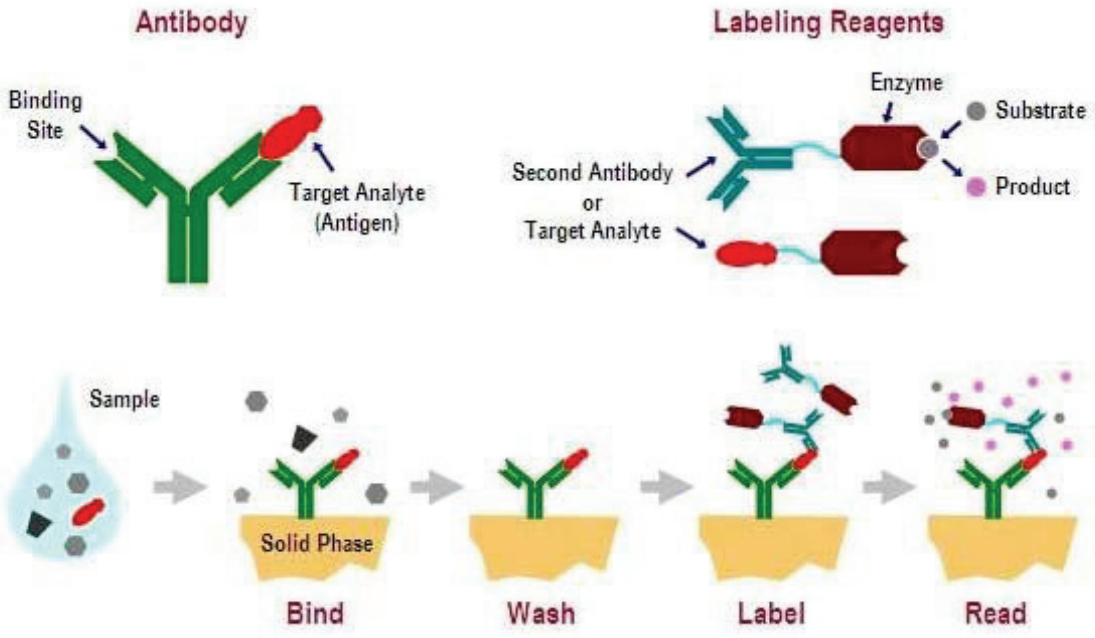


**Figure 2.** Illustration of the different steps in the ELISA assay.

Sixteen years ago it has been invented the first DNA sensor, as a tool for the rapid sequencing of DNA (7). The DNA microarray consists of an arrayed series of thousands of microscopic spots of DNA oligonucleotides, each containing picomoles ($10^{-12}$ moles) of a specific DNA sequence, the *probes*. The probes can be a short section of a gene or other DNA element that are used to hybridize a cDNA (complementary DNA), the *target*. The target is fluorescently labeled so that a successful hybridization event with the probe results in an increase of fluorescence intensity over a background level. The fluorescent intensity is measured using a fluorescent scanner (13,16). A detailed example is given in Figure 3.

This DNA microarray device has been exploited since the beginning as high capacity technology for analyzing viral or cellular functions, ranging from analysis gene expression to analysis of the contents and composition of proteins, carbohydrates, lipids and pro-metabolic products (8-15). Microarray technology is a very powerful tool: it allows the simultaneous examination of tens of thousands of genes through the use of slides or chips.

The advancement in micro-fabrications, robotics, and bioinformatics, has continued to improve efficiency, discriminatory power, reproducibility, sensitivity, and specificity the microarray technology. These improvements have allowed the transition of microarrays from strictly research settings to clinical diagnostic applications (17-18).

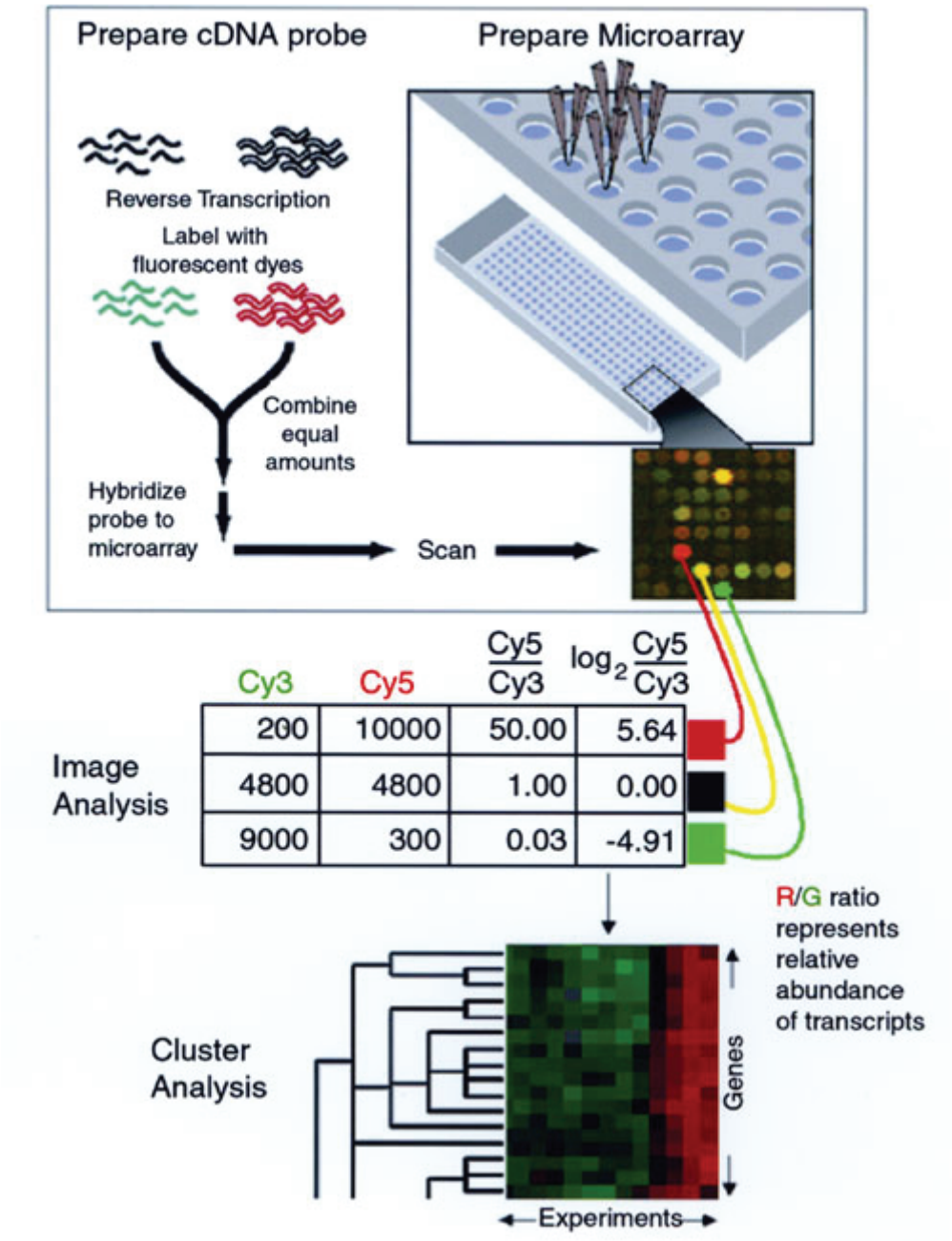


**Figure 3.** Schematic illustration of the relative gene expression measured with a DNA Microarray. RNA is prepared from the two samples to be compared, and labeled cDNA is prepared by reverse transcription, incorporating either Cy3 (green) or Cy5 (red). The two labeled cDNA mixtures are mixed and hybridized to the microarray, and the slide is scanned. In the resulting pseudo-color image, the green Cy3 and red Cy5 signals are overlaid (yellow spots indicate equal intensity for the dyes). With the use of image analysis software, signal intensities are determined for each dye at each element of the array, and the logarithm of the

ratio of Cy5 intensity to Cy3 intensity is calculated (center). Positive log(Cy5/Cy3) ratios indicate relative excess of the transcript in the Cy5-labeled sample, and negative log(Cy5/Cy3) ratios indicate relative excess of the transcript in the Cy3-labeled sample. Values near zero indicate equal abundance in the two samples. In this display, red boxes indicate positive log(Cy5/Cy3) values, and green boxes indicate negative log(Cy5/Cy3) values, with intensity representing magnitude of the value. Black boxes indicate log(Cy5/Cy3) values near zero. Hierarchical clustering of genes (vertical axis) and experiments (horizontal axis) has identified a group of co regulated genes and has divided the experiments into distinct classes. (Illustration by J. Boldrick, Stanford University). Copyright 2000 by Genomics.

The progress of the nanotechnology opened the door to the development of new and different kind of biosensors. Thanks to the miniaturization processes, the sensors are characterized by nanometer length scale. The size of a nanomaterial can be an advantage over a bulk structure, because a target binding event involving the nanomaterial can have a significant effect on its physical and chemical properties, thereby providing a new mode of signal transduction not necessarily available with a bulk structure made of the same material.

Today several techniques permit to generate the nanobioarray made from biomaterials as:Dip-Pen Nanolithography (DPN) (19), Electron-Beam Lithography (EBL) (20), NanoImprinting Lithography (NIL) (21), nano-ContactPrinting (nCP) (22), Supramolecular Nano-Stamping (SuNS) (23-24).

The optical nanobiosensors are sensors that can be devised using nanostructured metals, which are expected to cover unmet needs for label-free and high-throughput analysis in diagnostics. The home pregnancy test is an excellent example of how nano-properties of metal nanostructures can be used to provide practical solutions to real-world problems. The story behind some of the color change urine dipstick tests is related to the presence in pregnant women's urine of a significant excess of HcG, human gonadotropic hormone, which has a certain protein structure that binds to a complementary DNA base pair sequence. That very specific complementary lock for the HcG key is attached to gold nanoparticles which reflect red light. If HcG is detected, the spot or line of the dipstick reflects red; if there is not excess of HcG, the line results to be blue or clear (25).

The signal of biosensors based on optical properties of the nanostructured metals can be detected by a change in color as in the pregnancy test or by Localized Surface Plasmon Resonance (LSPR) spectroscopy. The use of these optical properties allows the development of nanobiosensors, able to detect the biological interactions for the clinical diagnostic in a label free way, this is one of most important goals that can be obtained. Indeed, biosensors that use the fluorescent molecules are very expensive as the technology necessary to their detection that moreover is not friendly to use. In addition the development of optical biosensors of nanometer scale with an easy instrumentation allowed have point of care testing (POCT), that's a medical testing at or near the site of patient care.

## 1.2 Surface Plasmon Spectroscopy

### 1.2.1 Surface Plasmons (SPs)

The existence of surface plasmons was first predicted in 1957 by R.H. Ritchie (26); he also suggested how they might be observed experimentally, and made many contributions related to this topic.

The plasmons are charge-density oscillations of free electrons of a metal. Plasma oscillations that can propagate at the interface of a metal and a dielectric medium are called Surface Plasmons (SPs) (Figure 4).

For SPs to exist at an interface the two media must have dielectric permittivity constants (ε) of opposite signs. The dielectric constant of the material is a function of the wavelength of the light and therefore, the excitation of SP is possible only at determinate wavelengths (27).

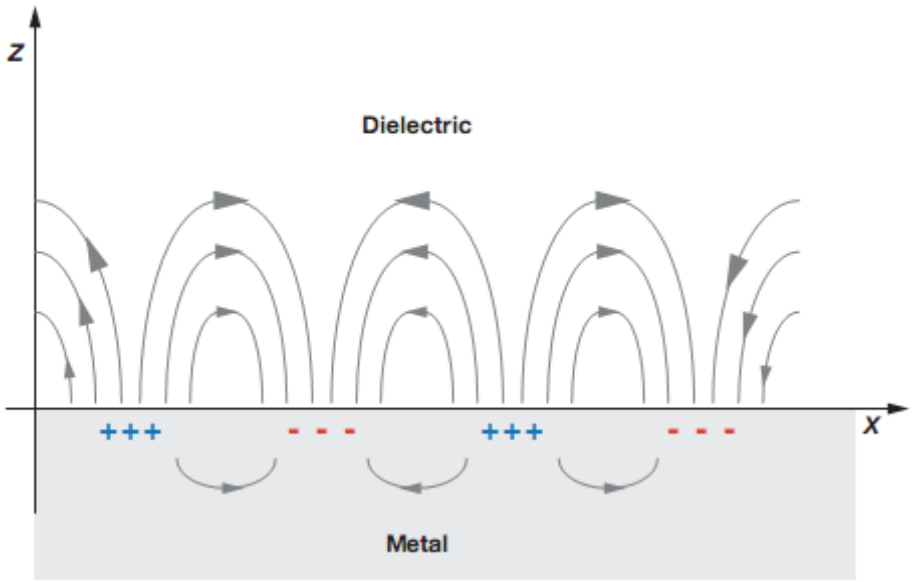


**Figure 4.** Schematic diagram of surface plasmons propagating in x- and y- directions between the two different dielectric surfaces. Copyright 2007 by Annual Reviews.

The charge density wave is associated with an electromagnetic wave which reaches its maxima at the interface and decay evanescently into both media. This surface plasma wave is a transverse magnetic (TM)-polarized wave (magnetic vector is perpendicular to the direction of propagation of the surface plasmon wave and parallel to the plane of interface) (28).

The surface plasmons propagate in the x- and y-directions along the metal-dielectric interface, for distances on the order of tens to hundreds of microns, and decay evanescently in the z-direction with 1/e decay lengths *l* on the order of 200 nm (29) (Figure 5).

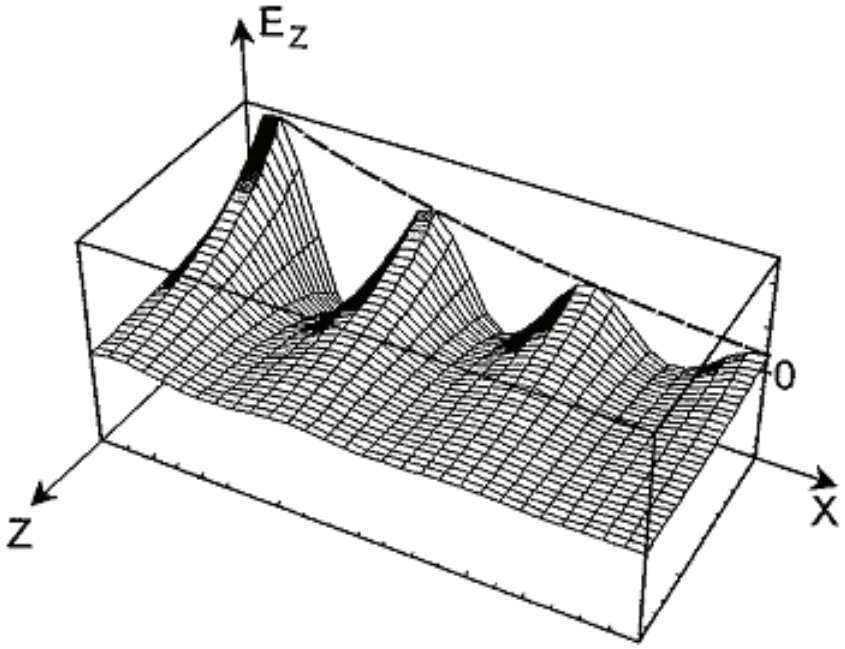


**Figure 5.** Schematic of the evanescent character of a surface plasmon mode excited at a metal/dielectric interface in the x-, y-plane propagating as a damped oscillatory wave in the x-direction. The electric field components along the z-direction, normal to the interface, decay exponentially, here shown for the *Ez* component. Copyright 1998 by The Annual Review of Physical Chemistry.

The term “evanescent wave optics” summarizes a number of optical phenomena associated with the total internal reflection of light at the boundary between two media of different optical properties described by their different dielectric functions $\varepsilon$. The optical E-field along the propagation direction, *Ex*, has the usual oscillatory character of an electromagnetic mode. The component perpendicular to the interface, *Ez*, does not fall to zero abruptly, but decays exponentially with a decay length *l* which is a function of the angle of incidence θ (30):

$$l = \frac{\lambda}{2\pi\sqrt{(n \cdot \sin\theta)^2 - 1}} \tag{1.1}$$

where *l* is the decay length, $\lambda$ is the wavelength and *n* is the refractive index.

The surface plasmon cannot be excited directly by an incident optical wave at a planar metal–dielectric interface. Therefore the momentum of the incident optical wave has to be enhanced to match that of the surface plasmon wave. This momentum change is commonly achieved using attenuated total reflection (ATR) in prism couplers and optical waveguides, and diffraction at the surface of diffraction gratings. As the excitation of surface plasmons by optical wave results in resonant transfer of energy into the surface plasmon wave, Surface Plasmon Resonance manifests itself by resonant absorption of the energy of the optical wave (28).

### 1.2.2 Surface Plasmon Resonance (SPR)

As the propagation length of SP wave is very limited in space (28), the sensing action is performed directly in the area where the SP is excited by an optical wave. The optical system used to excite the SP is simultaneously used for the interrogation of Surface Plasmon Resonance.

The first SPR system commercially available was under the name of BIAcore™ (Pharmacia Biosensor, Uppsala, Sweden) (31). This optical biosensor represents the most advanced and developed optical label-free biosensor technology. In the last three decades numerous progresses have been made in the SPR instrument and data processing for achieve the best performance (32).

SPR technology relies on the covalent immobilization of one of the interacting species (the ligand) onto a solid phase and the observation of the interaction binding of the soluble ligate.

Because the interaction is observed in real time, the data obtained contains information on the kinetics of interaction of the macromolecules.

Many macromolecular interactions in biology occur between solid and liquid phases, and in dynamic flow, such as is the case in BIAcore™, this technology may be a reasonable mimic of many important interactions in vivo (33).

The SPR sensor has been applied in many chemical and biological processes: gas detection (34), determination of affinity constants (35), study of binding kinetic (33), screening of new ligands (36), cell-cell interaction (37), antibody-antigen interaction (38), study of protein-protein interaction (39), DNA hybridization (40), DNA-protein binding (41), genetic mutations analysis (42).

The SPR is an optical phenomenon in which light is focused through a prism onto a thin gold film on a glass support, where at a particular angle of incidence, the intensity of the reflected light is decreased due to the energy transfer from the light beam to the surface electrons on the film (Figure 6). The angle of the reflected light is dependent on the refractive index near the surface of the thin gold film. Such changes are proportional to changes in the adsorbed molecule layer present on the surface: a ligand is immobilized on the surface of the sensor and interactions between it and a target molecule can be monitored in real time via changes occurring in the refractive index expressed in resonance units (RU) (34).

The monitoring of molecular process in the SPR can be observed in three modes: angle resolved, wavelength shift, and imaging. In the first two modes, one measures the reflectivity of light from the metal surface as a function of either angle of incidence (at constant wavelength) or wavelength (at constant angle of incidence). The third method uses light of both constant wavelength and incident angle to interrogate a two-dimensional region of the sample, mapping the reflectivity of the surface as a function of position (43).

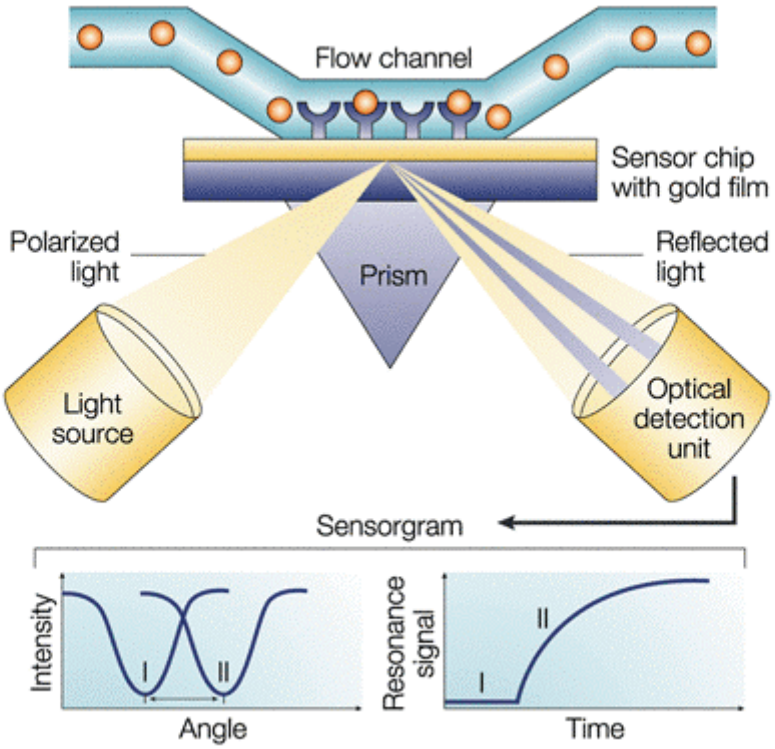


**Figure 6.** Surface plasmon resonance (SPR) detects changes in the refractive index in the immediate vicinity of the surface layer of a sensor chip. The SPR angle shifts (from I to II in the lower left-hand diagram) when biomolecules bind to the surface and change the mass of the surface layer. This change in resonant angle can be monitored non-invasively in real time as a plot of resonance signal (proportional to mass change) versus time. Copyright 2002 by Nature Reviews Drug Discovery.

The response (R) of SPR as the shift in wavelength (λ) or angle (θ) associated with changes in the refraction index of the medium of solution in contact with the metal surface, without adsorption on the surface, can be measured by the equation (29):

$$R = m\,\Delta\eta = (\eta_{final} - \eta_{initial}) \quad (1.2)$$

where $m$ is the sensitivity factor (nm/RIU(refractive index unit)), $\Delta\eta$ is the difference of refraction index of metal and medium. Plotting the refractive index of several solutions in contact with a metallic surface respect to the relative wavelength shift ($\Delta\lambda$) we obtain the sensitivity factor of the sensor analyzed. This parameter permits to compare the sensitivity of different sensors, and it's a 'universal' value for comparing different kind of sensors based on surface plasmons.

Chemosensors and biosensors based on SPR spectroscopy possess many desirable characteristics including: (a) capacity to detect changing in bulk index of refraction of $2x10^{-6}$ RIU (29); (b) large sensitivity factor about $2x10^{6}$ nm/RIU, ~15-25% of the light's wavelength (29); (c) the average thickness of an adsorbed layer is typically ~ $10^{-2}$ nm. The dynamic range is therefore rather large, from ~$10^{-2}$ to 200 nm in average film thickness (29); (d) a long range sensing length scale determined by the exponential decay of the evanescent electromagnetic field, $l$ ~ 200 nm (29); (e) multiple instrumental modes of detection (43); (f) real-time detection on the $10^{-1}$ $10^{3}$ s time scale for measurement of binding kinetics (30); (g) lateral spatial resolution on the order of 10 μm enabling multiplexing and miniaturization (43); (h) it's a label free sensor; (i) capable of probing complex mixtures, such as clinical material, without prior purification.

### 1.2.3 Localized Surface Plasmon Resonance (LSPR)

Noble metals of nanometric dimensions, that are metal nanoparticles (NPs), exhibit a strong UV-Vis absorption bands that is not present in the spectrum of the bulk metal.

These absorption bands result when the incident photon frequency is resonant with the collective oscillation of the conduction electrons and is known as Localized Surface Plasmon Resonance (LSPR) (44-45) (Figure 7). What happen exactly?

When the electron cloud is displaced relative to the nuclei, net charge separation appears at the surface of the nanostructure, which produces a restoring force arises from Coulomb

attraction between electrons and nuclei that results in oscillation of the electron cloud (Figure 7). The oscillating electron cloud has its own resonance frequency that depends by the density of electrons, the effective electron mass, and the shape and size of the charge distribution (46). When the frequency of the irradiated light matches the frequency of the electron cloud, its energy is completely absorbed by the electrons, and the incident light is completely extinguished. The amount of extinguished light determines the optical extinction of the nanostructure. The electron cloud oscillation produces an oscillating dipole which emits a dipolar radiation said to be scattered. Any energy from the incident light which does not contribute to scattering is said to be absorbed.

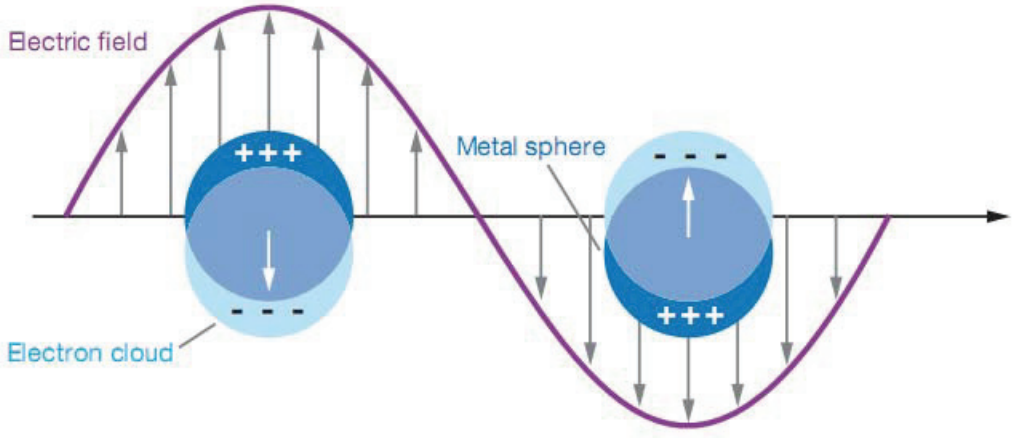


**Figure 7..** Schematic illustration of the Localized Surface Plasmon Resonance (LSPR) of a metal sphere showing the displacement of the electron charge cloud relative to the nuclei. Copyright 2007 by Annual Reviews.

In 1908 Gustav Mie (47) explained the phenomena by solving Maxwell's equations for the absorption and scattering of electromagnetic radiation by spherical metallic particles. This theory has been used to calculate the spectra of particles smaller than the wavelength of light, whose metallic dielectric function is known and which are embedded in an environment of known dielectric constant (44).

In Mie's formulation, the extinction E(λ) (scattering + absorption) of a sphere metal nanoparticle is related to the properties of the system by the equation:

$$E(\lambda) = \frac{24\pi N_A a^3 \varepsilon_m^{3/2}}{\lambda \cdot \ln(10)} \left[ \frac{\varepsilon_i}{(\varepsilon_r + \chi\varepsilon_m)^2 + \varepsilon_i^2} \right] \quad (1.3)$$

where$N_A$ is the areal density of nanoparticles, $a$ is the radius of the metallic nanosphere, $\varepsilon_m$ is the dielectric constant of the medium surrounding the metallic nanosphere (assumed to be a positive, real number and wavelength independent), λ is the wavelength of the absorbing radiation, $\varepsilon_i$ is the imaginary portion of the metallic nanoparticle's dielectric function, $\varepsilon_r$ is the real portion of the metallic nanoparticle's dielectric function, and $\chi$ is the term that describes the aspect ratio of the nanoparticle (equal to 2 for a sphere). It is evident from Eq. (1.3) that the LSPR spectrum of a metallic nanosphere depends on the nanoparticle radius $a$, the nanoparticle material ($\varepsilon_i$ and $\varepsilon_r$), the environment's dielectric constant ($\varepsilon_m$), and the shape of the nanoparticle ($\chi$).

The Mie's theory has provided a deep understanding of the interactions of light with metal nanoparticles, but it has been developed for ideal systems and results to be inadequate for most practical uses. A less rigorous approach is based on the assumption that the equations describing the extinction of the SPR of large metal surfaces (29) hold also for the nanoparticles (48). In this case, in analogy with the SPR, the LSPR bands are expected to show a spectral shift (Δλ) qualitatively described by:

$$\Delta\lambda = m(\eta_{ads} - \eta_{medium})\,(1 - e^{-2d/l}) \quad (1.4)$$

where $m$ is the sensitivity factor (nm/RIU (refractive index unit)) $n_{ads}$ and $n_{medium}$ are respectively the refractive index of the adsorbed layer and of the medium, $d$ is the thickness of the adsorbed layer, and $l$ is the characteristic electromagnetic decay length of the evanescent electromagnetic field (49-52).

According to Eq. (1.4), the binding of organic molecules to nanoparticles induces an increase of the local refractive index and, in turn, a red shift of the extinction spectrum, as experimentally observed (53-54). It is thus evident, that *LSPR response of plasmonic nanoparticles (NPs) acts as transducer of changes in the refractive index occurring at the surfaces*. When the Eq. (1.4) is applied to the LSPR, the equation approximates the response for adsorbate layers but does not provide a fully quantitative explanation of its response (48).

Though the SPR spectroscopy possesses many desirable characteristics, as listed before, the LSPR spectroscopy can be competitive with to SPR. The LSPR sensor shows modest refractive index sensitivity of ~ $2x10^2$ nm/RIU (29). A reduction of refractive index sensitivity of four orders of magnitude respect to the SPR sensor, could lead to think that the LSPR sensor can be less sensitive than the SPR sensor. But this is not the case. The characteristic short electromagnetic field decay length, *l* is ~5-25 nm (~1-3% of the light's wavelength), provides to LSPR sensors an enhanced sensitivity (48). This implies that the space surrounding the nanoparticles can be probed with electromagnetic field 20-50 times more intense than that of SPR. Therefore, for LSPR sensing, the spot size can be reduced from to a large number of individual sensing nanoparticles down to a single nanoparticle (55). Thanks to the lower refractive index sensitivity, the LSPR sensors do not require temperature control as the SPR sensor. Therefore, the LSPR and SPR sensors are very competitive in sensitivity.

The final and strong difference between the two sensors is the cost. Commercialized SPR instruments can vary between $150K-$300K (plus supplies), whereas the prototype and portable LSPR system costs less than $5K (plus supplies).

Hence, LSPR based sensors can provide an effective and easy route for monitoring in real time the binding of molecules or molecular interactions occurring at the nanoparticles surface. However, it is important to underline that the LSPR (in analogy with the SPR) is a non-specific technique because the signal is only dependent on the refractive index around the metal particle, and the specificity is only achieved through biomolecular recognition elements.

## 1.3 Fabrication of Metal Nanoparticles

For fabrication of metal nanostructures both *bottom up* and *top down* approaches can be used. While the latter involves the use of lithographic and related techniques, bottom up methods are based on chemical reactions giving rise to nanomaterials with composition, size and shape determined by the reaction conditions.

Typical materials for plasmonic applications are noble metals, especially silver or gold. Despite silver displays sharper and more intense LSPR bands than gold (56), the gold metal has a number of favorable properties. It has an higher chemical stability (57), is does not oxidize at temperature below its melting point, it does not react with atmospheric $O_2$, it does not react with most chemicals, it is compatible with biological element like the cells (58); all that has favored its preferential application for biosensing.

### 1.3.1 Bottom Up: Colloidal Nanoparticles

Nanoparticles are generally defined as discrete particles between 1 and 50 nm in size. They can be dispersed in water ("hydrosols") or organic solvents ("organosols"), depending on the preparation conditions and capping agents surrounding the particles (59).

The colloidal nanoparticles derive from chemical reduction of a metal salt in the presence of a stabilizer, which limits the growth of the particles, directs their shape, and provides colloidal stability (60). The stabilizers commonly ligands, surfactants, ions, organic acids, or polymers adsorbs or coordinates to the surface of the NPs and inhibits aggregation by Coulombic repulsion (61-62) and/or steric hindrance (60). The specific choice of reductant, stabilizer, temperature, and relative concentrations of the reagents can all affect the size and shape of the NPs. In review of Stewart et al. (63), we can find an exhaustive and detailed list of the broadly methods used for synthesizing the NPs (64,59).

The most frequently used procedure for making spherical Au NPs is the citrate reduction of $HAuCl_4$ in an aqueous solution reported by Turkevitch et al. in 1951 (65). In this protocol the citrate acts as both a reducing agent and an electrostatic stabilizer, and the size of the NPs can be tuned by controlling the citrate to $HAuCl_4$ ratio. Another largely used method, that yields highly stable particles monodisperse and protected them by thiol, is the Brust-Schiffrin method (66). This approach uses a biphasic synthesis (an aqueous and organic phase) and

tetraoctylammonium bromide as a phase-transfer agent to reduce the $[AuCl_4]^{-1}$ anion with $NaBH_4$ in the presence of alkanethiols to yield thiol-stabilized particles that are one to several nanometers in size. The thiols that protect the Au NPs can be easily replaced by thiolated oligonucleotides (67) or proteins (68), through simple place-exchange reactions (64).

Localized Surface Plasmon Resonance of colloidal NPs dispersed in a solution has been exploited in a variety of applications for sensing and monitoring of molecular interaction (69-78). However, the use of metal nanoparticles in solution requires a careful synthetic procedure to obtain monodisperse NPs, a fine control of ionic strength, pH, temperature in order to avoid the flocculation, and a stabilization of the synthesized nanoparticles with a proper molecular shell which can limit a further functionalization for sensing purpose (59,66).

### 1.3.2 Top Down: Nanoparticles Deposited on Substrate

As an alternative to colloidal dispersions, metal nanoparticles deposited on a transparent support result to be a promising plasmonic material.

For generate this kind of nanoparticles advanced lithographic techniques as Electron-Beam Lithography (EBL) (79) or Focused-Ion Beam (FIB) (80) allows for the fabrication of metal nanostructures with perfect control of size, shape and spatial distribution. However, these techniques are expensive and inappropriate to handle the large variety of organic and biological systems available in nanotechnology.

An alternative, inexpensive and large scale lithographic method is the so-called NanoSphere Lithography (NLS) (81-82,51) (Figure 8). This is a powerful fabrication technique that inexpensively produces arrays of nanoparticles with controlled shape, size, and interparticle spacing. The methodology consists in the self assembly of monodisperse nanospheres of latex, silica or polystyrene, to form a two-dimensional colloidal mask. A substrate is prepared so that the nanospheres freely diffuse until they reach their lowest energy configuration. This is achieved by chemically modifying the nanosphere surface with a negative charge that is electrostatically repelled by the negatively charged substrate such as mica or chemically treated glass. As the solvent, normally water evaporates, capillary forces draw the nanospheres together, and the nanospheres crystallize in a hexagonally close-packed pattern on the substrate. Sometimes nanosphere masks include a variety of defects that arise as a result of nanosphere polydispersity, site randomness, point defects, line defects, and

polycrystalline domains. Following self-assembly of the nanosphere mask, a metal or other material is then deposited by thermal evaporation or electron beam deposition to the substrate through the nanosphere mask. Then, the nanosphere mask is removed, typically by sonicating the entire sample in a solvent, leaving behind surface-confined nanoparticles that have a triangular footprint (Figure 8). The optical properties of these nanoparticles can be easily tuned throughout the visible region of the spectrum by changing the size or shape of the nanoparticles (51).

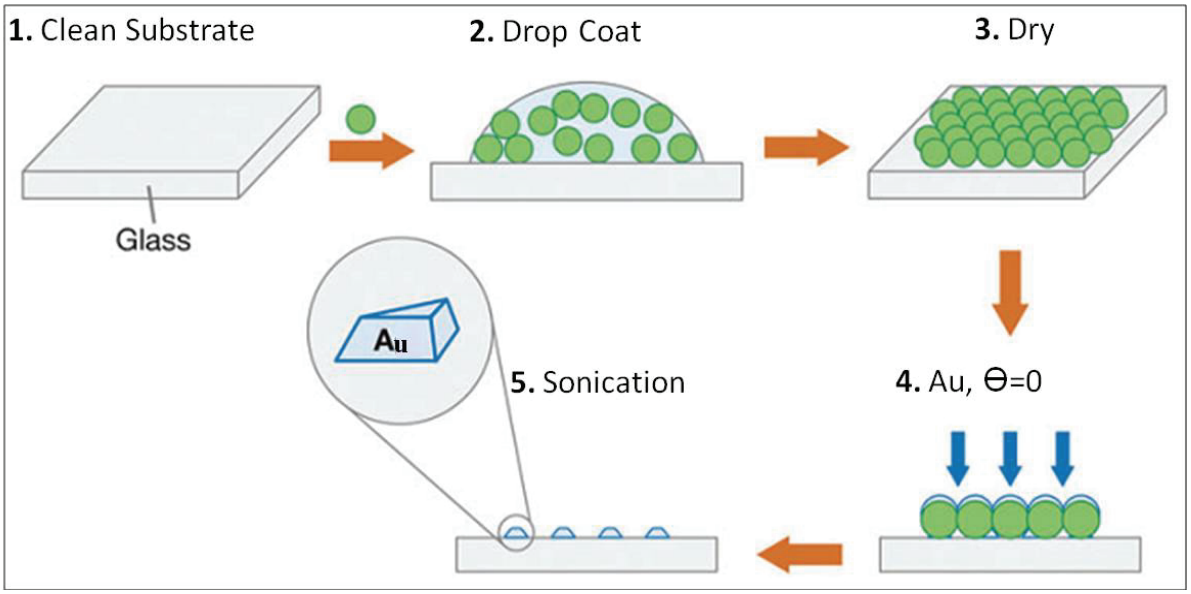


**Figure 8.** Illustration of the process of NanoSphere Lithography (NSL) in which nanospheres are drop coated onto a surface and allowed to self-assemble into a hexagonally close-packed array (steps 1–3), followed by metal deposition (step 4), and removal of the nanosphere mask. Copyright 2007 by Annual Review of Physical Chemistry.

An alternative, easier and inexpensive method is the classical deposition through thermal evaporation of a metallic layer on substrate, followed by thermal annealing (83-89).

The evaporation deposition techniques, called physical vapor depositions (PVD) (90), are atomistic deposition processes in which material is vaporized from a solid or liquid source in

the form of atoms or molecules, transported in the form of vapor through a vacuum or low pressure gaseous environment to the substrate where it condenses.

The Vacuum Deposition is a PVD process in which material from a thermal vaporization source reaches the substrate with little or no collision with gas molecules. Usually the deposition process occurs in high vacuum: from $10^{-5}$ to $10^{-9}$ Torr. At low pressures, the mean free path of vapor atoms is the same order as the vacuum chamber dimensions, so these particles travel in straight lines from the evaporation source towards the substrate. In thermal evaporation the average energy of vapor atoms reaching the substrate surface is generally low (tenths of eV). This process affects seriously the morphology of the films, often resulting in a porous and poorly adherent material. Thermal evaporation is generally done by using thermally heated source such a tungsten wire coils. This technique has the advantage to be easy to use, and to allow for a rapid evaporation of low melting point metals like gold and silver.

The electron beam evaporation is another thermal evaporation technique that allows using metal more hard to evaporate like titanium and tungsten (91).

We believe that the use of a thermal evaporation as deposition technique is a surface-based approach that it allows the development of chip-based sensors, and gives the opportunity to design arrays of plasmonic material which can be used in multiplex bio-recognition (92-95).

A series of recent studies have shown that monodisperse nanoparticles (NPs) of Ag and Au deposited on transparent substrates can provide a convenient approach to detect metal-surface/molecule interaction (96-113).

## 1.4 Self-Assembled Monolayers (SAMs)

The biosensors, as mentioned before, are based generally on a transducer system functionalized by a chemical interface layer. Since this chemical layer constitutes the interface with the analyte sample, this component strongly determines the stability, the specificity, and the reproducibility of the sensor. In particular, nonspecific signals are the major problem in diagnostic applications, where an analyte at low concentration must be detected in the presence of an excess of nonspecific molecules. Then, the construction of a specific and stable interface layer is therefore mandatory for the final biosensor application.

The adsorbate layers i) act as a physical or electrostatic barrier against aggregation or as an electrically insulating film, ii) decrease the reactivity of the surface atoms, and iii) alter interfacial properties of metal surface.

An excellent method for building the interface layer is based on the properties of self-Assembled Monolayers (SAMs). Self-assembled monolayers are ordered molecular assemblies that form spontaneously by adsorption of organic molecules via a specific affinity of the headgroup to the substrate. The most studied and used molecules for building the SAMs are the alkanethiols (58). The molecules that form SAMs can be divided in three parts.

The headgroup, that has a chemical function, provides to adsorption of the molecule to the metal surface (Figure 9). In this case the headgroup is the thiol group that has high affinity for gold (114). When the thiol group comes into contact with the gold surface it lost a hydrogen atom and it changes in thiolate group. Then, the thiolate group reacts with a surface gold atom forming covalent bond and developing hydrogen.

$$R\text{-}S\text{-}H + Au_n^0 \rightarrow R\text{-}S^-\text{-}Au^+ Au_n^0 + \tfrac{1}{2} H_2$$

The spacer, that's the alkane chain, is responsible of the strong lateral interaction, arising from the van der Waals forces (Figure 9). In fact, to minimize the free energy of the organic layer, the molecules adopt conformations that allow high degrees of van der Waals interactions with the neighboring molecules; these arrangements yield a secondary level of organization in the monolayer. This lateral interaction can be controlled by changing the length of the hydrocarbon (58).

The terminal functional group makes possible to generate well-defined organic surfaces with different functional chemical group exposed at the interface. These terminal functional groups determine the surface properties.

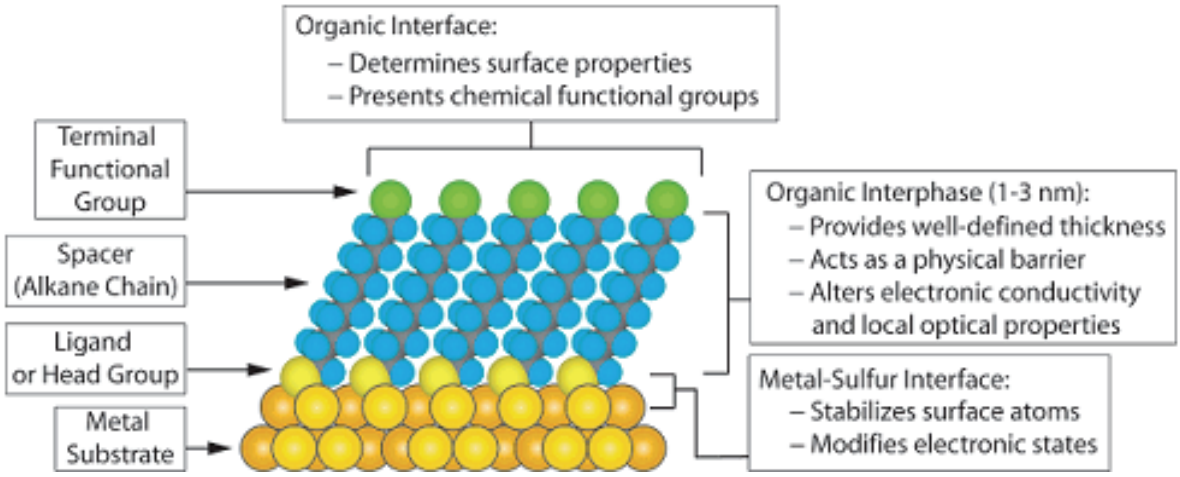


**Figure 9.** Schematic diagram of an ideal single-crystalline SAM of alkanethiolates supported on a gold surface with a (111) texture. The anatomy and characteristics of the SAM are highlighted. Copyright 2005 by Chemical Reviews.

The most common protocol for preparing SAMs on gold and other metals is immersion of a freshly prepared or clean substrate into a dilute 1-10 mM ethanolic solution of thiols for ~ 12-18 h at room temperature. Dense coverages of adsorbates are obtained quickly from millimolar solutions (milliseconds to minutes), but a slow reorganization process requires times on the order of hours to maximize the density of molecules and minimize the defects in the SAM (58). There are, however, a number of experimental factors that can affect the structure of the resulting SAM and the rate of formation: solvent, temperature, concentration of adsorbate, immersion time, purity of the adsorbate, concentration of oxygen in solution, cleanliness of the substrate, and chain length.

In the SAM formation, the molecules tend to adopt structural arrangements that are similar to simple adlayer structures formed by elemental sulfur on that metal. The SAMs formed from n-alkanethiols on gold adopt a quasi-crystalline structure where the chains are fully extended

in a nearly all-trans conformation. The tilts angle $\alpha$, defined with respect to the surface normal direction, of these chains on gold surface is 30°. The metal sulfur interaction drives the assembly to the limiting case where the gold surface is covered by a ($\sqrt{3}$ x $\sqrt{3}$)-R30° (R=rotated) overlayer of thiolates, but the attractive lateral interactions promote the secondary organization of the alkane chains that defines the fine details of the c(4 x 2) superlattice structure (115-117). This configuration gives the idea of the competition between the SAM ordering, driven by the lateral van der Waals interaction between alkyl chains, and disordering of interfacial Au atoms, driven by the sulfur-gold interaction. The Scoles's group found that the sulfur atoms of the short alkanethiol molecules bind at two distinct surface sites, and that the first gold surface layer contains gold atom vacancies (which are partially redistributed over different sites) as well as gold adatoms that are laterally bound to two sulfur atoms (118).

The SAMs formed on the metal nanoparticle surface can have different properties respect to the SAM formed on the bulk metal surface. The first difference derive from the percentage of the total number of metal atoms present at nanoparticles interface, in fact, the nanoparticles have higher percentage of metal atoms available to bind (58). In addition, the SAM's structure will depend on the curvature and atom defects of the nanoparticles surface. A consequence of the surface curvature is a decrease in the chain density that translates into enhanced mobility of the molecule (119).

Self-assembly is a general principle in nature, as seen in the formation of, e.g., membranes from lipid molecules, or the living cell as probably the most important paradigm. For their property to reproduce a like biological environment, the SAMs are also used to study the biologic element as cells, proteins, DNA, and other many biological components. Therefore SAMs should have the follows characteristics: i) they should be able to prevent nonspecific adsorption of proteins or other biomolecules on the surface, that is, they should only allow for interactions between the molecules and the ligands of interest; ii) they should allow for modifications of the composition and density of the immobilized ligands or biomolecules; and iii) they should incorporate ligands in a structurally well-defined manner in order to that minimizes the interaction with surface (58).

The best protein-resistant surfaces presently known are those formed by oligo- or poly-(ethylene glycol) (OEG or PEG) (120-123). Alkanethiols terminated with ethylene glycol groups are standard components of SAMs often used to study biological and biochemical interactions (124-128). On gold, the alkane chains of the oligo (ethylene glycol) form a dense,

ordered monolayer with the same molecular conformation found for n-alkanethiols, i.e., all-trans chains with a 30° tilt; the ethylene glycol terminal group adopts either a helical conformation aligned perpendicular to the surface or an amorphous conformation (58). The combination of several factors, that is the hydrophilicity of the terminal group, the hydrophilicity of the internal units, and the lateral packing density, allows the formation of a SAM which is fully protein resistant. If the ability of a polyether SAM to coordinate water both in its interior and on its surface is reduced when one of these factors is unfavorable or absent, the overall protein resistance decreases (121). This suggests that protein resistance of OEG-terminated self-assembled monolayers is a consequence of the stability of the interfacial water layer, which prevents direct contact between the surface and the protein (129).

## References


1. L. C. Clark Jr., C. Lyons. Electrode systems for continuous monitoring in cardiovascular surgery. *Annals of the New York Academy of Sciences*. **1962**, 102, 29-45.

2. S. J. Updije, G. P. Hicks. The Enzyme Electrode. *Nature*. **1967**, 214, 986-988.

3. E.-H. Yoo, S.-Y. Lee. Glucose biosensors: an overview of use in clinical practice. *Sensors*. **2010**, 10, 4558-4576.

4. J. Wang. Glucose biosensors: 40 years of advances and challenges. *Electroanalysis*. **2001**, 13(12), 983-988.

5. E. Engvall, P. Perlmann. Enzyme-linked immunosorbent assay (ELISA) quantitative assay of immunoglobulin G . *Immunochemistry*. **1971**, 8(9), 871-874.

6. B. K. Van Weemen, A. H. W. M. Schuurs. Immunoassay using antigen-enzyme conjugates. *FEBS Letters*. **1971**, 15(3), 232-236.

7. M. Schena, D. Shalon, R. W. Davis, P. O. Brown. Quantitative monitoring of gene expression patterns with a complementary DNA microarray. *Science*. **1995**, 270, 467-470.

8. J. DeRisi, L. Penland, P. O. Brown, M. L. Bittner, P. S. Meltzer, M. Ray, Y. Chen, Y. A. Su, J. M. Trent. Use of a cDNA microarray to analyse gene expression patterns in human cancer. *Nature Genetics*. **1996**, 14, 457-460.

9. M. Schena, D. Shalon, R. Heller, A. Chai, P. 0. Brown, R. W. Davis. Parallel human genome analysis: microarray-based expression monitoring of 1000 genes. *Proceedings of the National Academy of Sciences of the United States of America*. **1996**, 93, 10614-10619.

10. M. J. Marton, J. L. DeRisi, H. A. Bennett, V. R. Iyer, M. R. Meyer, C. J. Roberts, R. Stoughton, J. Burchard, D. Slade, H. Dai, D. E. Bassett Jr., L. H. Hartwell, P. O. Brown, S. H. Friend. Drug target validation and identification of secondary drug target effects using DNA microarrays. *Nature Medicine*. **1998**, 4(11), 1293-1301.

11. P. O. Brown, D. Botstein. Exploring the new world of the genome with DNA microarrays. *Nature Genetics Supplement*. **1999**, 21, 33-37.

12. C. A. Afshari, E. F. Nuwaysir, J. C. Barrett. Application of complementary DNA microarray technology to carcinogen identification, toxicology, and drug safety evaluation. *Cancer Research*. **1999**, 59, 4759-4760.

13. M. B. Miller, Y.-W. Tang. Basic concepts of microarrays and potential applications in clinical microbiology. *Clinical Microbiology Reviews*. **2009**, 22(4), 611-633.

14. M. L. Bulyk. Protein binding microarrays for the characterization of DNA-protein interactions. *Advances in Biochemical Engineering / Biotechnology*. **2007**, 104, 65-85.

15. M. Uttamchandani, J. Wang, S. Q. Yao. Protein and small molecule microarrays: powerful tools for high-throughput proteomics. *Molecular BioSystems*. **2006**, 2, 58-68.

16. D. Shalon, S. J. Smith, P. O. Brown. A DNA microarray system for analyzing complex DNA samples using two-color fluorescent probe hybridization. *Genome Research*. **1996**, 6, 639-645.

17. AmpliChip® CYP450 Test. *La Roche Ltd.*, **2003**. http://www.roche.com/products/product-details.htm?type=product&id=17

18. Protein Array kits. *APiX™ and PANDEIA Array™ Kits.* Gentel Biosciences, Inc. http://www.gentelbio.com/products/protein-array-kits.html

19. K. B. Lee, S. J. Park, C. A. Mirkin. Protein nanoarrays generated by dip-pen nanolitography. *Science*. **2002**, 295, 1702-1705.

20. A. A. Tseng, K. Chen, C. D. Chen, K. J. Ma. Electron beam litography in nanoscale fabrication: recent development. *IEEE Trans. Electronics Packaging Manufactur*. **2003**, 26, 141-149.

21. J. D. Hoff, L. J. Cheng, E. Meyhofer, L. J. Guo, A. J. Hunt. Nanoscale protein patterning by imprint lithography. *Nano Letters*. **2004**, 4, 853-857.

22. H. W. Li, B. V. O. Muir, G. Fichet, W. T. S. Huck. Nanocontact printing: A route to sub-50-nm-scale chemical and biological patterning. *Langmuir*. **2003**, 19, 1963-1965.

23. A. A. Yu, T. A. Savas, G. S. Taylor, A. Guiseppe-Elie, H. I. Smith, F. Stellacci. Supramolecular Nanostamping: using DNA as movable type. *Nano Letters*. **2005**, 5(6), 1061-1064.

24. A. A. Yu, T. Savas, S. Cabrini, E. diFabrizio, H. I. Smith, F. Stellacci. High resolution printing of DNA feature on poly(methyl methacrylate) substrates using supramolecular nano-stamping. *Journal of the American Chemical Society*. **2005**, 127(48), 1677-16775.

25. R. Tanaka, T. Yuhi, N. Nagatani, T. Endo, K. Kerman, Y. Takamura, E. Tamiya. A novel enhancement assay for immunochromatographic test strips using gold nanoparticles. *Analytical and Bioanalytical Chemistry*. **2006**, 385(8), 1414-1420.

26. R. H. Ritchie. Plasma losses by fast electrons in thin films. *Physical Review*. **1957**, 106(5), 874-881.

27. V. Silin, A. Plant. Biotechnological applications of surface plasmon resonance. *Trends in Biotechnology*. **1997**, 15(9), 353-359.

28. J. Homola, S. S. Yee, G. Gauglitz. Surface plasmon resonance sensors: review. *Sensors and Actuators B: Chemical*. **1999**, 54, 3-15.

29. L. S. Jung, C. T. Campbell, T. M. Chinowsky, M. N. Mar, S. S. Yee. Quantitative interpretation of the response of surface plasmon resonance sensors to adsorbed films. *Langmuir*. **1998**, 14, 5636-5648.

30. W. Knoll. Interfaces and thin films as seen by bound eectromagnetic waves. *The Annual Review of Physical Chemistry*. **1998**, 49, 569-638.

31. B. Liedberg, C. Nylander, I. Lundstrom. Biosensing with surface plasmon resonance - how it all started. *Biosensors & Bioelectronics*. **1995**, 10, i-ix.

32. J. Homola. Surface plasmone resonance based sensors. Berlin-Heidelberg-New York: *Springer-Verlag*, **2006**.

33. D. J. O'Shannessy. Determination of kinetic rate and equilibrium binding constants for macromolecular interactions: a critique of the surface plasmon resonance literature. *Current Opinion in Biotechnology*. **1993**, 5, 65-71.

34. B. Liedberg, C. Nylander, I. Lundstrom. Surface plasmon resonance for gas detection and biosensing. *Sensors and Actuactors*. **1983**, 4, 299-304.

35. L. Masson, A. Mazza, G. De Crescenzo. Determination of Affinity and Kinetic Rate Constants Using Surface Plasmon Resonance. *Bacterial Toxins: Methods and Protocols*. **2000**, 145, 189-201.

36. T. N. Stitt, C. Conn, M. Gore, C. Lat, J. Bruno, C. Radziejewski, K. Mattsson, J. Fisher, D. R. Ceiss, P. F. Jones. The anticoagulation factor protein S and its relative, CasC, are ligands for the Tyro 3/Axl family of receptor tyrosine kinases. *Current Biology*. **1995**, 4, 74-83.

37. P. A. Van der Merwe, A. N. Barclav, D. W. Mason, E. A. Davies, B. P. Morgan, M. Tone, A. K. C. Krishna, C. lanelli, S. J. Davis. Human cell-adhesion molecule CD2 binds CD58 (LFA-3) with a very low affinity and an extremely fast dissociation rate but does not bind CD48 or CD49. *Biochemestry*. **1994**, 33, 10149-10160.

38. A. C. Malborg, A. Michaelsson, M. Ohlin, B. Jansson, C. Borrebaeck. Real time analysis of antibody-antigen reaction kinetics. *Scandinavian Journal of Immunology*. **1992**, 35, 643-650.

39. H. Mach, D B. Volkin, C. Burke, C. R. Middaugh, R. J. Linhardt, J. R. Fromm, D. Loganathan, L. Mattisson. Nature of the Interaction of Heparin with Acidic Fibroblast Growth Factor. *Biochemestry*. **1993**, 32, 5480-5489.

40. C. E. Jordan, A. G. Frutos, A. J. Thiel, R. M. Corn. Surface plasmon resonance imaging measurements of DNA hybridization adsorption and streptavidin/DNA multilayer formation at chemically modified gold surfaces. *Analytical Chemistry*. **1997**, Vol. 69, 4939-4947.

41. C. Boozer, J. Ladd, S. F. Chen, S. T. Jiang. DNA-directed protein immobilization for simultaneous detection of multiple analytes by surface plasmon resonance biosensor. *Analytcal Chemistry*. **2006**, 78, 1515-1519.

42. G. Feriotto, G. Breveglieri, A. Finotti, S. Gardenghi, R. Gambari. Real-time multiplex analysis of four beta-thalassemia mutations employing surface plasmon resonance and biosensor technology. *Laboratory Investigation*. **2004**, 84, 796–803.

43. J. M. Brockman, B. P. Nelson, R. M. Corn. Surface plasmone resonance imaging measurments of ultrathin organics films. *Annual Review of Physical Chemistry*. **2000**, 51, 41-63.

44. U. Kreibig, M. Vollmer. Optical Properties of Metal Clusters. Berlin: *Springer*, **1995**.

45. M. A. El-Sayed. Some interesting properties of metals confined in time and nanometer space of different shapes. *Accounts of Chemical Research*. **2001**, 34(4), 257-264.

46. K. L. Kelly, E. Coronado, L. L. Zhao, G. C. Schatz. The optical properties of metal nanoparticles: the influence of size, shape, and dielectric enviroment. *The Journal of Physical Chemistry B*. **2003**, 107, 668-677.

47. G. Mie. Optical properties of colloidal gold solutions. *Annals of Physics*. **1908**, 25, 329-371.

48. A. J. Haes, S. Zou, G. C. Schatz, R. P. Van Duyne. A nanoscale optical biosensor: the short range distance dependence of the localized surface plasmon resonance of silver and gold nanoparticles. *The Journal of Physical Chemistry B*. **2004**, 108, 109-116.

49. A. J. Haes, R. P. Van Duyne. A unified view of propagating and localized surface plasmon resonance biosensors. *Analytical and Bioanalytical Chemistry*. **2004**, 379, 920-930.

50. K. A.Willets, R. P. Van Duyne. Localized surface plasmon spectroscopy and sensing. *Annual Review of Physical Chemistry*. **2008**, 58, 267-297.

51. C. L. Haynes, R. P. Van Duyne. Nanosphere lithography: a versatile nanofabrication tool for studies of size-dependent nanoparticle optics. *The Journal of Physical Chemistry B*. **2001**, 105 (24), 5599-5611.

52. A. J. Haes, D. A. Stuart, S. Nie, R. P. Van Duyne. Using solution-phase nanoparticles, surface-confined nanoparticle arrays and single nanoparticles as biological sensing platforms. *Journal of Fluorescence*. **2004**, 14 (4), 355-367.

53. M. E. Stewart, C .R. Anderton, L. B. Thompson, J. Maria, S. K. Gray, J. A. Rogers, R. G. Nuzzo. Nanostructured plasmonic sensors. *Chemical Reviews*. **2008**, 108, 494-521.

54. B. Sepulveda, P. C. Angelomé, L. M. Lechuga, L. M. Liz-Marzàn. LSPR-based nanobiosensors. *Nano Today*. **2009**, 4(3), 244-251.

55. A. D. McFarland, R. P. Van Duyne. Single silver nanoparticles as real-time optical sensors with zeptomole sensitivity. *Nano Letters*. **2003**, 3(8), 1057-1062.

56. C. Sönnichsen, T. Franzl, T. Wilk, G. von Plessen, J. Feldmann. Plasmon resonances in large noble-metal clusters. *New Journal of Physics*. **2002**, 4, 93.1-93.8.

57. J. Biener, A. Wittstock, M. M. Biener, T. Nowitzki, A. V. Hamza, M. Baeumer. Effect of surface chemistry on the stability of gold nanostructures. *Langmuir*. **2010**, 26(17), 13736-13740.

58. J. C. Love, L. A. Estroff, J. K. Kriebel, R. G. Nuzzo, G. M. Whitesides. Self-assembled monolayers of thiolates on metals as a form of nanotechnology. *Chemical Reviews*. **2005**, 105(4), 1103-1169.

59. J. Zhou, J. Ralston, R. Sedev, D. A. Beattie. Functionalized gold nanoparticles: synthesis, structure and colloid stability. *Journal of Colloid and Interface Science*. **2009**, 331, 251-262.

60. G. B. Khomutov, Y. A. Koksharov. Effects of organic ligands, electrostatic and magnetic interactions in formation of colloidal and interfacial inorganic nanostructures. *Advances in Colloid and Interface Science*. **2006**, 122, 119-147.

61. Z. S. Pillai, P. V. Kamat. What factors control the size and shape of silver nanoparticles in the citrate ion reduction method? *The Journal of Physical Chemestry B*. **2004**, 108, 945-951.

62. M. Geneviève, C. Vieu, R. Carles, A. Zwick, G. Brière, L. Salomé, E. Trévisiol. Biofunctionalization of gold nanoparticles and their spectral properties. *Microelectronic Engineering*. **2007**, 84, 1710-1713.

63. M. E. Stewart, C. R. Anderton, L. B. Thompson, J. Maria, S. K. Gray, J. A. Rogers, R. G. Nuzzo. Nanostructured plasmonic sensors. *Chemical Reviews*. **2008**, 108, 494-521.

64. R. Sardar, A. M. Funston, P. Mulvaney, R. W. Murray. Gold nanoparticles: past, present, and future. *Langmuir*. **2009**, 25(24), 13840-13851.

65. J. Turkevich, P. C. Stevenson, J. Hillier. A study of the nucleation and growth processes in the synthesis of colloidal gold. *Discussions of the Faraday Society*. **1951**, 11, 55-75.

66. M. Brust, M. Walker, D, Bethell, D. J. Schiffrin, R. Whyman. Synthesis of thiol-derivatised gold nanoparticles in a two-phase liquid-liquid system. *Journal of the Chemical Society, Chemical Communications*. **1994**, 801-802.

67. C. J. Ackerson, M. T. Sykes, R. D. Kornberg. Defined DNA/nanoparticle conjugates. *Proceedings of the National Academy of Sciences*. **2005**, 102(38), 13383-13385.

68. C. F. W. Becker, Y. Marsac, P. Hazarika, J. Moser, R. S. Goody, C. M. Niemeyer. Functional immobilization of the small GTPase Rab6A on DNA–gold nanoparticles by using a site-specifically attached poly(ethylene glycol) linker and thiol place-exchange reaction. *ChemBioChem*. **2007**, 8(1), 32-36.

69. S.Tokonami, H. Shiigi, T. Nagaoka. Open bridge-structured gold nanoparticle array for label-free DNA detection. *Analytical Chemestry*. **2008**, 80, 8071-8075.

70. M. Cai, F. Li, Y. Zhang, Q. Wang. One-pot polymerase chain reaction with gold nanoparticles for rapid and ultrasensitive DNA detection. *Nano Research*. **2010**, Vol. 3, 557-563 .

71. N. J. Wittenberg, C. L. Haynes. Using nanoparticles to push the limits of detection. *Advanced Review*. **2009**, 1, 237-254.

72. G. L. Liu, Y. Yin, S. Kunchakarra, B. Mukherjee, D. Gerion, S. D. Jett, D. G. Bear, J. W. Gray, A. P. Alivisatos, L. P. Lee, F. F. Chen. A nanoplasmonic molecular ruler for measuring nuclease activity and DNA footprinting. *Nature Nanotechnology*. **2006**, 1, 47-52.

73. K. E. Sapsford, D. Park, E. R. Goldman, E. E. Foos, S. A. Trammell, D. A. Lowy, M. G. Ancona. Selective DNA-mediated assembly of gold nanoparticles on electroded substrates. *Langmuir*. **2008**, 24, 10245-10252.

74. D. A. Giljohann, D. S. Seferos, A. E. Prigodich, P. C. Patel, C. A. Mirkin. Gene regulation with polyvalent siRNA nanoparticle conjugates. *Journal of the American Chemical Society*. **2009**, 131, 2072-2073.

75. A. K. R. Lytton-Jean, M. S. Han, C. A. Mirkin. Microarray detection of duplex and triplex DNA Binders with DNA-modified gold nanoparticles. *Analytical Chemistry*. **2007**, 79, 6037-6041.

76. S. J. Hurst, M. S. Han, A. K. R. Lytton-Jean, C. A. Mirkin. Screening the sequence selectivity of DNA-binding molecules using a gold nanoparticle-based colorimetric approach. *Analytical Chemistry*. **2007**, 79, 7201-7205.

77. S. I. Stoeva, J.-S. Lee, C. S. Thaxton, C. A. Mirkin. Multiplexed DNA detection with biobarcoded nanoparticle probes. *Angewandte Chemie International Edition*. **2006**, 45, 3303-3306.

78. X. Wanga, Y. Lia, H. Wangb, Q. Fua, J. Penga, Y. Wanga, J. Dua, Y. Zhoua, L. Zhan. Gold nanorod-based localized surface plasmon resonance biosensor for sensitive detection of hepatitis B virus in buffer, blood serum and plasma. *Biosensors and Bioelectronics*. **2010**, 26(2), 404-410.

79. C. Vieu, F. Carcenac, A. Pépin, Y. Chen, M. Mejias, A. Lebib, L. Manin-Ferlazzo, L. Couraud, H. Launois. Electron beam lithography: resolution limits and applications. *Applied Surface Science*. **2000**, 164, 111-117.

80. C. A. Volkert, A. M. Minor. Focused ion beam microscopy and micromachining. *Materials Research Society Bulletin*. **2007**, 32, 389-399.

81. T. R. Jensen, M. D. Malinsky, C. L. Haynes, R. P. Van Duyne. Nanosphere lithography: tunable localized surface plasmon resonance spectra of silver nanoparticles. *The Journal of Physical Chemistry B*. **2000**, 104(45), 10549-10556.

82. J. C. Hulteen, R. P. Van Duyne. Nanosphere lithography: a materials general fabrication process for periodic particle array surfaces. *Journal of Vacuum Science and Technology A*. **1995**, 13(3), 1553-1558.

83. V. Cantale, F. C. Simeone, R. Gambari, M. A. Rampi. Gold nano-islands on FTO as plasmonic nanostructures for biosensors. *Sensors and Actuators B: Chemical*. **2011**, 152(2), 206-213.

84. G. Kalyuzhny, A. Vaskevich, G. Ashkenasy, A. Shanzer, I. Rubinstein. UV/vis spectroscopy of metalloporphyrin and metallophthalocyanine monolayers self-assembled on ultrathin gold films. *The Journal of Physical Chemistry B*. **2000**, 104(34), 8238-8244.

85. G. Kalyuzhny, A. Vaskevich, M. A. Schneeweiss, I. Rubinstein. Transmission surface-plasmon resonance (T-SPR) measurements for monitoring adsorption on ultrathin gold island films. *Chemistry - A European Journal*. **2002**, 8(17), 3849-3857.

86. I. Doron-Mor, H. Cohen, Z. Barkay, A. Shanzer, A. Vaskevich, I. Rubinstein. Sensitivity of transmission surface plasmon resonance (T-SPR) spectroscopy: self-assembled multilayers on evaporated gold island films. *Chemistry - A European Journal*. **2005**, 11(19), 5555-5562.

87. E. Hutter, M.-P. Pileni. Detection of DNA hybridization by gold nanoparticle enhanced transmission surface plasmon resonance spectroscopy. *The Journal of Phical Chemistry B*. **2003**, 107(27), 6497-6499.

88. K.-C. Leea, S.-J. Lina, C.-H. Lina, C.-S. Tsaib, Y.-J. Lu. Size effect of Ag nanoparticles on surface plasmon resonance. *Surface and Coatings Technology*. **2008**, 202, 5339-5342.

89. S. Szunerits, V. G. Praig, M. Manesse, R. Boukherroub. Gold island films on indium tin oxide for localized surface plasmon sensing. *Nanotechnology*. **2008**, 19, 195712-195719.

90. D. M. Mattox. Handbook of physical vapor deposition (PVD) processing: film formation, adhesion, surface preparation and contamination control. *William Andrew*, **1998**.

91. S. Franssila. Introduction to Microfabrication. *John Wiley and Sons*, **2010**.

92. N. Nath, A. Chilkoti. A colorimetric gold nanoparticle sensor to interrogate biomolecular interactions in real time on a surface. *Analytical Chemistry*. **2002**, 74, 504-509.

93. N. Nath, A. Chilkoti. Label-free biosensing by surface plasmon resonance of nanoparticles on glass: optimization of nanoparticle size. *Analytical Chemistry*. **2004**, 76, 5370-5378.

94. C. Huang, K. Bonroy, G. Reekman, K. Verstreken, L. Lagae, G. Borghs. An on-chip localized surface plasmon resonance-based biosensorfor label-free monitoring of antigen-antibody reaction. *Microelectronic Engineering*. **2009**, 86, 2437-2441.

95. T. Endo, K. Kerman, N. Nagatani, H. M. Hiepa, D.-K. Kim, Y. Yonezawa, K. Nakano, E. Tamiya. Multiple label-free detection of antigen-antibody reaction Using localized surface plasmon resonance-based core−shell structured nanoparticle layer nanochip. *Analytical Chemistry*. **2006**, 78(18), 6465-6475.

96. Y.-B. Shin, J.-M. Lee, M.-R. Park, M.-G. Kim, B. H. Chung, H.-B. Pyo, S. Maeng. Analysis of recombinant protein expression using localized surface plasmon resonance (LSPR). *Biosensors and Bioelectronics*. **2007**, 22, 2301-2307.

97. H. M. Kim, S. M. Jin, S. K. Lee, M.-G. Kim, Y.-B. Shin. Detection of biomolecular binding through enhancement of localized surface plasmon resonance (LSPR) by gold nanoparticles. *Sensors*. **2009**, 9, 2334-2344.

98. M. Vestergaard, K. Kerman, D.-K. Kim, H. M. Hiep, E. Tamiya. Detection of Alzheimer's tau protein using localised surface plasmon resonance-based immunochip. *Talanta*. **2008**, 74, 1038-1042.

99. M. Lahav, A. Vaskevich, I. Rubinstein. Biological sensing using transmission surface plasmon resonance spectroscopy. *Langmuir*. **2004**, 20, 7365-7367.

100. C. Sönnichsen, B. M. Reinhard, J. Liphardt, A, P. Alivisatos. A molecular ruler based on plasmon coupling of single gold and silver nanoparticles. *Nature Biotechnology*. **2005**, 23, 741-745.

101. C. R. Yonzon, E. Jeoung, S. Zou, G. C. Schatz, M. Mrksich, R. P. Van Duyne. A comparative analysis of localized and propagating surface plasmon resonance sensors: the binding of Concanavalin A to a monosaccharide functionalized self-assembled monolayer. *Journal of the American Chemical Society*. **2004**, 126(39), 12669-12676.

102. A. J. Haes, L. Chang, W. L. Klein, R. P. Van Duyne. Detection of a biomarker for Alzheimer's disease from synthetic and clinical samples using a nanoscale optical biosensor. *Journal of the American Chemical Society*. **2005**, 127(7), 2264-2271.

103. A. J. Haes, S. Zou, J. Zhao, G. C. Schatz, R. P. Van Duyne. Localized surface plasmon resonance spectroscopy near molecular resonances. *Journal of the American Chemical Society*. **2006**, 128(33), 10905-10914.

104. W. P. Hall, J. N. Anker, Y. Lin, J. Modica, M. Mrksich, R. P. Van Duyne. A calcium-modulated plasmonic switch. *Journal of the American Chemical Society.* 2008, 130(18), 5836-5837.

105. A. Das, J. Zhao, G. C. Schatz, S. G. Sligar, R. P. Van Duyne. Screening of type I and II drug binding to human cytochrome P450-3A4 in nanodiscs by localized surface plasmon resonance spectroscopy. *Analytical Chemistry*. **2009**, 81(10), 3754-3759.

106. T. A. Bendikov, A. Rabinkov, T. Karakouz, A. Vaskevich, I. Rubinstein. Biological sensing and interface design in gold island film based localized plasmon transducers. *Analytical Chemestry*. **2008**, 80(19), 7487-7498.

107. I. Tokareva, I. Tokarev, S. Minko, E. Hutter, J. H. Fendler. Ultrathin molecularly imprinted polymer sensors employing enhanced transmission surface plasmon resonance spectroscopy. *Chemical Communications*. **2006**, 3343-3345.

108. Y. B. Zheng, Y.-W. Yang, L. Jensen, L. Fang, B. K. Juluri, A. H. Flood, P.l S. Weiss, J. F. Stoddart, T. J. Huang. Active molecular plasmonics: controlling plasmon resonances with molecular switches. *Nano Letters*. **2009**, 9(2), 819-825.

109. T. Endo, K. Kerman, N. Nagatani, Y. Takamura, E.Tamiya. Label-free detection of Peptide Nucleic Acid−DNA hybridization using localized surface plasmon resonance based optical biosensor. *Analytical Chemistry*. **2005**, 77(21), 6976-6984.

110. T. Endo, K. Kerman, N. Nagatani, E. Tamiya. Excitation of localized surface plasmon resonance using a core-shell structured nanoparticle layer substrate and its application for label-free detection of biomolecular interactions. *Journal of Physics: Condensed Matter*. **2007**, 19(21), 215201.

111. D.-K. Kim, K. Kerman, M. Saito, R. R. Sathuluri, T. Endo, S. Yamamura, Y.-S. Kwon, E. Tamiya. Label-free DNA biosensor based on localized surface plasmon resonance coupled with interferometry. *Analytical Chemistry*. **2007**, 79(5), 1855-1864.

112. T. Endo, S. Yamamurab, K. Kermanc, E. Tamiya. Label-free cell-based assay using localized surface plasmon resonance biosensor . *Analytica Chimica Acta*. **2008**, 614(2), 182-189.

113. T. Lai, Q. Hou, H. Yang, X. Luo, M. Xi,. Clinical application of a novel sliver nanoparticles biosensor based on localized surface plasmon resonance for detecting the microalbuminuria. *Acta Biochimica et Biophysica Sinica*. **2010**, 42(11), 787-792.

114. H. Grönbeck, A. Curioni, W. Andreoni. Thiols and disulfides on the Au(111) surface: the headgroup gold interaction. *Journal of American Chemistry Society*. **2000**, 122, 3839-3842.

115. L. H. Dubois, B. R. Zegarski, R. G. Nuzzo. Molecular ordering of organosulfur compounds on Au(111) and Au(100): adsorption from solution and in ultrahigh vacuum. *Journal of Chemical Physics*. **1993**, 98(1), 678-688.

116. F. Schreiber. Structure and growth of self-assembling monolayers. *Progress in Surface Science*. **2000**, 65, 151-257.

117. C. Vericat, M. E. Vela, G. A. Benitez, J. A. Martin Gago, X. Torrelles, R. C. Salvarezza. Surface characterization of sulfur and alkanethiol self-assembled monolayers on Au(111). *Journal of Physics: Condensed Matter*. **2006**, 8, R867-R900.

118. A. Cossaro, R. Mazzarello, R. Rousseau, L. Casalis, A. Verdini, A. Kohlmeyer, L. Floreano, S. Scandolo, A. Morgante, M. L. Klein, G. Scoles. X-ray diffraction and computation yield the structure of alkanethiols on gold(111). *Science*. **2008**, 321, 943-946.

119. M. J. Hostetler, J. E. Wingate, C.-J. Zhong, J. E. Harris, R. W. Vachet, M. R. Clark, J. D. Londono, S. J. Green, J. J. Stokes, G. D. Wignall, G. L. Glish, M. D. Porter, N. D. Evans, R. W. Murray. Alkanethiolate Gold Cluster Molecules with Core Diameters from 1.5 to 5.2 nm: core and monolayer properties as a function of core size. *Langmuir*. **1998**, 14(1), 17-30.

120. R. G. Chapman, E. Ostuni, L. Yan, G. M. Whitesides. Preparation of mixed self-assembled monolayers (SAMs) that resist adsorption of proteins using the reaction of amines with a SAM that presents interchain carboxylic anhydride groups. *Langmuir*. **2000**, 16, 6927-6936.

121. S. Herrwerth, W. Eck, S. Reinhardt, M. Grunze. Factors that determine the protein resistance of oligoether self-assembled monolayers internal hydrophilicity, terminal hydrophilicity, and lateral packing density. *Journal of American Chemistry Society*. **2003**, 125, 9359-9366.

122. M. Mrksich. Using self-assembled monolayers to understand the biomaterials interface. *Current Opinion in Colloid and Interface Science*. **1997**, 2, 83-88.

123. P. Harder, M. Grunze, R. Dahint, G. M. Whitesides, P. E. Laibinis. Molecular conformation in oligo(ethylene glycol)-terminated self-assembled monolayers on gold and silver surfaces determines their ability to resist protein adsorption. *Journal of Physical Chemistry B*. **1998**, 102, 426-436.

124. R. Michel, S. Pasche, M. Textor, D. G. Castner. Influence of PEG architecture on protein adsorption and conformation. *Langmuir*. **2005**, 21, 12327-12332.

125. J. Trmcic-Cvitas, E. Hasan, M. Ramstedt, X. Li, M. A. Cooper, C. Abell, W. T. S. Huck, J. E. Gautrot. Biofunctionalized protein resistant oligo(ethylene glycol)-derived polymer brushes as selective immobilization and sensing platforms. *Biomacromolecules*. **2009**, 10, 2885-2894.

126. P. Kingshott, H. J. Griesser. Surfaces that resist bioadhesion. *Current Opinion in Solid State and Materials Science*. **1999**, 4, 403-412.

127. A. Larsson, B. Liedberg. Poly(ethylene glycol) gradient for biochip development. *Langmuir*. **2007**, 23, 11319-11325.

128. S. S. Shah, M. C. Howland, L.-J. Chen, J. Silangcruz, S. V. Verkhoturov, E. A. Schweikert, N. N. Parikh, A. Revzin. Micropatterning of proteins and mammalian cells on indium tin oxide. *Applied Materials & Interfaces*. **2009**, 1(11), 2592-2601.

129. R. L. C. Wang, H. J. Kreuzer, M. Grunze. Molecular conformation and solvation of oligo(ethylene glycol)-terminated self-assembled monolayers and their resistance to protein adsorption. *Journal of Physical Chemistry B*. **1997**, 101, 9767-9773.

130. J. Turkevich. Colloidal gold. *Gold Bulletin*. **1985**, 18(3), 86-91.

131. J. Homola. Surface plasmon resonance sensors for detection of chemical and biological species. *Chemical Reviews*. **2008**, 108, 462-493.

# Chapter 2

# Plasmonic Materials based on Au Nanoparticles

## 2.1 Introduction

With the aim of fabricating label-free, easy to use, and economically convenient biosensors for bio/organic molecular interactions, we have focused our attention on plasmonic materials and their optical properties.

The recently highly improved ability to fabricate and to study the properties of nanometer size metal particles provided an efficient and inexpensive approach to the fabrication of sensing devises. Nano-sized clusters of noble metals such gold and silver, exhibit unique optical properties: absorption and scattering of incident light, occurring when the photon frequency is resonant with collective oscillations of conduction electrons, results in strong UV-Vis bands. This effect is known as non-propagating or Localized Surface Plasmon Resonance (LSPR) (1). In particular, the energy of the peak extinction, the $\lambda_{max}$, the intensity, and the linewidth of the LSPR spectra are strongly dependent on their size, shape, interparticle spacing, and local dielectric environment (2-4), as described by the Mie theory.

In accord to the Mie's theory (equation (1.3)), the changes of the local dielectric environment lead to changes in the refractive index at the nanoparticles (NPs) surfaces. Therefore, the LSPR is the transducer of a chemical binding and interaction event into on optical signal. Hence, the sensitivity of the LSPR to the presence of adsorbates can provide an effective and easy route for monitoring in real time the binding of molecules or molecular interactions occurring at the nanoparticles surface.

Metal nanoparticles deposited on a transparent support results to be a promising plasmonic material, under the condition that their morphology is stable so that the LSPR band features are well set.

The main problem in using metal nanoparticles deposited on a transparent support as plasmonic material for biorecognition purposes is related to the degree of adhesion of the metal nanoparticles on the transparent surfaces (mainly quartz and glass), and the stability of the

metal nanoparticles (5-6). These problems are particularly severs for fabricating a sensor of biological interest, since the biochemical processes occurs in aqueous solutions.

The stability is related both to the *adhesion properties* of the NPs to solid surfaces and to the *restructuration processes* of the metal surface. These phenomena are responsible for large and difficult-to-control variations of their optical properties, and specifically of the LSPR bands feature (7).

The widely used approach for increasing the adhesion of Au based on pre-deposition of Ti and Ni layers would requires expensive apparatuses like electron beam evaporator. On the other hand, the more accessible deposition of Cr inter-layers (8) can affect and attenuate the response because of Cr diffusion into the Au NPs (9-11). In addition, the adhesion layers are known to block the plasmon resonance phenomena and to broaden the plasmon resonance band (12).

The relevance of the NPs stability problem is well represented by the large number of studies suggesting different approaches to reach "stable" metal NPs. A useful approach to increase the adhesion of the NPs to the surface is based on precoating the glass or quartz surfaces with an organic adhesive monolayer terminating with a thiol group, such as 3-mercaptopropyl-tri-methoxysilane (MPTS). Layers of mercapto-silane have been used for improving the adhesion of NPs to glass (13-14). Van Duyne reported structural changes of Ag NPs in organic solvents, and faced the restructuration problem by solvent preconditioning prior to the NPs functionalization (15). This procedure could be suitable for certain studies, but inappropriate for most biological applications. Rubinstein has proposed two different approaches: i) to coat Au NPs by a robust and transparent layer of ultra thin films of silica (16), or ii) to sink Au NPs into the glass by a controlled thermal treatment (17). This last method is a simple, one-step procedure for achieving stable and strongly-bonded Au particles film on glass substrates, consisting in high-temperature annealing close to the glass transition temperature $T_g$. This method allows for the preparation of a plasmonic material by using glass substrates, but is not easily applicable on quartz substrate, which is well known to enable a large range of optical monitoring. Stable Au nanorods and Au NPs were obtained by embedding them respectively into glass (18), and into an $Al_2O_3$ matrix (19).

An enhanced adhesion of Au NPs at rough surfaces has been reported when ITO (indium-doped tin oxide) is used as support (20). We stress that, besides the high cost of ITO substrates, the diffusion of indium at the interface could preclude the right functioning of ITO-based sensor (21-23).

In this chapter we describe a number of approaches we have adopted in order to obtain stable NPs.

The first approach was based on using, as transparent surfaces, glass and quartz slides. To improve the adhesion of the deposited NPs we have anchored the NPs to the surfaces by using an organic adhesion layer of 3-mercaptopropyl-tri-methoxysilane, on quartz surface.

In the second approach we have used a procedure reported by Rubistein's (17) based on embedding gold NPs onto glass surfaces. We performed the tests in different media, in particular in aqueous buffer solution used normally in biology.

The third approach is based on the use as transparent substrate commercially available surfaces of Fluorine Tin Oxide (FTO). The rational of this choice is based on the porosity of $SnO_2$ where gold can penetrate during thermal annealing and enhance the adhesion of Au onto FTO substrates (24-26). We report a study on the stability of these NPs evaporated on FTO when immersed in different media, in particular: water aqueous buffers solutions as sodium chloride-Tris-EDTA (STE) and phosphate-buffered saline (PBS) solutions; ethanol, as one of the most common solvent used for self assembled monolayers (SAMs) formation (27).

## 2.2 Materials and Methods

### Materials

3-mercaptopropyl-tri-methoxysilane (MPTS) (Sigma Aldrich), 1-dodecanthiol (DT) (Fluka), and 6-mercapto-1-hexanol (MCH) (Sigma Aldrich). Dimethyl sulfoxide (DMSO) (Sigma Aldrich), sulfuric acid, hydrogen peroxide, chloridric acid, nitric acid and ethanol (Fluka), acetone and 2-propanol (Sigma Aldrich). STE buffer (10 mM Tris-HCl pH 8.00, 1 mM EDTA pH 8.00, 1 M NaCl) was purchased from Sigma Aldrich, and phosphate-buffered saline (PBS) solutions from Lonza Walkersville Inc. (Walkersville, MD). The glass microscope slides D 263 T were purchased from Schott AG (Mainz, Germany), the quartz slides were purchased from Chemglass (Vineland, NJ), and the Fluorine Tin Oxide (FTO) (TEC 8) surfaces were purchased from Pilkington North America Inc. (Toledo, OH).

### Au NPs fabrication

*First approach*. On clean glass microscope slides, 5 nm of nominal thickness of gold was evaporated by a thermal evaporator at deposition rate of 0.008 nm $s^{-1}$. The NPs were thermal annealed at 350°C for 2 hours.

The clean quartz slides were treated according to the description reported in literature (13) for the silanization process. In this case, the gold nanoparticles were formed by using a thermal evaporator, at a pressure of $10^{-6}$ mB and at deposition rate of 0.0017 nm $s^{-1}$.

The nominal thickness was controlled by a built-in system consisting of a quartz crystal mechanically oscillating at its natural resonance frequency (6 MHz). Finally, the samples were annealed in oven for 2 hours to 200°C of temperature.

*Second approach.* The glass microscope slides were treated with Piranha solution (sulphuric acid and hydrogen peroxide 30% in ratio of 3:1) for 30 minutes, and then, rinsed copiously with MilliQ water. The Au NPs were formed by thermal evaporation of a nominal thickness of 5 nm of gold with a rate deposition of 0.005 nm $s^{-1}$. The samples were immediately placed in the oven for the annealing treatment at 562°C of temperature for 10 hours. Some samples, were subsequently cleaned with aqua regia (nitric acid and chloride acid in ratio 1:3).

*Third approach.* The FTO surfaces were cleaned by a solution 1:1 of acetone and 2-propanol in ultrasounds bath for 15 minutes, then repeatedly rinsed with copious amounts of water MilliQ and lastly dried with a pure nitrogen stream. The gold nanoparticles were deposited on the FTO

surfaces by thermal evaporation at deposition rate of 0.0016 nm $s^{-1}$. The deposition process of NPs is controlled by measuring a nominal thickness of 5nm with a built-in quartz balance. The samples were then annealed for 10 hours at to 200°C.

**Characterization methods**

The UV-Vis measurements were carried out by using a Jasco V-570 UV-Vis-NIR spectrophotometer in transmittance mode by placing the samples into the spectrophotometer cavity (scan speed 200 nm/min, band width 1 nm). All the spectra were recorded in air and by using air as reference. A series of measurements performed by repetitive removing and replacing the same sample into the spectrophotometer cavity showed an error in $\lambda_{max}$ values of 1 nm.

Atomic Force Microscope (AFM) measurements were performed in non contact mode using a Nanoscope IIIa - Digital Instruments.

The Au NPs/FTO images were obtained using a Scanning Electron Microscopy (SEM FEI XLF30-SFEG of FEI Company Eindhoven) equipped with ultra high resolution lens and in-lens SE (secondary-electron) detector.

**Stabilization of Au NPs**

Incubation of Au NPs on glass surface was carried in the MilliQ water, while incubation of the Au NPs on quartz surface were carried in both water and STE buffer solution for several hours. Incubation of Au NPs on FTO surface performed by immersion in different media: H2O, STE buffer, PBS buffer and ethanol, for 24 hours. Then the samples were rinsed with water MilliQ or ethanol and dried with pure nitrogen. LSPR spectra were recorded before and after immersion in the various media.

**Functionalization with organic molecules**

Self-assembled monolayer (SAM) of 1-dodecanthiol (DT) was prepared by incubating the samples into a 10 mM solution of DT in ethanol for 24 hours. The 6-mercapto-1-hexanol (MCH) SAM was obtained incubating the samples into a 10 mM solution of MCH in MilliQ water for 24 hours. All SAMs was rinsed with ethanol or MilliQ water and drying under nitrogen stream.

## 2.3 Results and Discussion

### *2.3.1 Au NPs onto glass and quartz surfaces*

***Deposition and Adhesion of Au NPs on glass surface***

To test the degree of adhesion of Au NPs on glass surface, we have incubated the samples in water for 1 hour. After incubation, we have washed and dried the samples. In Figure 1 are reported the spectra UV-Vis in transmittance mode of gold nanoparticles taken in air before and after incubation.

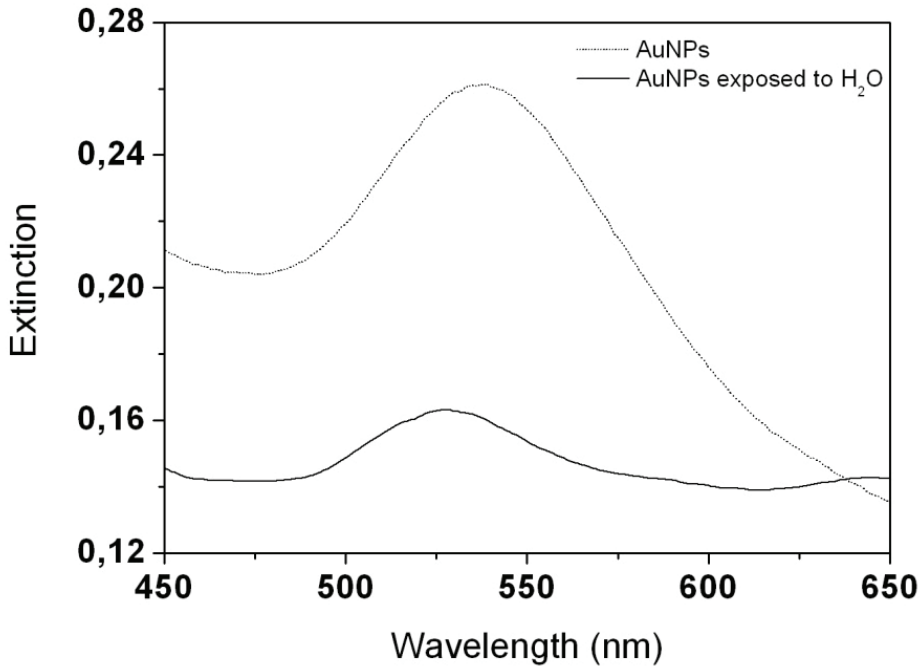


**Figure 1.** Spectra of Au NPs (short dot) and the Au NPs after incubation with water (solid)

The LSPR band of Au NPs shows large changes after incubation in water: the absorbance value has decreased dramatically and the maximum wavelength is shifted toward the blue. This result, in agreement with the literature, indicates that the Au NPs deposited by thermal evaporation on glass are poorly adhesive (8,14,28).

***Deposition and Adhesion of Au NPs on quartz surface***

A further attempt was based on using quartz slides as different substrate; the use of this substrate is reported in literature to be convenient for the preparation of plasmonic material (29-31).

In Figure 2 are reported the AFM images of the Au NPs deposited on quartz surface before (Figure 2A) and after (Figure 2B) over night incubation of the sample in STE buffer solutions, a medium typically used in biology. The Au NPs show a different morphology before and after STE incubation. The STE buffer seems to induce a reorganization of the gold atoms of NPs.

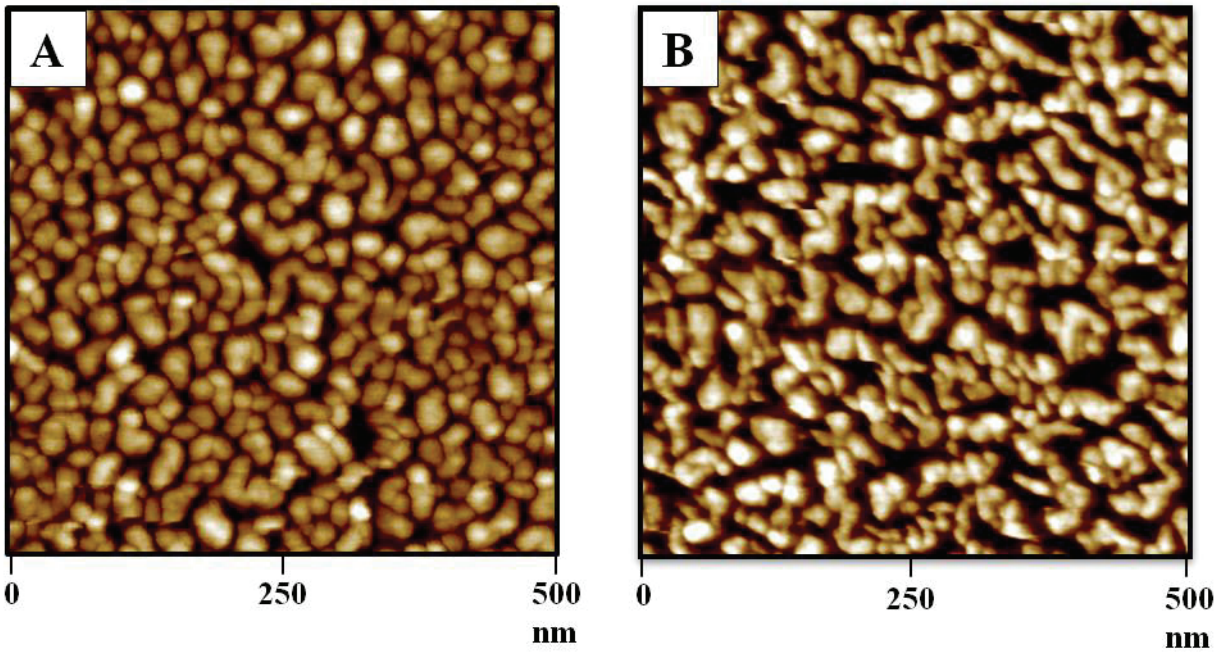


**Figure 2.** AFM images of not annealed Au NPs deposited on quartz surfaces, before (**A**) and after (**B**) incubation in aqueous buffer solution STE.

Figure 3 shows the spectra of Au NPs on quartz, incubated both in water and in STE buffer for several hours. After each incubation, the absorbance value decreases, and the SP band widens. The dramatic changes of the features of the SP band indicate a poor adhesion of the Au NPs when deposited on quartz.

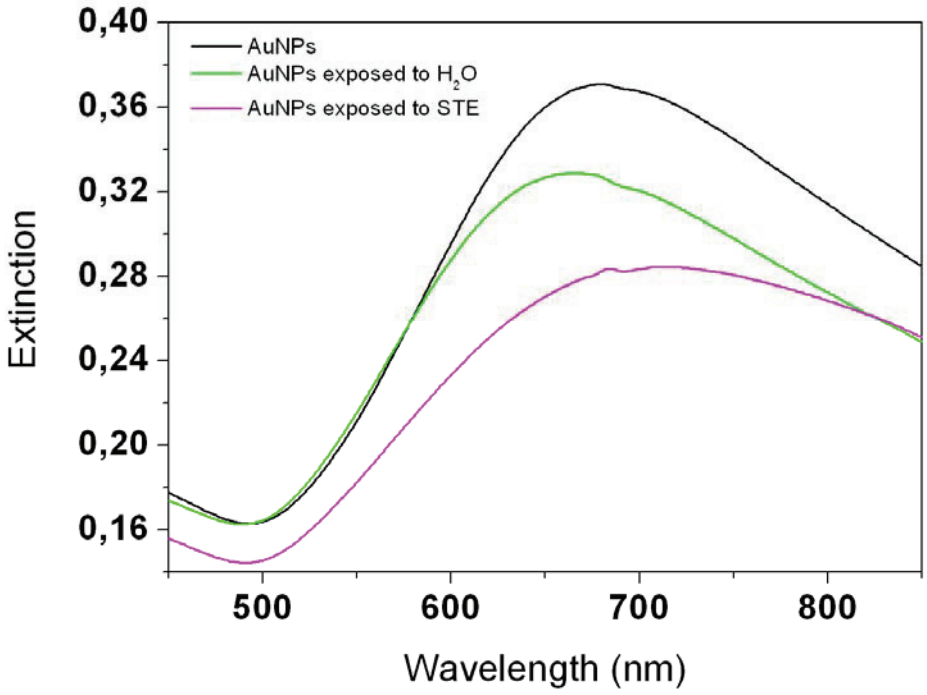


**Figure 3.** Spectra of Au NPs deposited on quartz and after incubation with water and STE buffer.

Despite positive examples reported in literature on the good adhesion of Au NPs deposited on quartz surface, we obtain negative results similar to those obtained on glass. The poor adhesion of Au NPs causes changes in the SP bands.

***Deposition of Au NPs on silanized quartz surface***

For increasing the adhesion, we have functionalized the quartz surface with 3-mercaptopropyl-tri-methoxysilane (MPTS) (13). This approach involves a chemical modification of the quartz surface by a covalent bond of the silane moieties of the MPTS, while the terminal thiol groups can provide a strong binding to the evaporated gold atoms.

Figure 4 shows the AFM topographic images of gold NPs under deposition of nominal thickness of 3 nm onto (A) not silanized and (B) silanized quartz slides, while (C) shows corresponding UV-Vis absorption spectra.

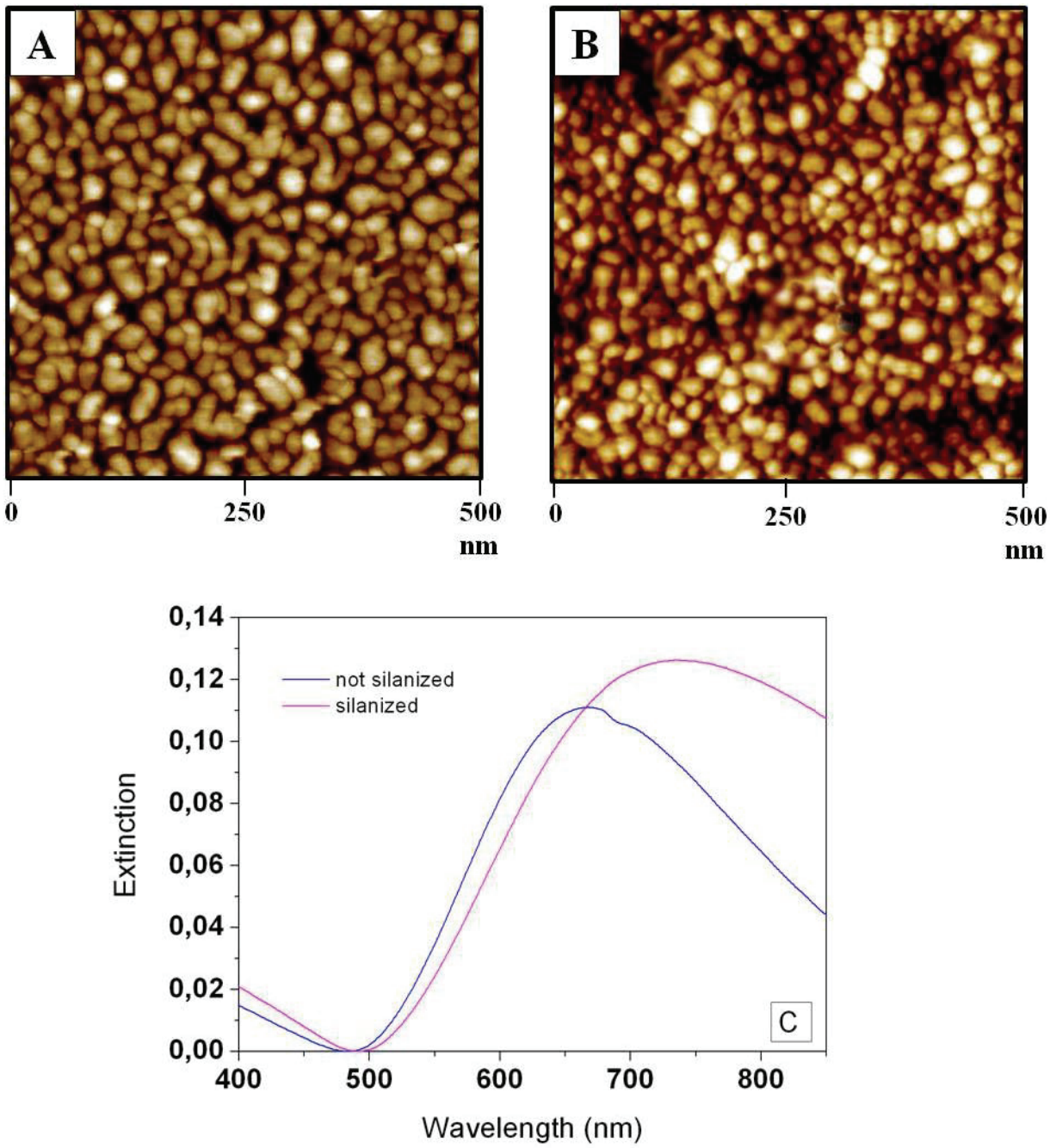


**Figure 4.** AFM image (10 nm z-scale) of 3 nm Au thin film deposited onto (**A**) not silanized and (**B**) silanized quartz slides and (**C**) the corresponding UV-Vis spectra detected in air.

Even if it is difficult to estimate the difference in particles separation, due to AFM tip convolution (14), the comparison of Figures 4A and 4B shows that gold nanoparticles evaporated onto MPTS-treated surfaces have a more rounded shape.

Interestingly, the presence of the MPTS on the quartz surface, has a great influence on the morphology of the Au NPs (Figures 4A and 4B), as reflected by the respective optical properties (Figure 4C).

Figure 5 reports the SP band absorption of NPs prepared by evaporating on silanized quartz three different nominal thicknesses, 1.5, 2, 3 nm.

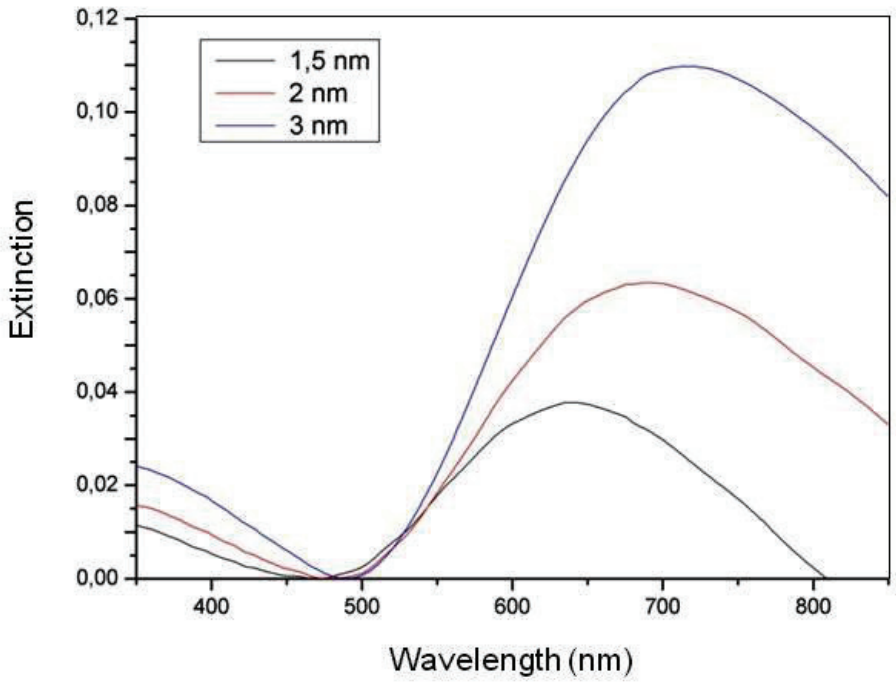


**Figure 5.** Detection of SP bands absorption of samples, measured in transmittance mode after evaporation, of different nominal thickness (1.5, 2, 3 nm) of Au deposited on silanized quartz.

The spectra show well defined peaks with maximum shifting from ~ 630 to 730 nm for increasing size, accompanied by a constant increase in peak intensity (Figure 5). For greater thickness values, the plasmon band become very broad, making difficult the identification of the peak maximum (not shown). It is well known that the energy position of the SP band depends on the size, shape and kind of metal of the NPs (3) and the interparticle distance (2,4). The progressive red-shift of the absorption maximum of the plasmon band to longer wavelength, is the result of increasing the aspect ratio (*a/b* where *a* is height and *b* is width) (2).

***Stabilization of Au NPs on silanized quartz surface by Solvent Annealing***

Measurements of the LSPR bands show marked changes of in energy and features, as function of the environment in which the sample is kept. We have found that, even the air humidity has an important effect on the optical properties of the samples. SP bands of 3 nm thick samples (chosen as representative ones), show a blue-shift when kept in air and a red-shift when kept overnight under vacuum (not shown).

The annealing solvent effects have been studied on 3 nm of nominal thickness Au NPs under overnight immersion in STE buffer. In particular, Figures 6A and 6B show AFM measurements respectively before and after the incubation. The red and blue curves of Figure 6C are the corresponding spectra of these samples. We observe that, after incubation process, the average particle height slightly increase, and the size of NPs decreases. The SP band of the incubated sample, exhibits a blue shift of 30 nm accompanied by an intensity decrease.

Figures 6 demonstrate the effects on the LSPR induced by STE solvent annealing. These solvent effects have been reported in literature (15,32): the dominant factor in solvent-induced nanoparticles reconstruction is likely to be related to the strong decrease in surface tension at to interface between the hydrophilic surface and the solvent.

We have also tested a possible correlation between the NPs stability (λ max shift) and their sizes ($\lambda_{max}$ value). Figure 7 reports the λ max shift as function of $\lambda_{max}$: the results indicate a larger blue shift measured for larger λ of the maximum SP band, with a qualitative trend.

The results reported in Figure 7 suggest that morphological changes induced by STE are larger for larger particles average diameter.

The solvent annealing process is a methodology used by Van Duyne's group for stabilizing the NPs evaporated on glass surface and for facing the restructuration problem by solvent preconditioning prior to the NPs functionalization (15). In our case, under further immersion in the solvent, we have observed additional changes of the LSPR band (not shown). Therefore, this approach shows certainly an improved adhesion, but the optical response of the Au NPs remains too sensitive to further solvent immersion, even after solvent stabilization/annealing process.

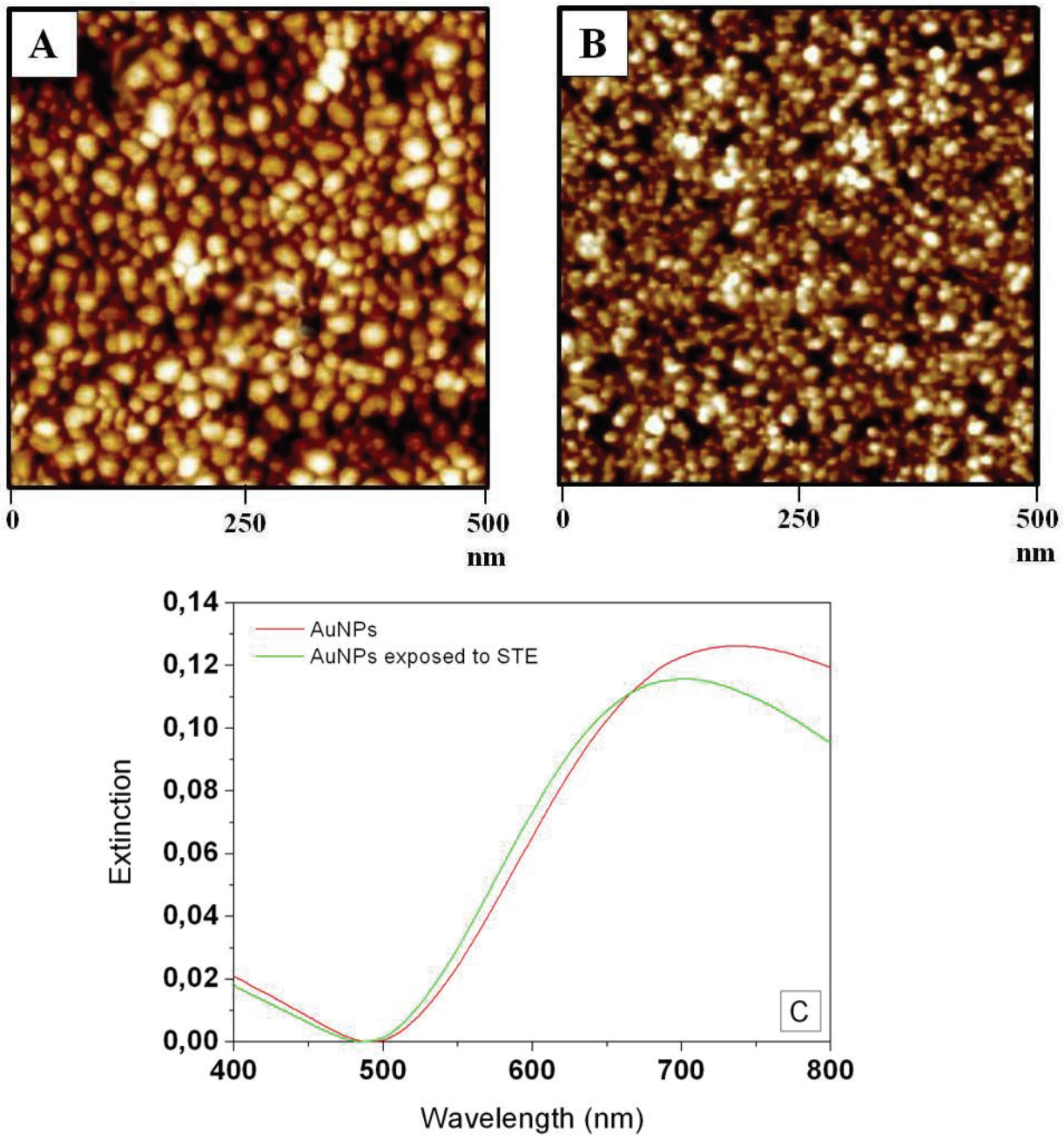


**Figure 6.** AFM topographic images (10 nm z-scale) of 3 nm Au thin film deposited onto silanized quartz slides (**A**) before and (**B**) after STE buffer incubation and (**C**) corresponding UV-Vis absorption spectra registered in air.

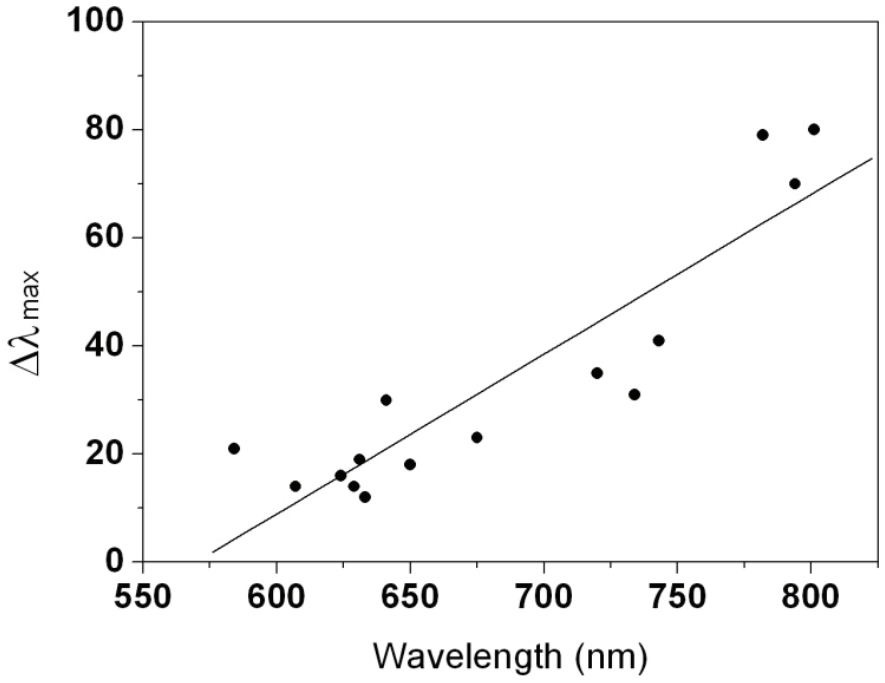


**Figure 7.** Qualitative dependence of the blue-shift induced by STE stabilization for silanized quartz samples of different $\lambda_{max}$ of the SP band initial position (different size). The line is a guide to the eye.

***Stabilization of Au NPs on silanized quartz surface by Thermal Annealing***

Could the thermal annealing improve the NPs stability?

To answer this question we have evaporated 3 nm of gold on silanized quartz surface, annealed, and then incubated the annealed sample in STE buffer.

Figure 8 reports the optical properties of Au NPs i) just evaporated, ii) thermally annealed, and iii) annealed and exposed to STE buffer.

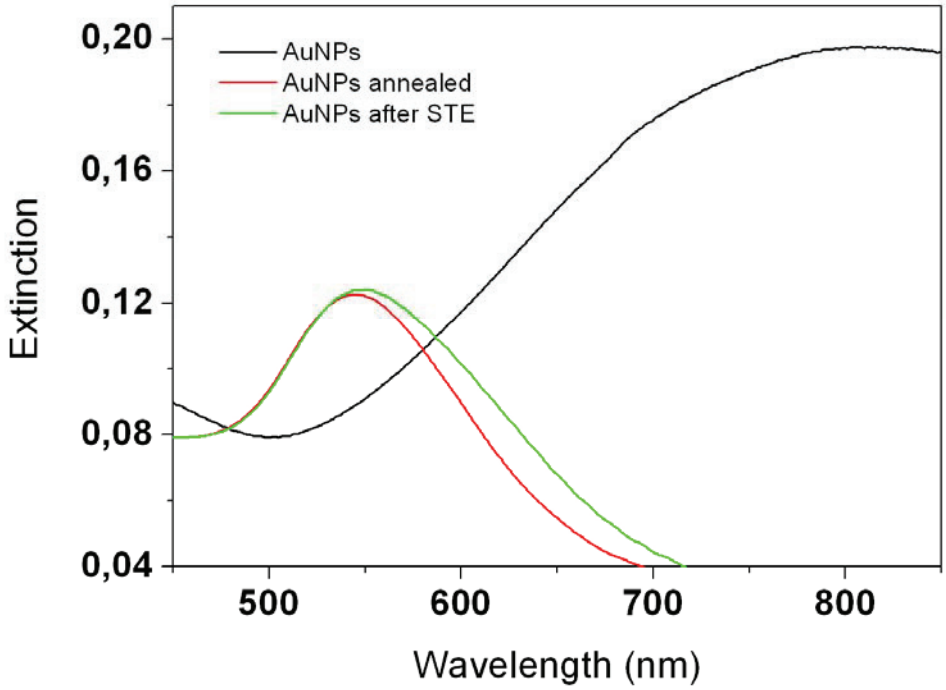


**Figure 8.** UV-Vis absorption spectra of 3 nm Au NP deposited onto silanized quartz slides in air (*black*), annealed at 200°C for 2 hours (*red*) and after STE incubation (*green*).

We observe a large LSPR $\lambda_{max}$ blue shift (258 nm) of the NPs under thermal annealing. This LSPR shift is in agreement with that observed by Van Duyne's group for annealed silver NPs on glass surface (2). The blue shift of the thermal annealing process has been well studied (2,6,31,33-34) and it is caused by a structural transition of Au NPs. It has reported that that

changes in the aspect ratio (height/diameter) results in a change in the LSPR oscillation frequency. When the aspect ratio of NPs decrease or increase respectively a blue shift or a red shift of SP band can be observed. The interparticle spacing is an additional factor that can contribute to SP band blue shift. In fact, the annealing process leads the coalescence of small particles into larger ones, increasing then the space between the NPs and therefore decoupling of surface plamons. In spatially closer NPs, the oscillation of conduction electrons of each NP is affected by a coupling with the nearest neighbour (2,4). A description of the process occurring during the thermal annealing can be the following: a few nanometers thick gold film deposited on glass substrate is polycrystalline in nature with deformed grainy structures. This film under the first annealing step nucleates to form discontinuous and irregular NPs; under prolonged annealing, the NPs grow in shape to give a more ordered structure. This transformation is governed by the surface energies at each interface (33).

Figure 8 shows also the SP band difference between the sample before and after incubation in STE buffer. The LSPR $\lambda_{max}$ is red shifted of 6 nm, and the shape of SP band has slightly changed.

***Functionalization of thermal annealed Au NPs on silanized quartz surfaces***

In order to test if these NPs are suitable as plasmonic materials for a biosensor, we tested the response under functionalization of the samples with organic SAMs. We have functionalized the thermal annealed sample with a self-assembled monolayer of 1-dodecanethiol (DT).

Figure 9 shows the SP bands measured in air before and after functionalization with DT SAMs. For a convenient comparison of the SP band features, we have reported the results obtained for different steps (annealed, STE incubation and SAMs).

Figure 9 reports a $\Delta\lambda_{max}$ of 26 nm toward the red region and an increase of the absorbance value under functionalization of Au NPs. In this case, the red shift of SP band is in agreement with literature data. The result indicates that the Au NPs annealed on silanized quartz surface are sensitivity to organic molecular layer. Nonetheless the SP band shape of the Au NPs functionalized with DT SAMs shows a too large increase in width, respect to the original. This result indicates that the modification of the SP band cannot be attributed exclusively to the SAMs formation.

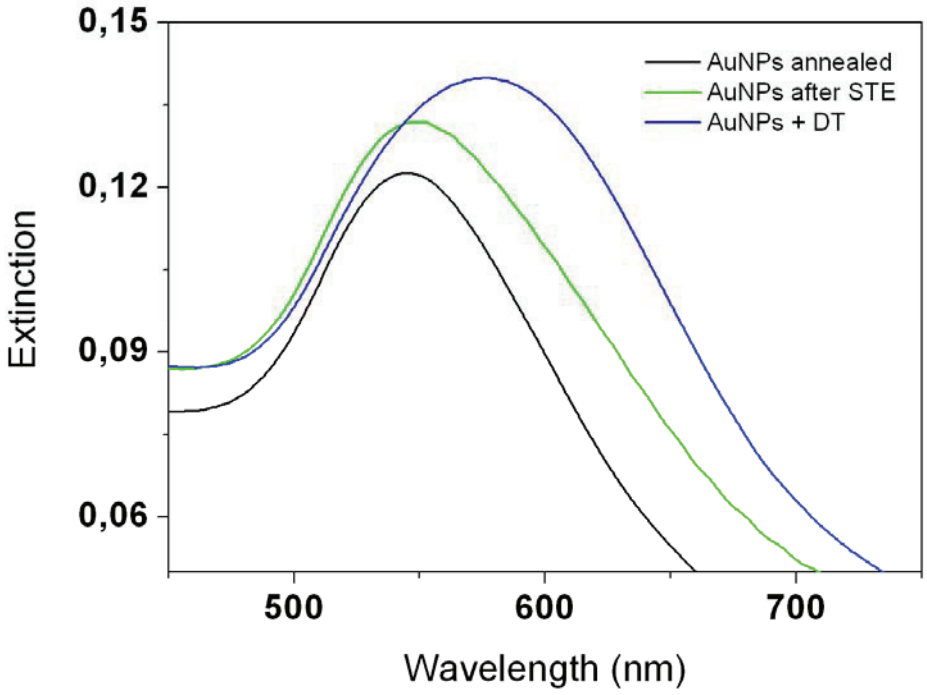


**Figure 9.** UV-Vis absorption spectra registered in air of Au NPs thermal annealed onto silanized quartz (*black*), after STE stabilization (*red*) and after DT SAM formation (*green*).

On the basis of these results, the Au NPs obtained according to this procedure cannot be considered a good plasmonic material for a biosensor. In fact, the biosensors require the use of aqueous solutions and the plasmonic material must be stable after several hours in these media. In conclusion, *the organic adhesion layers do not provides to the Au NPs the necessary stability*.

Other groups (17) have abandoned this approach for embracing new methods to obtain stable Au NPs.

### *2.3.2 Au NPs embedded on glass surface*

It is clear that the changes in the optical properties of Au NPs resulting from morphological changes induced by exposure to solvents and analytes, drying, etc., introduce uncertainty in interpreting the experimental data based on refractive index changes.

Rubinstein's group has presented a new procedure for obtaining morphologically stable Au NPs strongly bonded to glass substrates (17). We have followed the Rubistein's approach (see Materials and Methods), which is based on a thermal annealing treatment at temperature near the transition glass temperature, *Tg*. In our case the transition glass temperature of the glass slides was 567°C, and various tests have indicated that the optimal annealing occurs at 562°C.

In Figure 10 are represented the AFM images in plane and in 3D of Au NPs samples before and after the thermal annealing process. Figure 11 reports the respective LSPR optical properties. We observe that for a large number of NPs their height move from ~ 1 nm to 6-11 nm, and their width from 50-55 nm to 100-115 under annealing. The effect of the annealing process on Au NP morphology is evident: there is a coalescence process of many, small NPs in some larger ones. The image also show some bigger NPs (10 nm) as evidence of an inhomogeneous gold film.

From Figure 11 is evident a $\lambda_{max}$ blue shift of 188 nm related to the increase of the aspect ratio. It is know that the drastic film reshaping is practically complete in the first few minutes of annealing, while the embedding process (possibly accompanied by subtle morphological changes) takes hours (17).

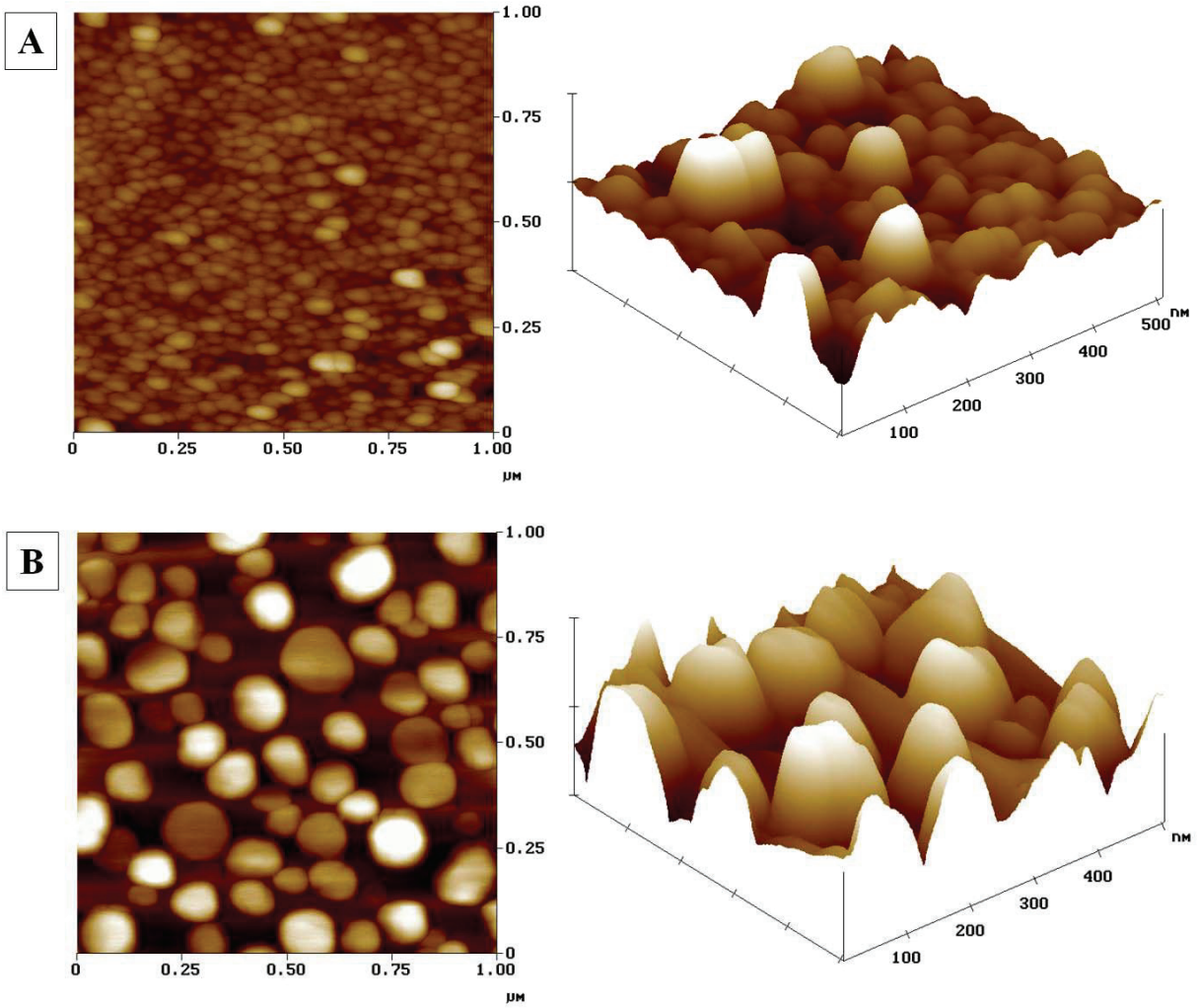


**Figure 10.** AFM topographic images in planes (x-y axis 1μm and z axis 30 nm) and in 3D (x-y axis 500 nm and z axis 20 nm) of 10 nm Au thin film deposited onto glass slides (**A**) before and (**B**) after thermal annealing treatment to 562°C for 10 hours.

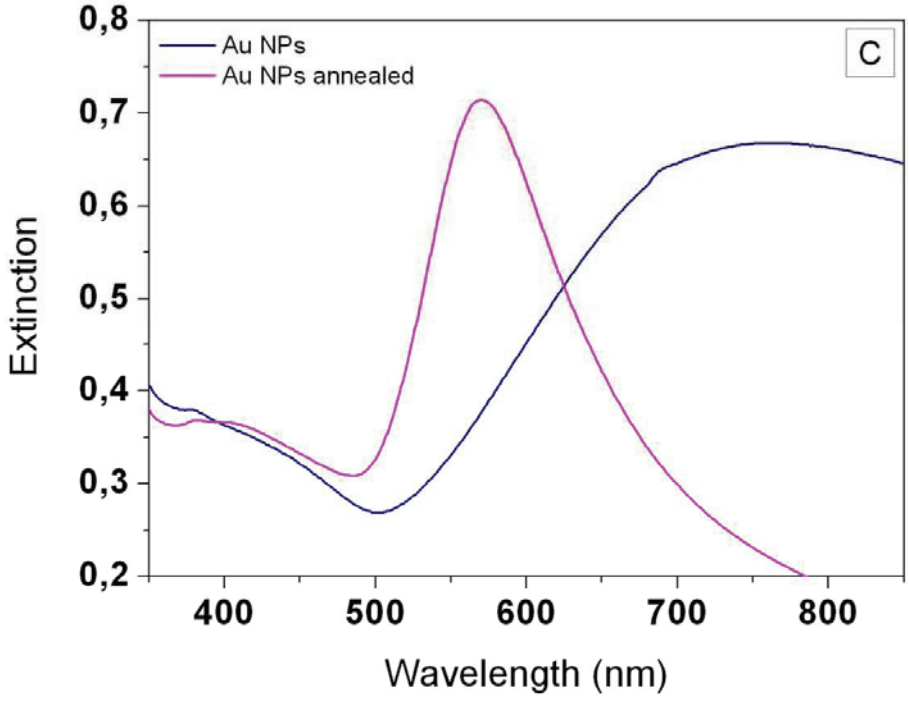


**Figure 11.** UV-Vis absorption spectra registered in air of Au NPs evaporated on glass slide (*blue navy*), and after Au NPs thermal annealed to (*magenta*).

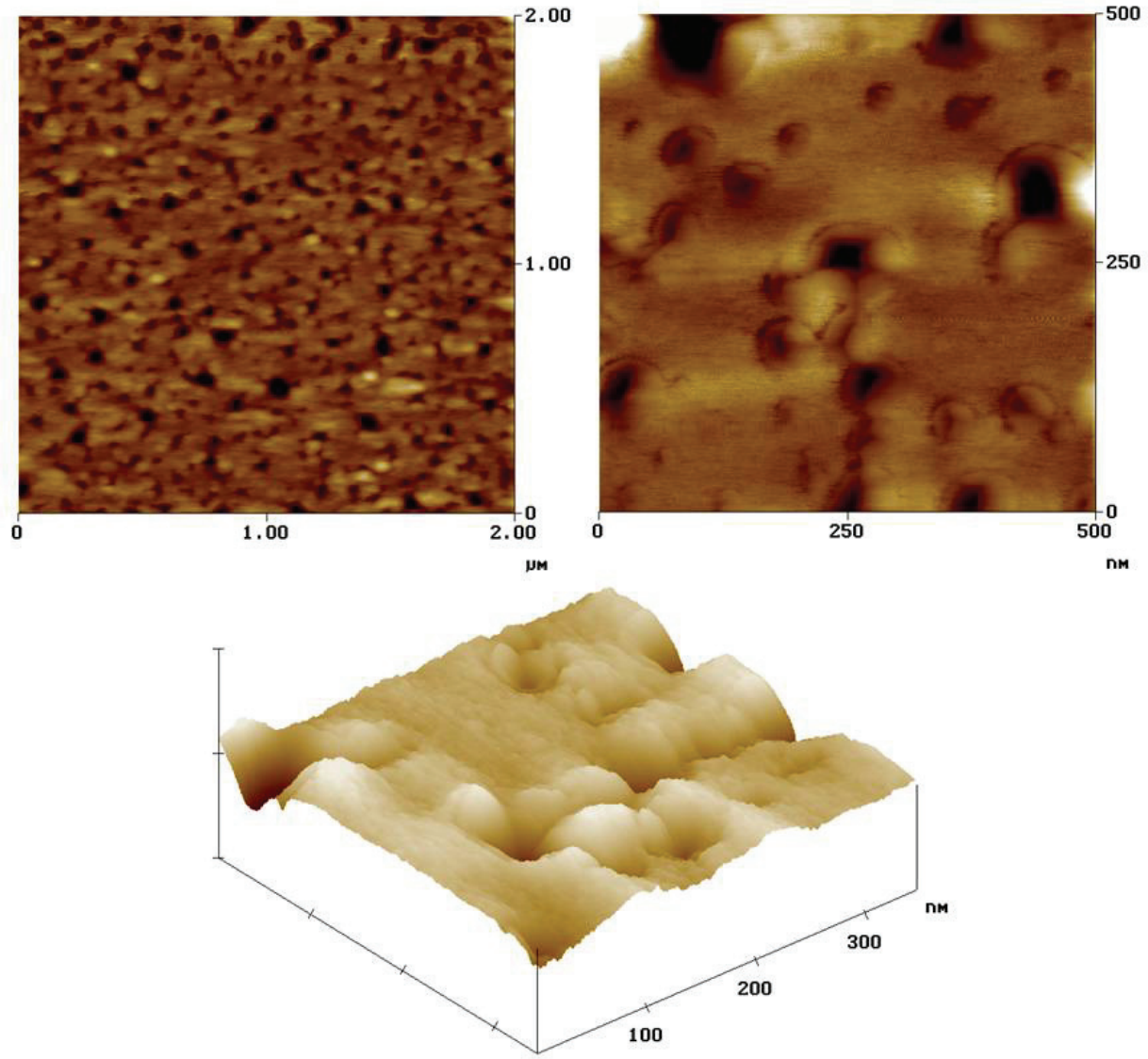


**Figure 12.** AFM topographic images in planes (x-y axis 2μm and z axis 30; x-y axis nm500 nm and 20 nm) and in 3D (x-y axis 350 nm and z axis 20 nm) of glass slides cleaned from the Au NPs after its thermal annealing treatment to 562°C for 10 hours.

The detailed morphology of the glass surface after the embedding treatment was studied by dissolution of the metal NPs in aqua regia.

In Figure 12 are reported the AFM images of a glass substrate after removal of the metal nanoparticles; numerous holes of different dimensions (from 100 nm to few nanometer of width and from 25 nm to few nanometer of depth) are evident on the surface. In the 3D figure, we note an increase of the glass thickness on the hole outline. On these bases, we can define the process as thermal embedding of Au NPs into the glass substrate. This procedure leads to a drastic enhancement of adhesion between Au NPs and the glass substrate.

The Rubistein's group has demonstrated that Au NPs on cover-glass annealed 10 h at 550 °C showed the same embedding pattern. Although the driving force and mechanism of the partial thermal embedding of Au particles into glass are not entirely clear, the experimental evidence suggests that i) the embedding process occurs in the vicinity of the glass transition of the substrate, ii) there is no gravitational effect, and iii) the presence of an oxidative atmosphere (oxygen) is required (17).

After the fabrication of the partially embedded Au nanoparticles, we have tested their stability towards aqueous solutions and solvents, as previously done with the Au NPs on quartz.

In Figure 13 are reported the UV-Vis spectra of the samples before and after incubation in different media for several hours as indicated on graphs: STE buffer (Figure 13A), MiliQ water (Figure 13B) and ethanol (Figure 13C).

From Figure 13A it is evident a $\lambda_{max}$ blue shift and an absorbance decrease already after 2 hours and thirty minutes incubation, while the Figures 13B and 13C show unchanged SP bands. The results show *a good stability of Au NPs when immersed on MilliQ water and ethanol, but non-stability in STE buffer*.

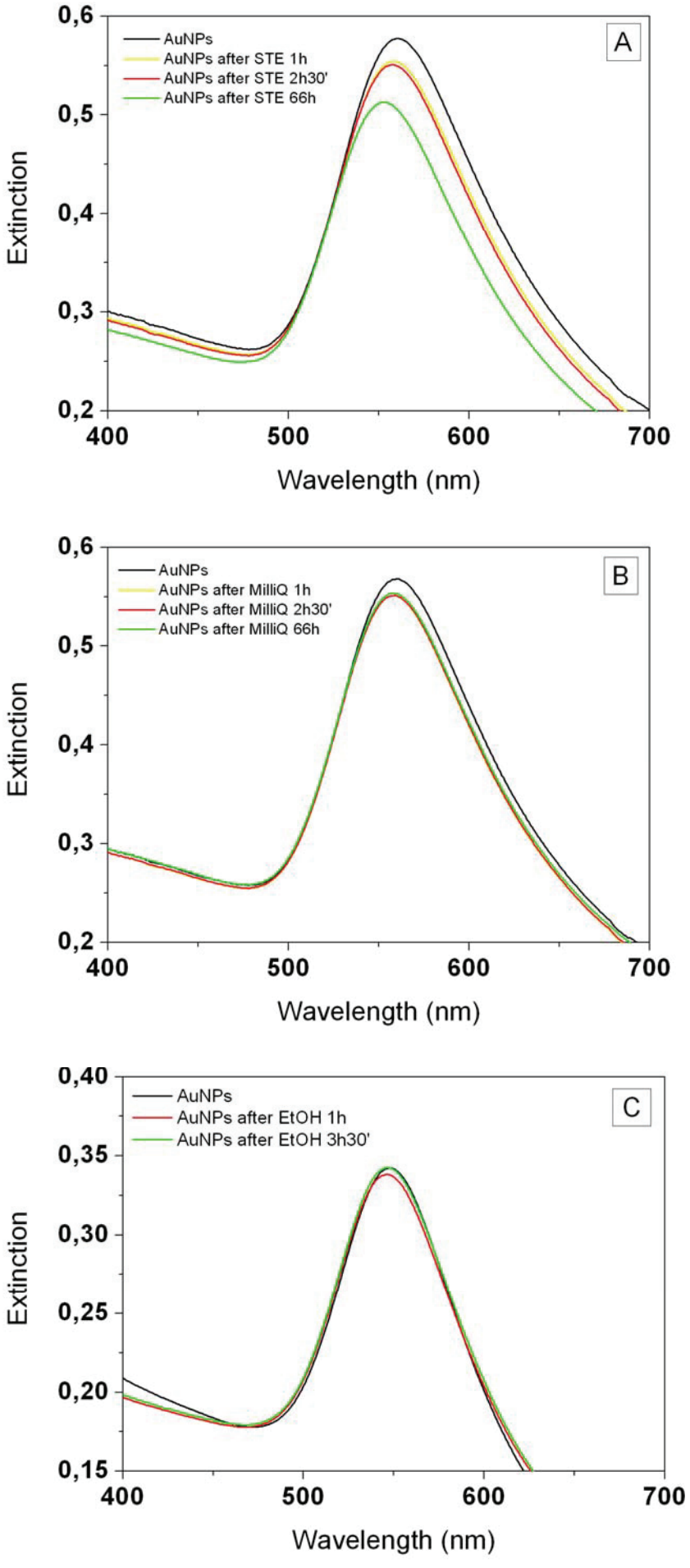


**Figure 13.** UV-Vis absorption spectra registered in air of (**A**) silanized Au NPs quartz (*black*),

after 1 h (*yellow*), 2 h 30 minutes (*red*), and 66 h (*green*) of STE. (**B**) silanized Au NPs (*black*), after 1 h (*yellow*), 2 h 30 minutes (*red*), and 66 h (*green*) of MilliQ water incubation. (**C**) silanized Au NPs (*black*), after 1 (*red*), and 3 h 30 minutes (*green*) of Ethanol incubation.

***Functionalization of Au NPs***

The stability of the embedded Au NPs both in water and ethanol has encouraged a test of their plasmonic response under functionalization. The samples are incubated for 24 hours in two different solutions: the 1-dodecanethiol (DT) in ethanol and the 6-mercapto-1-hexanol (MCH) in MilliQ water. In Figure 14 are reported the spectra of the respective samples taken in air.

The results of both organic incubations were surprising. The Figure 14A shows that the SP band after the DT SAM formation shifts towards the red region of 1 nm only. An analogous result is shown in Figure 14B, where after the MCH SAM formation the SP band does not shift in any direction. Both results have been confirmed by repeated experiments, with new products and different organic molecules. The results are in disagreement with both the literature (15) and the theory; in fact, when the molecules binding the NPs surface is expected to change the refractive index of the surrounding media and therefore the LSPR band features. In conclusion, these stable Au NPs seem to be unresponsive to functionalization.

This failure addressed our attention in a different direction as a search of a different substrate.

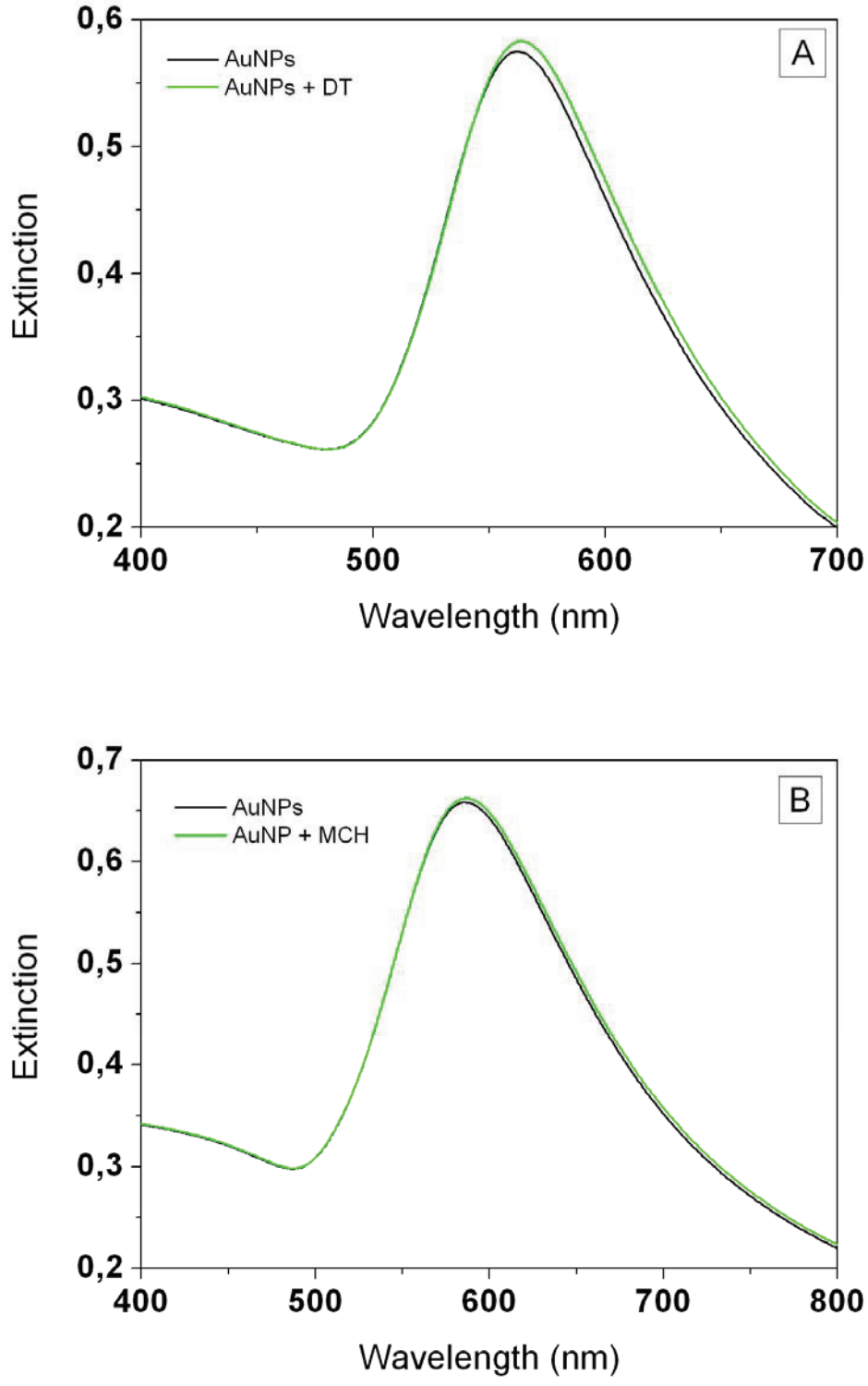


**Figure 14.** UV-Vis absorption spectra registered in air of (**A**) naked Au NPs (*black*) and Au NPs with 1-dodecanethiol (DT) SAM (*green*), and **(B**) naked Au NPs (*black*), and Au NPs with 6-mercapto-1-hexanol (MCH) SAM (*green*).

### *2.3.3 Au NPs deposited on FTO surface*

In search of a new substrate, we selected commercially available FTO. Figure 15 reports the SEM image of FTO surfaces.

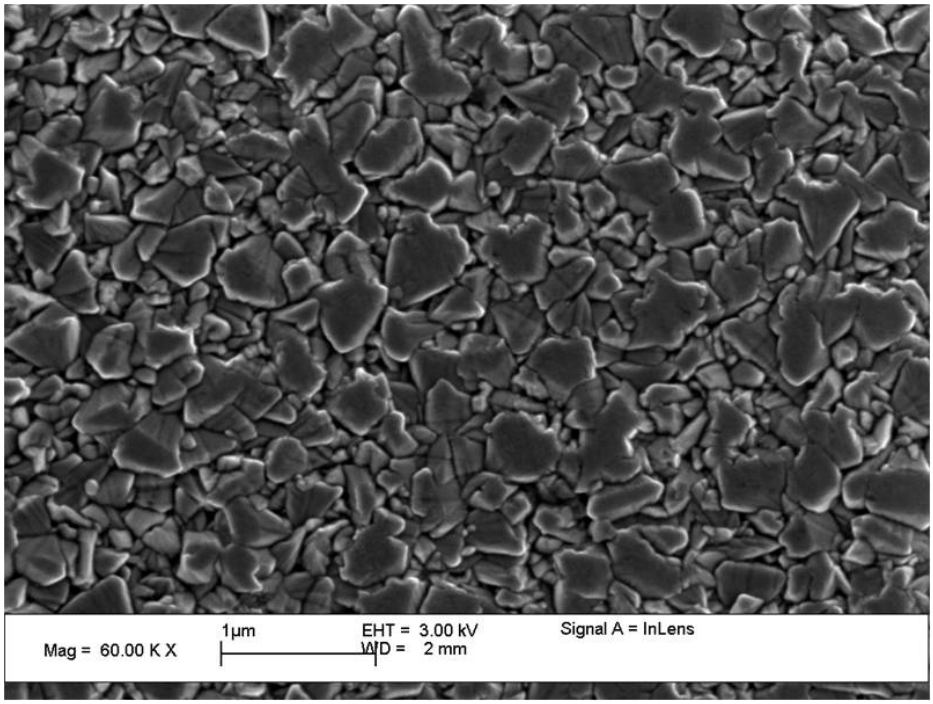


**Figure 15.** SEM image of naked FTO substrate.

Figures 16A and 16B report the SEM images of the Au NPs obtained by depositing Au respectively before and after the annealing process. Figure 17 shows the respective LSPR bands. The annealing process of NPs deposited on quartz or glass leads to a sharper LSPR band, with a $\lambda_{max}$ shift towards the blue, according to literature data, indicating that the aspect ratio (*a/b*, where *a* is height and *b* is width) decreases (35). Therefore the annealing process results to be a key step also for the fabrication of the plasmonic material on FTO.

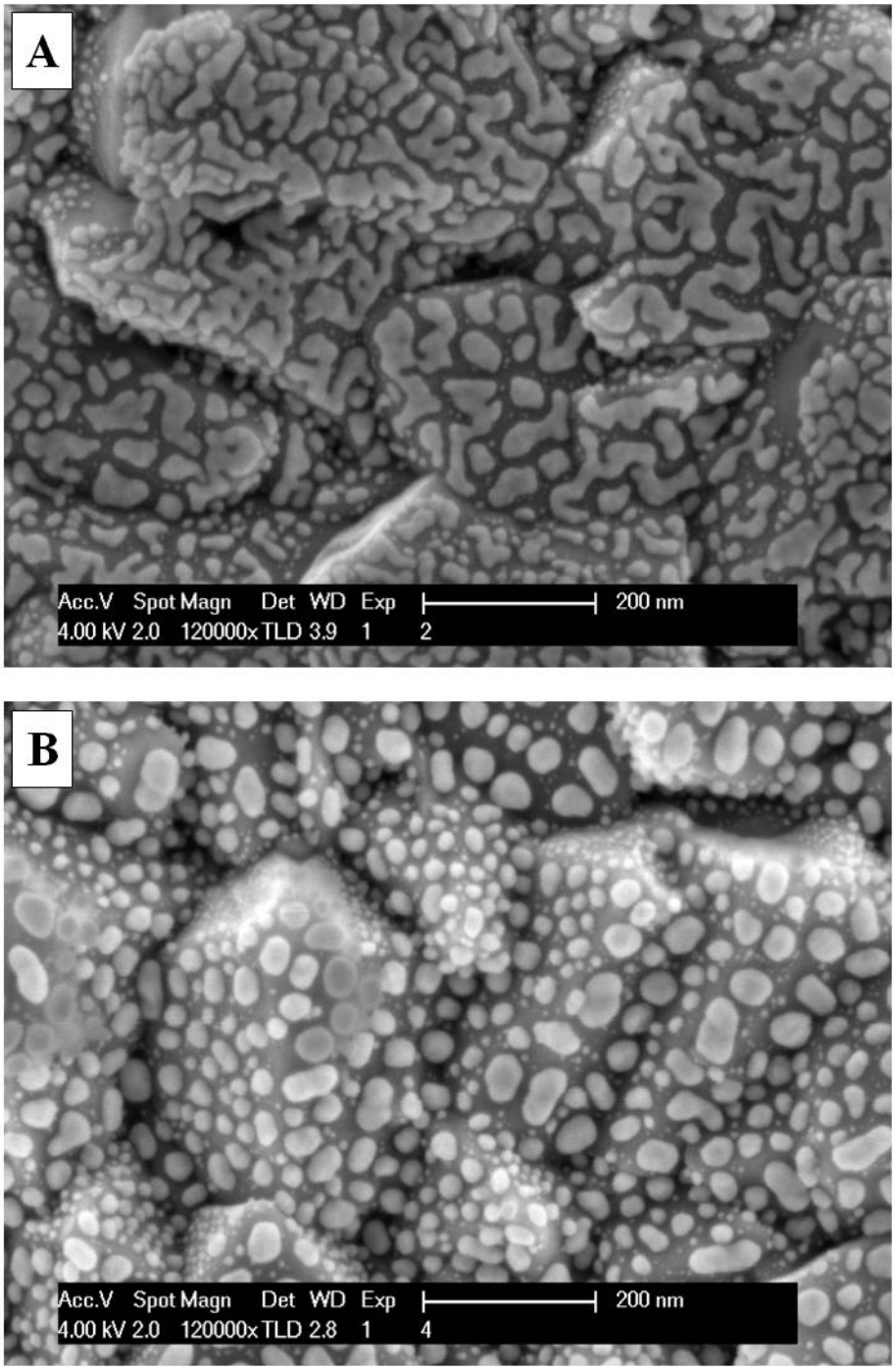


**Figure 16.** SEM images and respective T-LSPR bands of the Au NPs deposited on FTO with nominal thickness 5 nm; (**A**) and (**B**) images of the morphology of the Au NPs respectively immediately after the thermal evaporation and after annealing process for 10 hours at 200 °C.

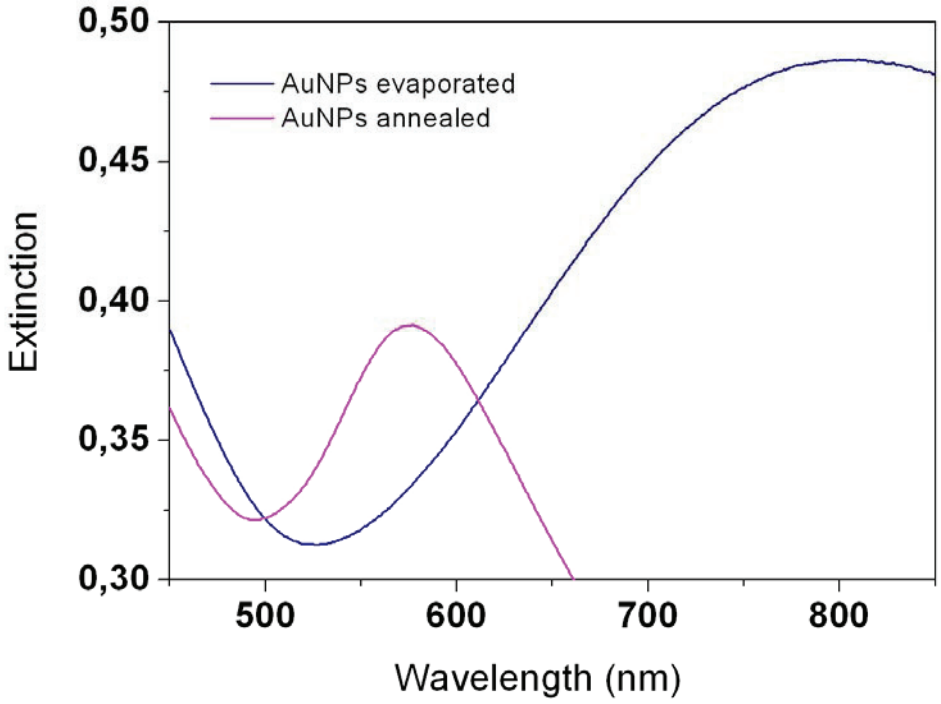


**Figure 17.** LSPR spectra of Au NPs deposited on FTO, with nominal thickness 5 nm, immediately after the thermal evaporation (*blue navy*), and after annealing process for 10 hours at 200°C (*magenta*).

Figure 18 shows a number of LSPR bands recorded for different samples of annealed Au NPs. The spectra show a relatively large bell shape, as expected for NPs of different aspect ratio, with $OD_{max}$ values that span from 0.39 to 0.42 and the $\lambda_{max}$ values that span between 555 to 585 nm. These data indicate that the samples resulting from such a simple fabrication differ in average morphology.

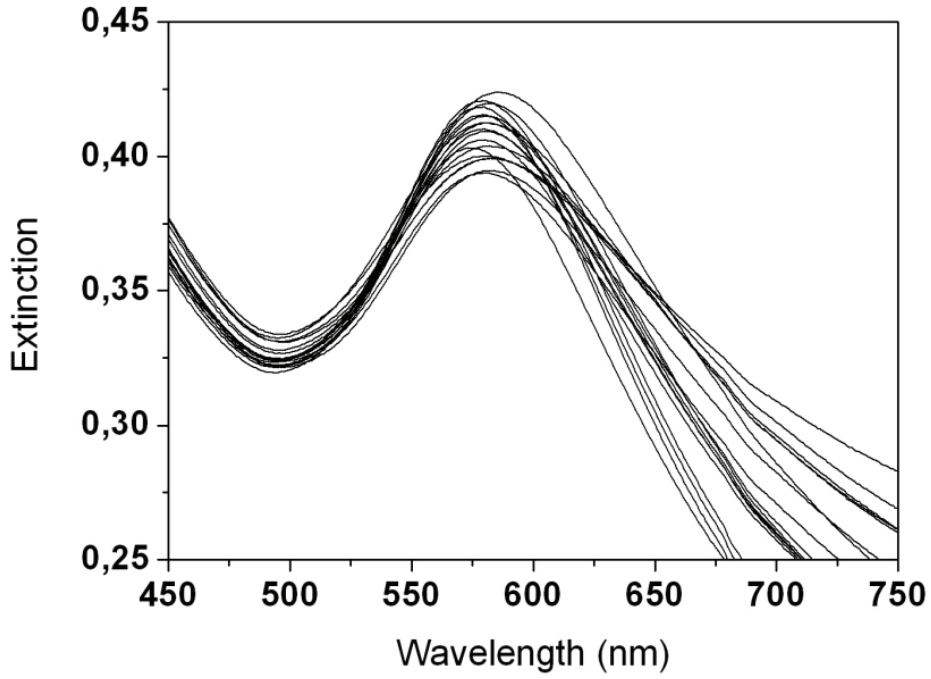


**Figure 18.** LSPR spectra measured in transmission mode of a number of different Au NPs samples of 5 nm nominal thickness and after annealing at 200°C for 10 hours.

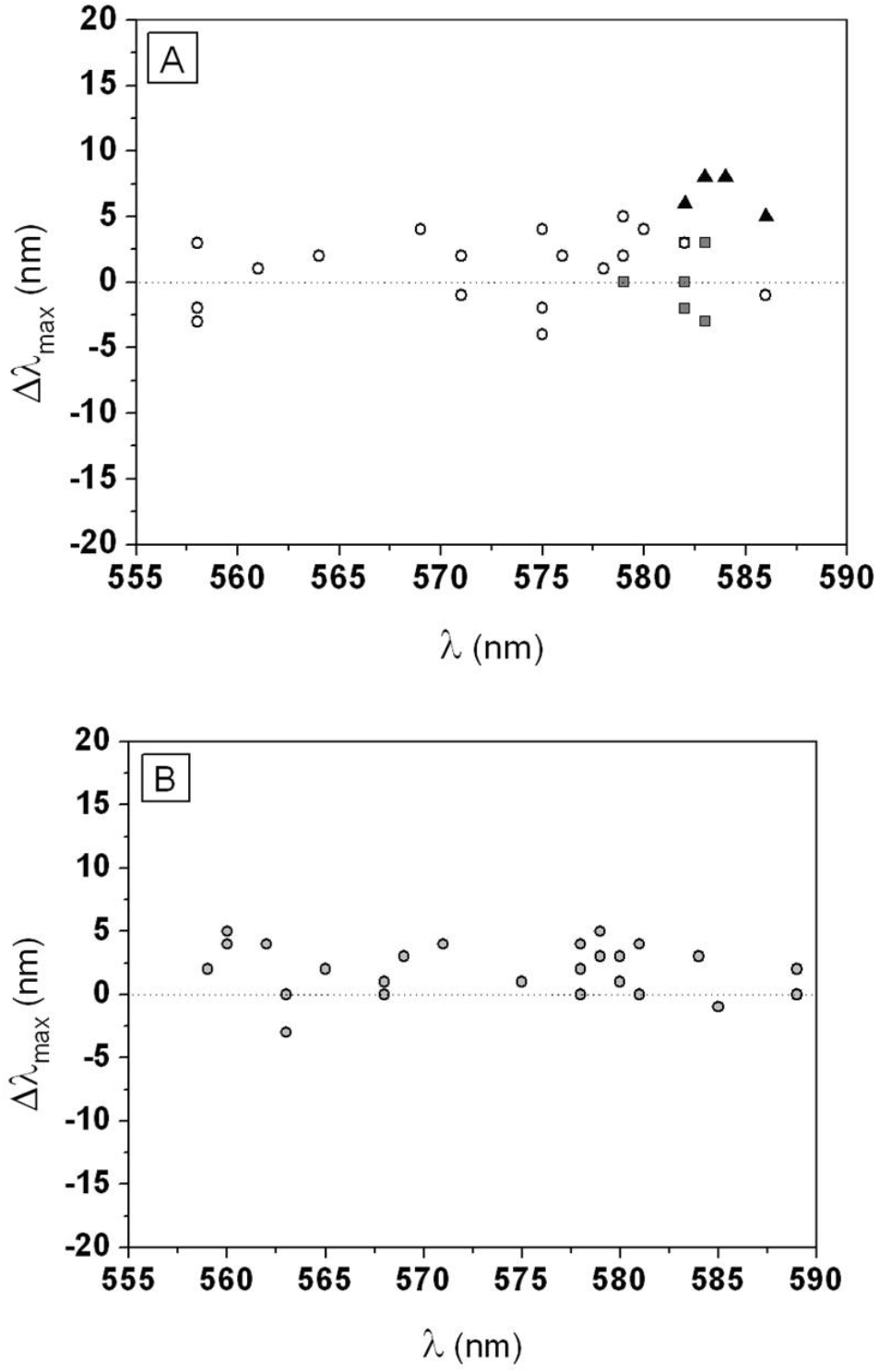


**Figures 19.** (**A**) shift of $\lambda_{max}$ ($\Delta\lambda_{max}$) of the LSPR spectra measured for different samples of Au NPs versus $\lambda_{max}$ values. Different $\lambda_{max}$ indicate that the samples have different average morphology. The shift is measured after immersion of 24 hours in water (o), STE ($\nabla$) and PBS

( ). (**B**) $\lambda_{max}$ shift measured for different samples of Au NPs versus $\lambda_{max}$ after immersion in ethanol for 24 hours.

***Stability of the Au NPs***

The stability of a large number of Au NPs/FTO samples (showing different values of $\lambda_{max}$) has been tested both in organic and aqueous solvents, in particular by incubation for 24 hours in pure $H_2O$, STE and PBS aqueous buffers and in ethanol. Importantly, the LSPR spectra measured before and after incubation do not show significant decrease in OD, indicating a good adhesion of the NPs to FTO surfaces. Figures 19A and 19B report the $\Delta\lambda_{max}$ of samples with different morphology (different values of $\lambda_{max}$) after incubation respectively in aqueous media and in ethanol. The results indicate that the shift of $\lambda_{max}$ is very small.

In particular, the incubation yields in pure water a $\Delta\lambda_{max,water}= 1 \pm 2.6$ and PBS buffer a $\Delta\lambda_{max,PBS}= 1.8 \pm 1.8$, while a bigger shift was detected for STE, $\Delta\lambda_{max,STE} = 6.75 \pm 1.5$, as shown in Figure 19A.

The reported $\lambda_{max}$ shifts could be related both to gold atom restructuration processes of the NPs or to contamination of gold by some impurity of the media (solvents/buffers). Possibly the larger shift measured for incubation in STE, consisting of concentrated salt solutions, could be related to impurity effects of the buffer salts.

Significantly, the data of Figure 19 show that the $\Delta\lambda_{max}$ shifts are randomly distributed respect to the relative values of $\lambda_{max}$, that is the adhesion/restructuration process is small regardless the morphology of the samples.

In Figure 19 we observe a trend in the LSPR feature toward red shift. The small value suggests that a possible restructuration process confined to the surface occurs upon immersion in a solvent. It is well known that under thermal treatment Au surfaces reconstruct to denser, contracted structures (36). The contact with solvents stabilizes the unreconstructed surface which relaxes to the bulk lattice leading to a red shift of the LSPR maximum. When using PBS, which is a buffer and not a pure solvent, the interaction of the dissolved ions with the Au surface can be the reason for the observed slightly different behavior.

## 2.4 Conclusions

After using different protocols for fabricating stable plasmonic materials, it is possible to draw the following conclusions.

The use of glass and quartz as substrate for the Au NPs deposition has showed a poor adhesion of the Au NPs to the surface and their unsuitability for a biosensor development. The use of an organic adhesion layer improved the Au NPs adhesion to the surface but did not help to over pass the main problem of metal nanoparticles on aqueous solution, their instability. The Rubinstein's methodology based on embedding the Au NPs into glass slides, provides NPs which are stable but not sensitive to the binding of organic molecules.

Very positive results have been obtained using fluorine tin oxide (FTO) as substrate. The Au NPs evaporated on FTO are highly stable in different organic and more importantly in aqueous solvents. We believe that the high stability of the gold deposits is related to the roughness of commercially available FTO and the annealing on this surface. The fabrication of Au nanoparticles is very simple: it consists on a simple standard thermal evaporation of gold on commercial FTO surfaces followed by a mild annealing process. The simple protocol of fabrication yields samples of Au NPs of different morphology which is reflected by LSPR bands with maximum energy $\lambda_{max}$ spanning of 30 nm. Significantly, all the fabricated samples, formed by polydisperse NPs, exhibit the same stability.

In conclusion we have shown that i) the best approach to fabricated a stable plasmonic material is based on the use of FTO as substrate, ii) deposition of Au NPs on FTO surfaces is easy and inexpensive, and ii) the Au NPs are stable in several media.

## References


1. U. Kreibig, M. Vollmer. Optical Properties of Metal Clusters. Berlin: *Springer*, **1995**.

2. C. L. Haynes, R. P. Van Duyne. Nanosphere lithography: a versatile nanofabrication tool for studies of size-dependent nanoparticle optics. *The Journal of Physical Chemistry B*. **2001**, 105(24), 5599-5611.

3. K. L. Kelly, E. Coronado, L. L. Zhao, G. C. Schatz. The optical properties of metal nanoparticles: the influence of size, shape, and dielectric enviroment. The *Journal of Physical Chemistry B*. **2003**, 107, 668-677.

4. W. Rechberger, A. Hohenau, A. Leitner, J. R. Krenn, B. Lamprecht, F. R. Aussenegg. Optical properties of two interacting gold nanoparticles. *Optics Communications*. **2003**, 220, 137-141.

5. G. Mie. Optical properties of colloidal gold solutions. *Annals of Physics*. **1908**, 25, 329-371.

6. H. Ishikawa, K. Kimura. Instability of gold nano-island in several organic media. *Nanostructured Materials*. **1997**, 9, 555-558.

7. M. Gluodenis, C. Manley, C. A. Foss Jr. In situ monitoring of the change in extinction of stabilized nanoscopic gold particles in contact with aqueous phenol solutions. *Analytical Chemistry*. **1999**, 71, 4554-4558.

8. P. Mulvaney. Surface plasmon spectroscopy of nanosized metal particles. *Langmuir*. **1996**, 12, 788-800.

9. P. A. Mosier-Boss, S. H. Liebermann. Comparison of three methods to improve adherence of thin gold films to glass substrates and their effect on the SERS response. *Applied Spectroscopy*. 1999, 53(7), 862-873.

10. N. R. Moody, D. P. Adams, D. Medlin, T. Headley, N. Yang, A. Volinsky. Effects of diffusion on interfacial fracture of gold-chromium hybrid microcircuit films. *International Journal of Fracture*. **2003**, 119(4), 407-419.

11. D. C. Miller, C. F. Herrmann, H. J. Maier, S. M. George, C. R. Stoldt, K. Gall. Intrinsic stress development and microstructure evolution of Au/Cr/Si multilayer thin films subject to annealing. *Scripta Materialia*. **2005**, 52, 873-879.

12. M. A. George, W. S. Glaunsinger, T. Thundat, S. M. Lindsay. Electrical, spectroscopic, and morphological investigation of chromium diffusion through gold films. *Thin Solid Films*. **1990**, 189(1), 59-72.

13. F. Frederix, J. M. Friedt, K. H. Choi, W. Laureyn, A. Campitelli, D. Mondelaers, G. Maes, G. Borghi. Biosensing based on light absorption of nanoscaled gold and silver particles. *Analytical Chemistry*. **2003**, 75, 6894-6900.

14. C. A. Goss, D. H. Charych, M. Majda. Application of (3-mercaptopropyl)trimethoxysilane as a molecular adhesive in the fabrication of vapor-deposited gold electrodes on glass substrates. *Analytical Chemestry*. **1991**, 63(1), 85-88.

15. I. Doron-Mor, Z. Barkay, N. Filip-Granit, A. Vaskevich, I. Rubinstein. Ultrathin gold island films on silanized glass morphology and optical properties. *Chemistry of Materials*. **2004**, 16, 3476-3483.

16. M. D. Malinsky, K. L. Kelly, G. C. Schatz, R. P. Van Duyne. Chain length dependence and sensing capabilities of the localized surface plasmon resonance of silver nanoparticles chemically modified with alkanethiol self-assembled monolayers. *Journal of American Chemical Society*. **2001**, 123, 1471-1482.

17. I. Ruach-Nir, T. A. Bendikov, I. Doron-Mor, Z. Barkay, A. Vaskevich, I. Rubinstein. Silica-stabilized gold island films for transmission localized surface plasmon sensing. *Journal of American Chemical Society*. **2007**, 129, 84-92.

18. T. Karakouz, A. B. Tesler, T. A. Bendikov, A. Vaskevich, I. Rubinstein. Highly stable localized plasmon transducers obtained by thermal embedding of gold island films on glass. *Advanced Materials*. **2008**, 20, 3893-3899.

19. C. Y. Hsu, J. W. Huang, S. Gwo, K. J. Lin. The facile fabrication of tunable plasmonic gold nanostructure arrays using microwave plasma. *Nanotechnology*. **2010**, 21(3), 35302.

20. S. Gao, N. Koshizaki, E. Koyama, H. Tokuhisa, T. Sasaki, J.-K. Kim, Y. Cho, D.-S. Kim, Y. Shimizu. Innovative platform for transmission localized surface plasmon transducers and its application in detecting heavy metal Pd(II). *Analytical Chemistry*. **2009**, 81, 7703-7712.

21. S. Szunerits, V. G. Praig, M. Manesse, R. Boukherroub. Gold island films on indium tin oxide for localized surface plasmon sensing. *Nanotechnology*. **2008**, 19, 195712-195719.

22. A. R. Schlatmann, D. W. Floet, A. Hilberer, F. Garten, P. J. M. Smulders, T. M. Klapwijk, G. Hadziioannou. Indium contamination from the indium-tin-oxide electrode in polymer light emitting diodes. *Applied Physics Letters*. **1996**, 69(12), 1764-1767.

23. M. P. de Jong, D. P. L. Simons, M. A. Reijme, L. J. van Ijzendoorn, A. W. D. van der Gon, M. J. A. de Voigt, H. H. Brongersma, R. W. Gymer. Indium diffusion in model polymer light-emitting diodes. *Synthetic Metals*. **2000**, 110, 1-6.

24. S. T. Lee, Z. Q. Gao, L. S. Hung. Metal diffusion from electrodes in organic light-emitting diodes. *Applied Physics Letters*. **1999**, 75, 1404-1406.

25. K. von Rottkay, M. Rubin. Optical indices of pyrolytic tin-oxide glass. *Materials Research Society Symposia Proceedings*. **1996**, 426, 449-454.

26. P. Montmeat, J.-C. Marchand, R. Lalauze, J.-P. Viricelle, G. Tournier, C. Pijolat. Physico-chemical contribution of gold metallic particles to the action of oxygen on tin dioxide sensors. *Sensors and Actuators B*. **2003**, 95, 83-89.

27. A. I. Martinez, L. Huerta, J. M. O-Rueda de León, D. Acosta, O. Malik, M. Aguilar. Physicochemical characteristics of fluorine doped tin oxide films. *Journal of Physics D: Applied Physics*. **2006**, 39, 5091-5096.

28. J. C. Love, L. A. Estroff, J. K. Kriebel, R. G. Nuzzo, G. M. Whitesides. Self-assembled monolayers of thiolates on metals as a form of nanotechnology. *Chemical Reviews*. **2005**, 105(4), 1103−1169.

29. J. C. Riboh, A. J. Haes, A. D. McFarland, C. R. Yonzon, R. P. Van Duyne. A nanoscale optical biosensor: real-time immunoassay in physiological buffer enabled by improved nanoparticle adhesion. *The Journal of Physical Chemistry B*. **2003**, 107(8), 1772-1780.

30. E. Hutter, M.-P. Pileni. Detection of DNA hybridization by gold nanoparticle enhanced transmission surface plasmon resonance spectroscopy. *The Journal of Phical Chemistry B*. **2003**, 107(27), 6497-6499.

31. G. Kalyuzhny, M. A. Schneeweiss, A. Shanzer, A. Vaskevich, I. Rubinstein. Differential plasmon spectroscopy as a tool for monitoring molecular binding to ultrathin gold films. *Journal of American Chemistry Society*. **2001**, 123, 3177-3178.

32. G. Kalyuzhny, A. Vaskevich, M. A. Schneeweiss, I. Rubinstein. Transmission surface-plasmon resonance (T-SPR) measurements for monitoring adsorption on ultrathin gold island films. *Chemistry - A European Journal*. **2002**, 8(17), 3849-3857.

33. S. E. Roark, K. L. Rowlen. Thin silver films: influence of substrate and postdeposition treatment on morphology and optical properties. *Analytical Chemistry*. **1994**, 66(2), 261-270.

34. G. Gupta, D. Tanaka, Y. Ito, D. Shibata, M. Shimojo, K. Furuya, K. Mitsui, K. Kajikawa. Absorption spectroscopy of gold nanoisland films: optical and structural characterization . *Nanotechnology*. **2009**, 20, 025703.

35. J. Tiggesbäumke, L. Köller, K.-H. Meiwes-Broer, A. Liebsch. Blue shift of the Mie plasma frequency in Ag clusters and particles. *Physical Review A*. **1993**, 48, R1749-R1752.

36. A. J. Haes, D. A. Stuart, S. Nie, R. P. Van Duyne. Using solution-phase nanoparticles, surface-confined nanoparticle arrays and single nanoparticles as biological sensing platforms. *Journal of Fluorescence*. **2004**, 14 (4), 355–367.

37. Kolb, D. M. Reconstruction phenomena at metal-electrolyte interfaces. *Progress in Surface Science*. **1996**, 51(2), 109-173.

# Chapter 3

# Sensitivity and Reversibility of Au Nanoparticles

## 3.1 Introduction

In Chapter 2 we have reported about i) the fabrication of Au NPs by simple thermal evaporation on fluorine tin oxide surfaces followed by a mild annealing process, and ii) the stability of this plasmonic material under exposure to different media (MilliQ water, STE and PBS buffers, and ethanol). This protocol of fabrication yields samples of polydisperse Au NPs of different morphology which exhibit the same stability. These successful results led us to focus on this material to understand its properties. It is this plasmonic material suitable to develop a molecular biosensor?

To answer this question, we have focused on two main issues: i) the response of the Au NPs LSPR to the formation SAMs of organic molecules of the different structures, and ii) the reversibility of the LSPR based sensor.

As discussed in the Chapter 1, the LSPR of noble metal nanoparticles arises when electromagnetic radiation induces a collective oscillation of the conduction electrons of the individual nanoparticles there are two primary consequences: i) a selective photon absorption which allows the optical properties of these nanoparticles to be monitored with UV-Vis spectroscopy and ii) an enhancement of the electromagnetic fields surrounding the nanoparticles which is responsible for all surface-enhanced spectroscopies.

In general, the sensitivity of a sensor is a critical parameter which determines the system performance. In particular, for sensors based on localized surface plasmon resonance (LSPR) the sensitivity is related to the response of the optical properties of the Au NPs to the changes of the refractive index of the surrounding medium. In a typical LSPR sensor, an analyte binds to a recognition layer on the LSPR transducer, effecting a local change of the refractive index.

According to equation (1.3) a change in the refractive index of the medium surrounding the NPs will induce a $\lambda_{max}$ shift of the LSPR band easily detectable with conventional UV-Vis spectroscopy.

A not much rigorous but valid equation for a qualitatively description of the LSPR band shift is the following:

$$\Delta\lambda = m(\eta_{ads} - \eta_{medium})\,(1 - e^{-2d/l}) \qquad (1.4)$$

where $m$ is the sensitivity factor (nm/RIU (refractive index unit)) $n_{ads}$ and $n_{medium}$ are respectively the refractive index of the adsorbed layer and of the medium, $d$ is the thickness of the adsorbed layer, and $l$ is the characteristic electromagnetic decay length of the evanescent electromagnetic field (1-4). The equation therefore provides the sensor sensibility, and the properties of the layers formed on the NPs surface.

According to equation (1.4) the binding of organic molecules to nanoparticles induces an increase of the local refractive index and, in turn, a red shift of the extinction spectrum, as experimentally observed (5-6). It is thus evident, that *the LSPR response of plasmonic nanoparticles acts as transducer of changes in the refractive index occurring at the surfaces*. The equation approximates the response for adsorbate layers but does not provide a fully quantitative explanation of its response (2).

The $m$ factor is a basic parameter determining the effectiveness of an LSPR system of an optical transducer. This factor is commonly determined by measuring the optical extinction of the LSPR transducer upon immersion in a uniform bulk medium of variable refractive index. Refractive index sensitive measurements have been reported for a variety of systems, including metal nanoparticles in solution and immobilized on substrates (7-9), and metal nanoparticles arrays evaporated through a mask (10-12). Data for random Au nanoparticles films are rather limited (13-16). Finally, it is known that in the presence of the thickest SAM the sensitive factor $m$ diminishes approximately of 20% (11); this behavior is a consequence of the spatial distribution of the electromagnetic field surrounding the Au NPs. In fact, when the LSPR is excited, the strength of the generated electromagnetic fields decays over the length scale of ~ 50 nm (17). Thus, the strongest sensing capabilities are in the near surface region of the nanoparticle.

In Chapter 3 we study the refractive index sensitivity, $m$, of the Au NPs deposited on FTO in solvent media and under functionalization by SAMs. To calculate the sensitivity factor $m$ of the plasmonic material we have measured the $\Delta\lambda_{max}$ of the LSPR band under exposition of the Au NPs to media of different dielectric constant, as air (n = 1.00), $H_2O$ (n =1.3325), $C_2H_3N$ (n = 1.344), $C_2H_5OH$ (n = 1.36168), $C_3H_8O$ (n = 1.3776), $(CH_3)_2SO$ (n = 1.479).

To test the sensing capability of the LSPR bands of Au NP to the formation of organic self assembled monolayers (SAMs), we have measured and compared the spectral shift of $\lambda_{max}$ of the LSPR bands under formation of 1-dodecanethiol (C12), 1-hexadecanethiol (C16), and 4-terphenylthiol (SAMs) in order to i) compare the response of the Au NPs system to those reported in literature, ii) to compare the shift induced by SAMs with same refractive index and different thickness, iii) to compare the shift induced by SAMs of the same thickness and different electronic structure.

We also measured the response of the LSPR band to the formation of SAMs of 6-mercapto-1-hexanol (MCH), a compound widely used to intercalate DNA strands on a metal surface (18).

For testing the reversibility of the LSPR response, we have recorded the LSPR bands when SAMs formed on the NPs surfaces by alkane-thiols are replaced by SAMs formed by aromatic molecules, and vice versa.

## 3.2 Materials and Methods

### Materials

1-hexadecanethiol, 1-dodecanethiol and 6-mercapto-1-hexanol, ethanol, acetonitrile, 2-propanol, dimethyl sulfoxide (DMSO) and STE buffer were purchased from Sigma Aldrich (Germany), 4-terphenylthiol from Frinton Laboratories Inc (Vineland, NJ) and phosphate-buffered saline (PBS) solutions from Lonza Walkersville Inc. (Walkersville, MD). The Fluorine Tin Oxide (FTO) (TEC 8) surfaces were purchased from Pilkington North America Inc. (Toledo, OH).

### Au NPs fabrication

The fluorine tin oxide surfaces was cleaned by a solution 1:1 of acetone and 2-propanol in ultrasounds bath for 15 minutes, then repeatedly rinsed with copious amounts of water MilliQ and lastly gently dried with a pure nitrogen stream. The gold nanoparticles were deposited on the FTO surfaces by thermal evaporation at a pressure of $10^{-6}$ mB and at deposition rate of 0.0016 nm $s^{-1}$. The deposition process of NPs is controlled by measuring a nominal thickness of 5nm with a built-in quartz balance. The samples were then annealed for 10 hours at to 200°C.

### Characterizations

The UV-Vis measurements were carried out by using a Jasco V-570 UV-Vis-NIR spectrophotometer in transmittance mode by placing the samples into the spectrophotometer cavity (scan speed 200 nm/min, band width 1 nm). All the spectra were recorded in air and by using air as reference. A series of measurements performed by repetitive removing and replacing the same sample into the spectrophotometer cavity showed an error in $\lambda_{max}$ values of 1 nm.

The Au NPs/FTO images were obtained using a Scanning Electron Microscopy (SEM FEI XLF30-SFEG of FEI Company Eindhoven) equipped with ultra high resolution lens and in-lens SE (secondary-electron) detector.

### Sensitive factor *m*

The LSPR absorption band of the Au NPs deposited on FTO was measured in air (n = 1.00) and under immersion in $H_2O$ (n =1.3325), $C_2H_3N$ (n = 1.344), $C_2H_5OH$ (n = 1.36168), $C_3H_8O$

(n = 1.3776), $(CH_3)_2SO$ (n = 1.479). The samples were washed accurately before immersion in a different solvent.

**Functionalization of Au NPs**

Self-assembled monolayers (SAMs) of 1-dodecanethiol (C12), 1-hexadecanethiol (C16), 4-terphenylthiol and 6-mercapto-1-hexanol (MCH), were formed by incubating the Au NPs samples into respectively 1 mM ethanol and 1 mM water solutions for 16 hours.

**Reversibility**

The C12 SAM formed on Au NPs has been replaced by a 4-terphenylthiol SAM upon immersion of the sample carrying the C12 SAM in 1mM ethanolic solution of 4-terphenylthiol for 16 hours. The 4-terphenylthiol SAM has been thus replaced by a new C12 SAM, by incubating the sample in 1mM ethanol solution of 1-dodecanethiol SAM for 16 hours. T-LSPR spectra have been recorded after the formation of each SAM.

## 3.3 Results and Discussion

### Sensitivity to various media

The sensitivity of the new plasmonic material, based on Au NPs deposited on FTO, was determined by measuring the change of its optical properties, that is, the size of the $\lambda_{max}$ shift by changing the surrounding dielectric medium.

In Figure 1 is reported the $\lambda_{max}$ shift ($\Delta\lambda_{max}$) versus the refractive index, *n*, of various solvents.

Figures 1A and 1B report the measurements performed on two samples of Au NPs annealed in a different annealing condition that differ for the amount of oxygen inside the oven chamber. Figure 1A reports the results obtained for samples annealed an "open" oven, under a constant circulation of oxygen, while Figure 1B shows the data collected on samples annealed in a "closed" oven , where the amount of oxygen decreases during the process.

Both figures show that the measured LSPR $\lambda_{max}$ values shift toward longer wavelengths as the solvent refractive index increases. This trend is in agreement with that reported in literature (3,11).

The plot of the solvent refractive index versus the LSPR $\lambda_{max}$ shift showed to be linear for both cases; the slope of the linear fit shows that the LSPR spectral sensitivity is 74 nm $RIU^{-1}$ (Figure 1A) and 63 nm $RIU^{-1}$ (Figure 1B). The difference between the two values, even if it is quite small, shows that the annealing step is one of the factors responsible for the substrate optical characteristics. We could say that, in our case, the presence continuous of new oxygen is more important for the preparation a more sensitive plasmonic material (19). Therefore, we have performed all the annealing processes in "open" oven.

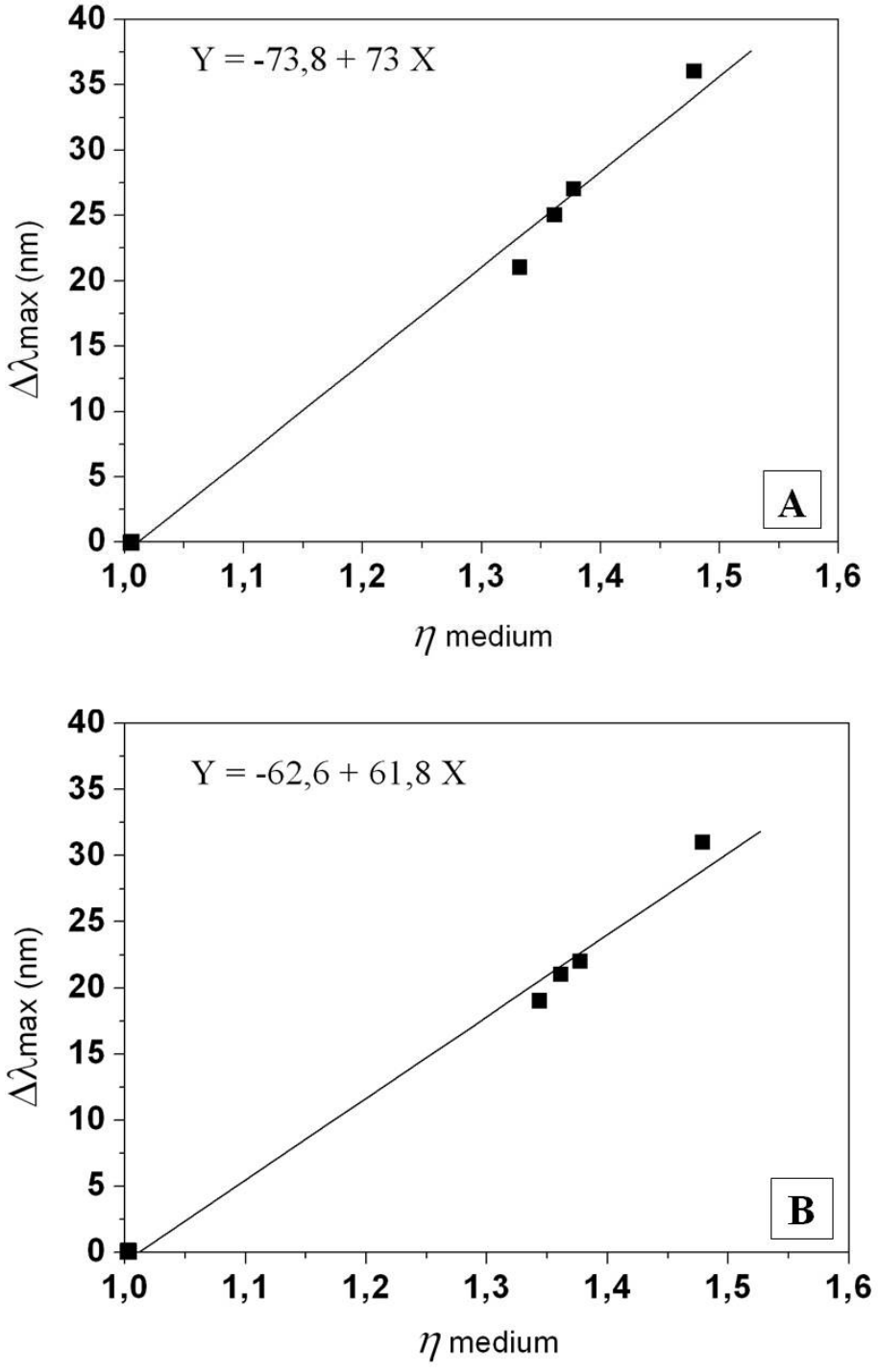


**Figure 1.** LSPR $\lambda_{max}$ of Au NPs on FTO surface versus refractive index of the medium solvent. The Figures 1A and 1B represent the results obtained on samples annealed at two different conditions (see text) that have a sensitive factor of 74 nm $RIU^{-1}$ and 63 nm $RIU^{-1}$ respectively.

The *m* factor obtained in our experiment (Figure 1A) is in agreement with the sensitivity factors reported in literature. The Chilcoti's group reports a sensitivity factor of 76.4 nm $RIU^{-1}$ for using colloid gold nanoparticles bind to glass substrate (8); the Rubinstein's group, by using a similar fabrication methodology and NPs of similar dimension, calculates a *m* factor of 80 nm $RIU^{-1}$ (13); a study of Szunerits et al. (16), on Au NPs thermally evaporated on indium tin oxide (ITO), reports a *m* factor of 65 nm $RIU^{-1}$ (16). It has been also reported that nanoparticles fabricated by metal thermal evaporation through a mask (3) show higher *m* factor of 200 nm $RIU^{-1}$, and that the same NPs when annealed show a *m* factor of 100 nm $RIU^{-1}$.

The Van Duyne's group has demonstrated that, by using substrates of different refractive index the sensitivity of the Au NPs does not change, that is that the *m* factor was not affected by the kind of substrate used (3).

If the sensitivity of a plasmonic material is not affected by the refractive index of the substrate, it can be affected by others properties, as for example the surface morphology. The substrate surface shows always some degree roughness, caused by inherent imperfections of fabrication processes. Thus, surface roughness could be a parameter that influences the LSPR sensitivity. It has been found (20) that when a surface has a roughness smaller than 2 nm in height deviation (δ, quantitatively defined as the root-mean-square (rms) deviation from a mean plane), the sensitivity of a LSPR biosensor is not significantly influenced regardless of correlation length (CL), a characteristic size of surface regions. However, the extinction peak amplitude and curve width are affected substantially by a decrease in correlation length. At a less than 100 nm of CL, surface roughness can induce interference in the localized surface plasmon resonance.

On the basis of these results, the *m* factor obtained for our plasmonic material, which at first sight seems too low, is well explained. It is understandable that our *m* value i) is slightly lower than that obtained by Rubinstein's group for NPs deposited on glass surfaces, certainly less rough than FTO and ii) is slightly higher than that reported by Szunerits for NPs deposited on ITO surfaces: these surfaces are well known to present a roughness higher than FTO.

We stress here that the roughness of the FTO surfaces slightly lower the sensitivity of the deposited NPs, but on the other side provide and outstanding stability to the plasmonic material. The strong adhesion of Au onto FTO substrates is enhanced by the porosity of $SnO_2$ where gold can penetrate during thermal annealing (21-23).

**Sensitivity of the Au NPs LSPR to SAMs formation**

In search of plasmonic materials suitable to detect molecular interactions, the first and simplest step is to test its sensitivity toward the formation of organic SAMs at the surface. The $\lambda_{max}$ shifts of SP bands of the Au NP deposited on FTO was measured under functionalization with self assembled monolayers (SAMs) of 1-dodecanethiol (C12), 1-hexadecanethiol (C16), 4-terphenylthiol and 6-mercapto-1-hexanol (MCH).

Figure 2 shows a SEM image of Au NPs annealed on FTO before (Figure 2A) and after functionalization with C16 SAM (Figure 2B). The morphology comparison shows that there are no evidences of gold depletion or restructuration of the Au NPs morphology. This result indicates that we can consider the Au NPs stable under functionalization.

Figures 3.1A, 3.1B, 3.2C and 3.2D show respectively T-LSPR spectra of representative Au NPs samples, before and after incubation in ethanol solution of C12, C16, terphenyl, and in aqueous solution of MCH. All the spectra show a red shift of the $\lambda_{max}$ and an increase of extinction. It is evident that each kind of SAMs leads a different shift and value of absorbance.

The values reported in Figures 3 were obtained in one of the 100 experiments of sensitivity tests. The average $\lambda_{max}$ shifts, calculated over more than 100 samples, are respectively $\Delta\lambda_{max,C12}$ = 9.8 ± 2.7 for C12, $\Delta\lambda_{max,C16}$ =11.7 ± 2.2 nm for C16, and $\Delta\lambda_{max,MCH}$ =10.2 ± 2 nm for MCH (Figure 4). In the present case the reported standard deviations represent the distribution of $\Delta\lambda$ over samples with different average morphology, and not, as usually, the error distribution of experimental measurement. In all experiments, always a higher shift was recorded after functionalization with C16 than after binding C12.

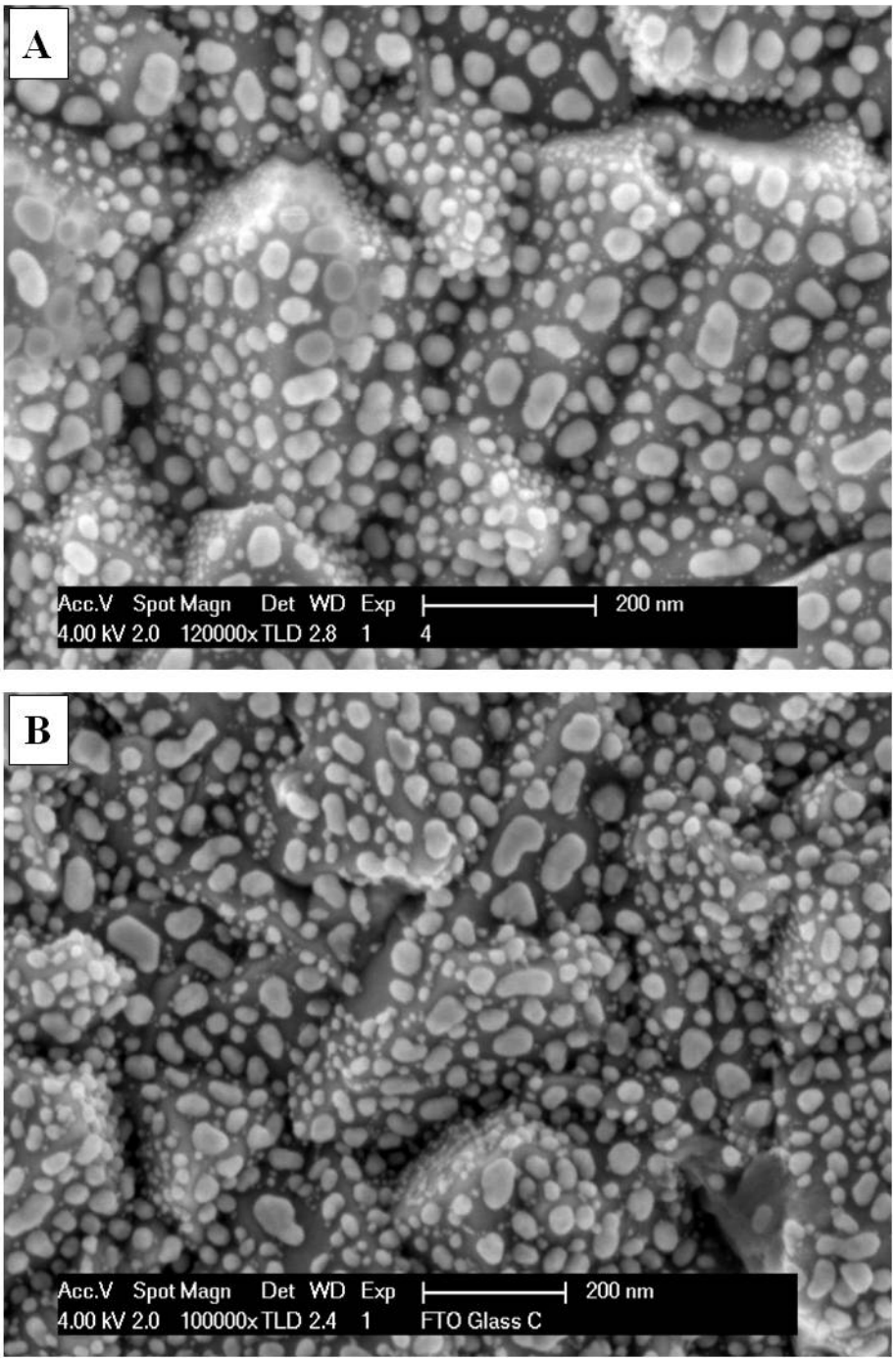


**Figure 2.** SEM images of annealed Au NPs on FTO surface, before (**A**) and after formation of a hexadecanethiol SAM (**B**).

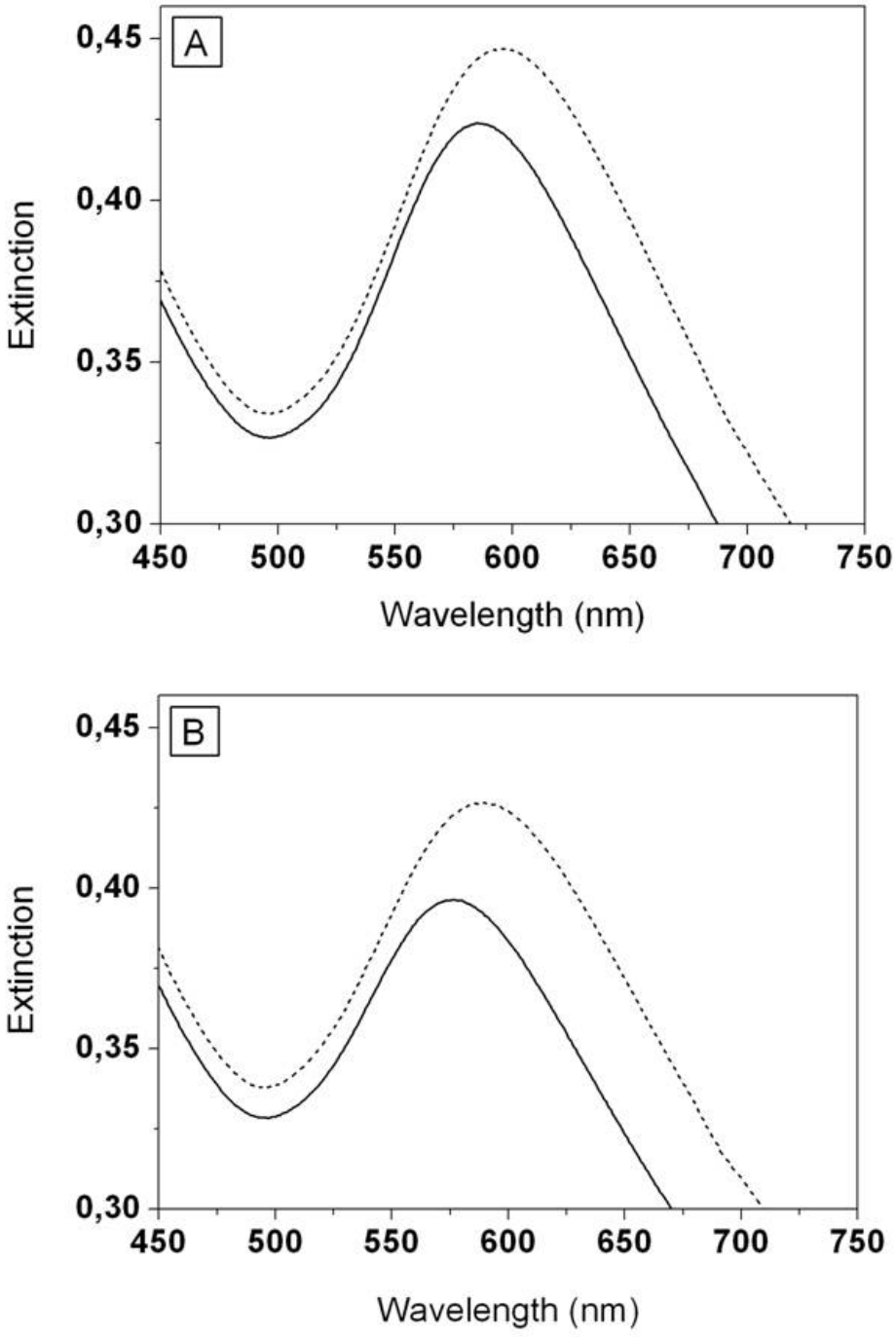


**Figure 3.1.** Surface Plasmon bands after formation of organic SAMs on Au NPs: (**A**) 1-dodecanethiol (C12), (**B**) 1-hexadecanethiol (C16).

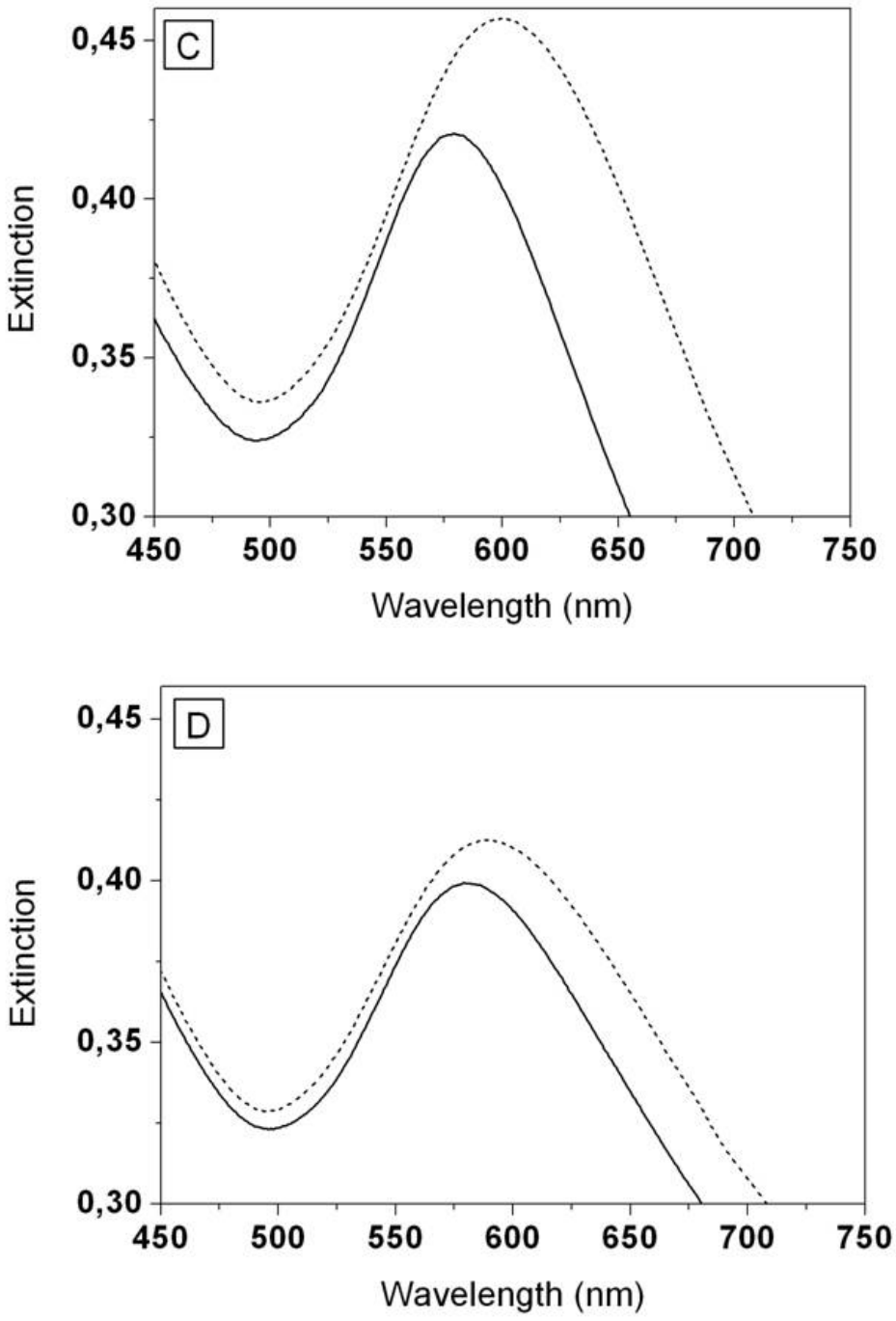


**Figure 3.2.** Surface Plasmon bands after formation of organic SAMs on Au NPs: (**C**) 4-terphenylthiol (TP), (**D**) 6-mercapto-1-hexanol (MCH).

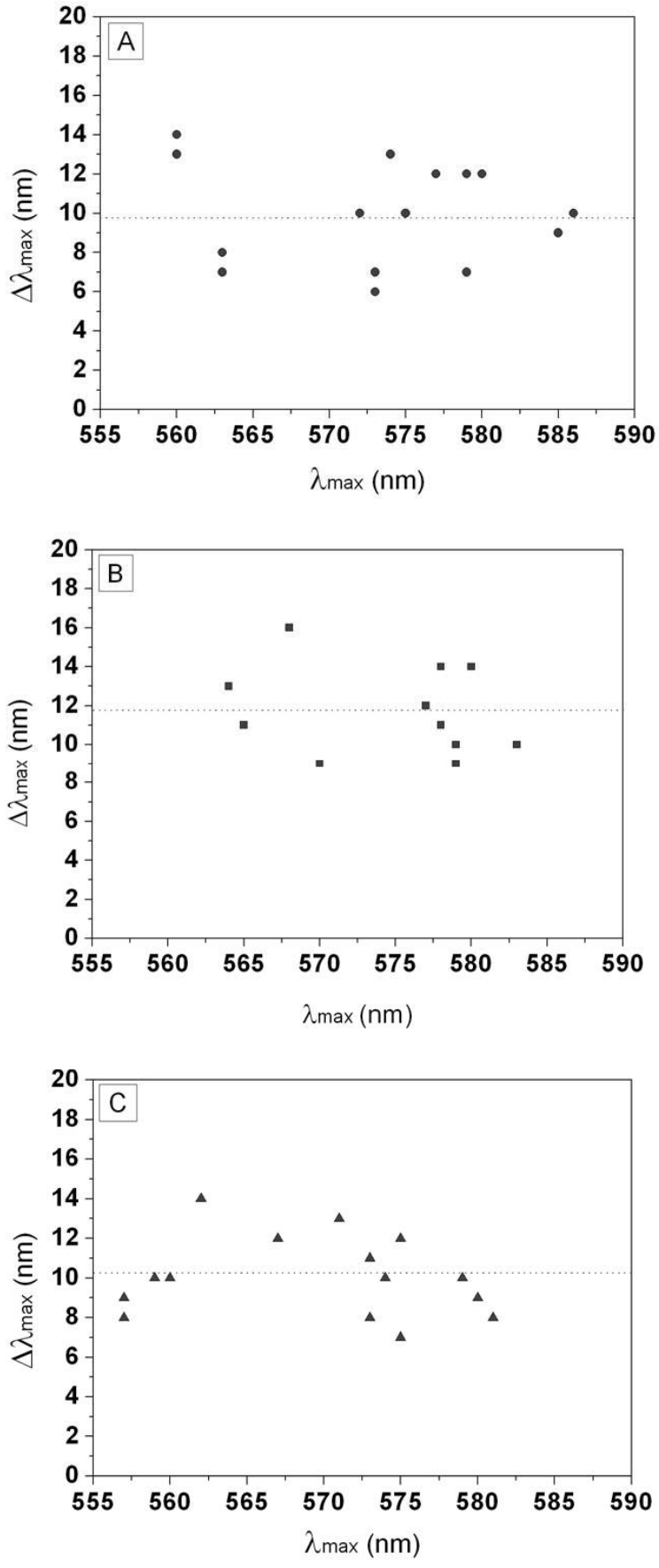


**Figure 4.** LSPR $\Delta\lambda_{max}$ shift of Au NPs versus $\lambda_{max}$ after formation of different SAMs: (**A**) 1-dodecanethiol, (**B**) 1-hexadecanethiol, and (**C**) 6-mercapto-1-hexanol.

Figure 4 reports the $\Delta\lambda_{max}$ shift of the LSPR bands after each functionalization of the Au NPs with MCH, C12 and C16 SAMs versus the $\lambda_{max}$. The results indicate that the LSPR bands of the Au NPs on FTO show a good sensitivity to the presence of organic SAMs and that we do not observe any correlation of the $\Delta\lambda_{max}$ with the $\lambda_{max,}$ that is, there is no correlation of the $\Delta\lambda_{max}$ with the morphology of the nanoparticles.

The difference between the $\Delta\lambda_{max,C12}$ = 9.8 ± 2.7 for C12 SAM and $\Delta\lambda_{max,terph}$= 21 nm± 2.1 for terphenyl SAM, are related to two SAMs having the same thickness (24-25) but different refractive index. Considering these shift values, we can affirm that the results allow of disentangle between aliphatic and aromatic electronic structure.

We have reported the data obtained from the Au NPs stabilizations and Au NPs functionalizations in Table 1. By comparing the data of Table 1, we observe that the $\Delta\lambda_{max}$ measured after stabilization is in the error of the $\Delta\lambda_{max}$ measured after SAM formation. These data indicate that the Au NPs samples do not need to undergo any stabilization process.

**Table 1. $\lambda_{max}$ shifts ($\Delta\lambda$) of the LSPR band of Au NPs-FTO samples after stabilization and functionalization with different SAMs in the same solvents (water and ethanol)**

| **stabilization** | | **functionalization** | |
|---|---|---|---|
| *solvent* | $\Delta\lambda_{max}$ / *nm* [a] | *SAM* | $\Delta\lambda_{max}$ / *nm* [a] |
| water | 1 ± 2.6 | MCH | 10.2 ± 2.8 |
| | | C12 | 9.8 ± 2.6 |
| ethanol | 1.8 ± 1.8 | C16 | 11.7 ± 2.2 |
| | | TerPh | 21 ± 2.1 |

[a] The $\Delta\lambda$ values report the standard deviation related to 100 samples

In order to confirm this conclusion we have compared the spectral shift measured after direct immersion in the thiol solution ($\Delta\lambda_{max,d}$), with that obtained after two processes, that is I) stabilization in pure solvents ($\Delta\lambda_{max,s}$), and II) subsequent incubation in the thiol solutions ($\Delta\lambda_{max,SAM}$). The results show that $\Delta\lambda_{max,d} = \Delta\lambda_{max,s} + \Delta\lambda_{max,SAM}$ for a large number of samples (>70) with different initial $\lambda_{max}$. These data represent a further confirmation that the Au NPs/FTO samples do not need to undergo any stabilization process in contrast to other plasmonic Au or Ag NPs reported in literature (11).

The plasmonic material based on Au nanoparticles deposited on FTO surfaces indicate that their LSPR are sensitive to the formation of organic SAM, showing a different response for SAMs formed by I) the same molecules of different lengths, II) molecules of different structure but same length. The slightly different morphology of the NPs does not affect the sensitivity of this material.

**Reversibility of the LSPR system**

Figure 5 reports the LSPR spectra recorded for a sample i)of bare Au NPs, ii) after formation of a C12 SAM, iii) after replacement of the C12 SAM by 4-terphenylthiol SAMs, and iv) after a second replacement of the 4-terphenylthiol SAM with the original C12 SAM.

These results show that the formation of 1-dodecanethiol SAM yields a red shift of 10 nm of $\Delta\lambda_{max,}$ in agreement with the results reported in Figure 4A and the Table 1. By replacing the C12 SAM with a terphenyl SAM, a further red shift of 11 nm is observed. Under restoration of C12 SAM, the value of $\lambda_{max}$ goes back exactly to the original value by a blue shift of 11 nm.

These results indicate a complete reversibility of the Au NPs plasmonic response under SAMs exchange and demonstrate that there is neither loss nor restructuration of the NPs gold atoms during the formation of different SAMs and their replacement. The completely reversibility indicate that the nanoparticles can be regenerated after a sensing episode, crucial event for a biosensor.

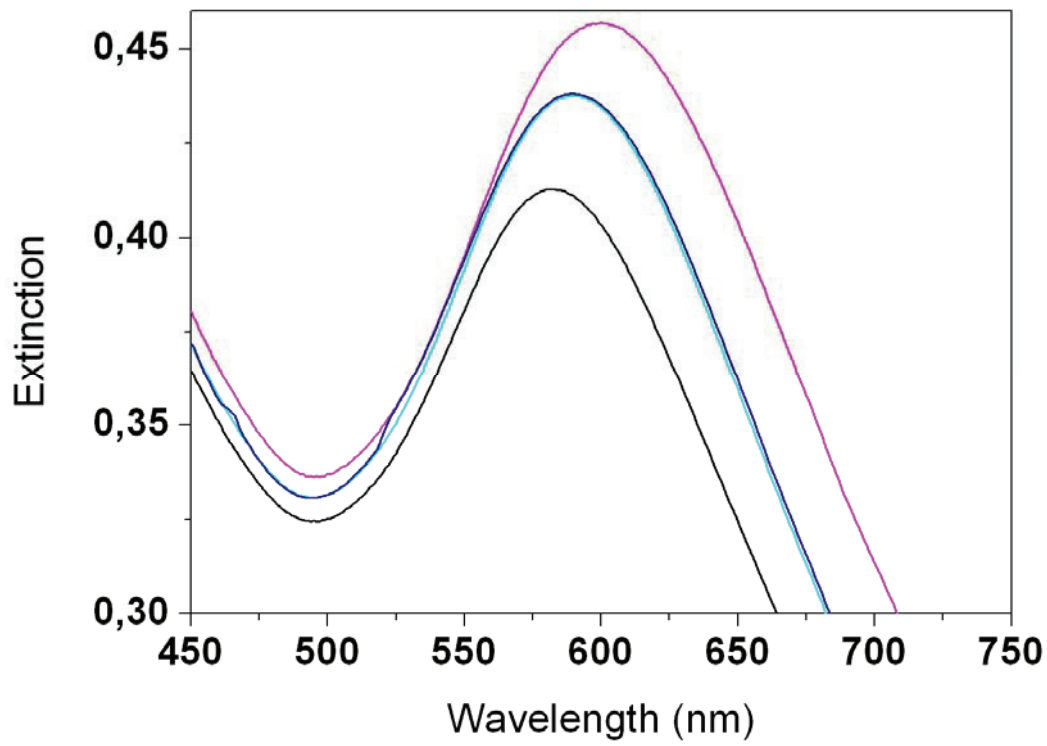


**Figure 5.** SP bands of bare Au NPs (*black*); after formation of dodecanthiol SAM (*turquoise*); after replacement of the dodecanthiol SAM by a terphenylthiol SAM (*pink*): after replacement of the terphenylthiol SAM by the original dodecanethiol SAM (*blue*).

By using the shift values measured for C12 and terphenyl SAMs, the refractive indices of the respective organic molecules (C12 (η=1.5), terphenyl (η=1.55) (26; 27)) found in literature for a bulk, the thickness values of these molecules for a bulk ($d_{C12}$=1.62 nm, $d_{Terphenyl}$=1.76 nm) (24-25), and by calculating the electromagnetic field decay length, $l$ (the decay length for a LSPR system is 1-3% of the light's wavelength(2,28), $l$=17 nm in our case), we can obtain the from equation (1.4) a sensitivity factor $m$ of 115 nm $RIU^{-1}$ for C12 and of 204 nm $RIU^{-1}$ for terphenyl.

We observe that the order of magnitude of these values of $m$ are not similar of that reported in literature for LSPR (2,28). The order of magnitude of our $m$ values are 50% higher than the $m$ values calculated by the Van Duyne's group (11) that he predicted a $m$ value decrease of 20% when on the Au NPs surface is present a SAM. The difference in $m$ cannot be attributed to a change in morphology, as indicated by the complete reversibility of the system; it can be rather

related to the fact that the refractive index of SAMs formed by these compounds are certainly different from the bulk, given the well know different architectures, organization and the packing of these molecules in the SAMs are very different.

## 3.4 Conclusions

The LSPR spectroscopy performed with Au NPs supported on transparent substrates is a convenient technique to monitor molecular interactions, provided two mandatory conditions: high stability of the Au NPs in different media, and a good sensitivity of their LSPR to molecular interactions occurring at the surface.

The Au NPs deposited on FTO, which are stable in different organic and more importantly in aqueous solvents (Chapter 2), show LSPR bands which results to be sensitive to absorption of organic SAMs and to the electronic structure of the molecules forming the SAMs (aliphatic versus aromatic).

The simple protocol of fabrication yields samples of Au NPs of different morphology. Significantly, all the fabricated samples, formed by polydisperse NPs, exhibit the same stability and sensitivity. Therefore the samples can been used directly after the fabrication, without stabilization processes and the recorded shift in $\lambda_{max}$ is related exclusively to the change in refractive index of the SAMs, without any contribution to restructuration processes.

Interestingly, the LSPR of the samples Au NPs/FTO recovers the same values after multiple SAM replacements, indicating high stability of the metal nanoparticles and the reversibility of this plasmonic material as molecular sensors. For a commercially practical LSPR biosensor means that it can be completely reusable. Reusability has a large impact on cost effectiveness and the simplicity of use of biosensors.

## References


1. A. J. Haes, D. A. Stuart, S. Nie, R. P. Van Duyne. Using solution-phase nanoparticles, surface-confined nanoparticle arrays and single nanoparticles as biological sensing platforms. *Journal of Fluorescence*. **2004**, 14 (4), 355-367.

2. A. J. Haes, R. P. Van Duyne. A unified view of propagating and localized surface plasmon resonance biosensors. *Analytical and Bioanalytical Chemistry*. **2004**, 379, 920-930.

3. C. L. Haynes, R. P. Van Duyne. Nanosphere lithography: a versatile nanofabrication tool for studies of size-dependent nanoparticle optics. *The Journal of Physical Chemistry B*. **2001**, 105 (24), 5599-5611.

4. K. A.Willets, R. P. Van Duyne. Localized surface plasmon spectroscopy and sensing. *Annual Review of Physical Chemistry*. **2008**, 58, 267-297.

5. M. E. Stewart, C. R. Anderton, L. B. Thompson, J. Maria, S. K. Gray, J. A. Rogers, R. G. Nuzzo. Nanostructured plasmonic sensors. *Chemical Reviews*. **2008**, 108, 494-521.

6. B. Sepulveda, P. C. Angelomé, L. M. Lechuga, L. M. Liz-Marzàn. LSPR-based nanobiosensors. *Nano Today*. **2009**, 4(3), 244-251.

7. H. Chen, X. Kou, Z. Yang, W. Ni, J. Wang. Shape- and size-dependent refractive index sensitivity of gold nanoparticles. *Langmuir*. **2008**, 24(10), 5233-5237.

8. N. Nath, A. Chilkoti. A colorimetric gold nanoparticle sensor to interrogate biomolecular interactions in real time on a surface. *Analytical Chemistry*. **2002**, 74(3), 504-509.

9. Y. Sun, Y. Xia. Increased sensitivity of surface plasmon resonance of gold nanoshells compared to that of gold solid colloids in response to environmental changes. *Analytical Chemistry*. **2002**, 74(20), 5297-5305.

10. T. R. Jensen, M. Duval Malinsky, C. L. Haynes, R. P. Van Duyne. Nanosphere lithography: tunable localized surface plasmon resonance spectra of silver nanoparticles. *The Journal of Physical Chemistry B*. **2000**, 104(45), 10549-10556.

11. M. D. Malinsky, K. L. Kelly, G. C. Schatz, R. P. Van Duyne. Chain length dependence and sensing capabilities of the localized surface plasmon resonance of silver nanoparticles

chemically modified with alkanethiol self-assembled monolayers. *Journal of American Chemical Society*. **2001**, 123, 1471-1482.

12. N. Nath, A. Chilkoti. Label-free biosensing by surface plasmon resonance of nanoparticles on glass: optimization of nanoparticle size. *Analytical Chemistry*. **2004**, 76, 5370-5378.

13. T. Karakouz, D. Holder, M. Goomanovsky, A. Vaskevich, I. Rubinstein. Morphology and refractive index sensitivity of gold island films. *Chemistry of Materials*. **2009**, 21, 5875-5885.

14. M. Gluodenis, C. Manley, C. A. Foss Jr. In situ monitoring of the change in extinction of stabilized nanoscopic gold particles in contact with aqueous phenol solutions. *Analytical Chemistry*. **1999**, 71, 4554-4558.

15. J. Denga, Y. Songa, Y. Wanga, J. Di. Label-free optical biosensor based on localized surface plasmon resonance of twin-linked gold nanoparticles electrodeposited on ITO glass. *Biosensors and Bioelectronics*. **2010**, 26(2), 615-619.

16. S. Szunerits, V. G. Praig, M. Manesse, R. Boukherroub. Gold island films on indium tin oxide for localized surface plasmon sensing. *Nanotechnology*. **2008**, 19, 195712-195719.

17. T. Jensen, L. Kelly, A. Lazarides, G. C. Schatz. Electrodynamics of noble metal nanoparticles and nanoparticle clusters. *Journal of Cluster Science*. **1999**, 10(2), 295-317.

18. T. M. Herne, M. J. Tarlov. Characterization of DNA probes immobilized on gold surfaces. *Journal of the American Chemical Society*. **1997**, 119(38), 8916-8920.

19. T. Karakuz, A. B. Tesler, T. A. Bendikov, A. Vaskevich, I. Rubinstein. Highly stable localized plasmon transducers obtained by thermal embedding of gold island films on glass. *Advanced Materials*. **2008**, 20(20), 3893-3899.

20. K. M. Byun, S. J. Yoon, D. Kim. Effect of surface roughness on the extinction-based localized surface plasmon resonance biosensors. *Applied optics*. **2008**, 47(31), 5886-5892.

21. A. I. Martinez, L. Huerta, J. M. O-Rueda de León, D. Acosta, O. Malik, M. Aguilar. Physicochemical characteristics of fluorine doped tin oxide films. *Journal of Physics D: Applied Physics*. **2006**, 39, 5091-5096.

22. K. von Rottkay, M. Rubin. Optical indices of pyrolytic tin-oxide glass. *Materials Research Society Symposia Proceedings*. **1996**, 426, 449-454.

23. P. Montmeat, J.-C. Marchand, R. Lalauze, J.-P. Viricelle, G. Tournier, C. Pijolat. Physico-chemical contribution of gold metallic particles to the action of oxygen on tin dioxide sensors. *Sensors and Actuators B*. **2003**, 95, 83-89.

24. T. Kondo, M. Yanagida, K. Shimazu, K. Uosaki. Determination of thickness of a self-assembled monolayer of dodecanethiol on Au(111) by angle-resolved X-ray photoelectron spectroscopy. *Langmuir*. **1998**, 14, 5656-5658.

25. H.-J. Himmel, A. Terfort, C. Wöll. Fabrication of a carboxyl-terminated organic surface with self-assembly of functionalized terphenylthiols: the importance of hydrogen bond formation. *Journal of the American Chemical Society*. **1998**, 120(46), 12069-12074.

26. D. A. Krapchetov, H. Ma, A. K. Y. Jen, D. A. Fischer, Y.-L. Loo. Solvent-dependent assembly of terphenyl- and quaterphenyldithiol on gold and gallium arsenide. *Langmuir*. **2005**, 21, 5887-5893.

27. R. F. DeBono, G. D. Loucks, D. Della Manna, U. J. Krull. Self-assembly of short and long-chain n-alkyl thiols onto gold surfaces: a real-time study using surface plasmon resonance techniques. *Canadian Journal of Chemistry*. **1996**, 74, 677-688.

28. A. J. Haes, S. Zou, G. C. Schatz, R. P. Van Duyne. A nanoscale optical biosensor: the long range distance dependence of the localized surface plasmon resonance of nobel metal nanoparticles. *The Journal of Physical Chemistry B*. **2004**, 108, 109-116.

# Chapter 4

# Localized Surface Plasmon Resonance Biosensing

## 4.1 Introduction

With the aim of developing a biosensor which is i) easy and inexpensive to fabricate, ii) simple to be used, and iii) reversible, we have focused on those based on plasmonic materials. Among the large number of approaches (1-13) used to develop biomedical sensor, those based on the Localized Surface Plasmon Resonance spectroscopy can be very convenient. For example, in the run towards miniaturization the sensors based on LSPR spectroscopy, could, in theory, use the single nanoparticle as transducer (14).

In particular, as described in the previous Chapters, we have fabricated plasmonic materials, based on metal nanoparticles, in order to detect changes in local refractive index by monitoring the LSPR $\lambda_{max}$ extinction maximum by UV-Vis spectroscopy (15). It is well established that the peak extinction wavelength, $\lambda_{max}$, of the LSPR spectrum is dependent upon the size, shape, and interparticle spacing of the nanoparticle as well as its own dielectric properties and those of its local environment including substrate, solvent, and adsorbates (16-20).

In Chapter 2 and 3 we have shown that our approach to fabricate a plasmonic material towards the development of biosensors is very promising. Thermal evaporation of Au on a FTO surfaces yield nanoparticles which show good adhesion, good stability toward restructuration, and reversibility. In addition, we have demonstrated that the LSPR spectrum of these metal nanoparticles shows a high sensitivity to the changes of local dielectric constant.

A number of studies are reported in literature based on the optical response of colloidal metal NPs dispersed in solution. The main part of these studies is based on color changes, visible by naked eye, arising from aggregation of the NPs, caused by molecular interaction between DNA (21-23), protein (24-25), and small molecules (26-27). However, biosensors based on colloidal metal nanoparticles requires a careful synthetic procedure in order to obtain monodisperse material: i) a fine control of ionic strength, pH, temperature (to avoid flocculation), and ii) a stabilization procedure with a proper molecular shell which can limit a further functionalization (28-29).

Alternatively, the use of nanoparticles deposited on surfaces present several advantages: they i) allow for the fabrication of "point of care testing" (POCT) to perform the patient diagnose "in situ" and in short time, ii) can be easily handled in the measurement processes: the sample to test is located in directly contact with the NPs surface, allowing for using a small probe volume.

In the present study, after the demonstration of the stability and sensitivity of the plasmonic material based on Au NPs deposited on a FTO surface, we focused on the response of this material to biomolecular *interaction* occurring at their surfaces.

As first approach, we are interested in detecting, by LSPR spectroscopy, the interaction between two complementary DNA single strands. In literature a large number of studies have been dedicated to fabricate sensors suitable for detecting DNA hybridization events, the major part focuses on label-based microarrays. These studies are very important in the biomedical field since they aim to identify genetic mutations caused by presence of even one base mismatch in the DNA sequence. In fact, the genetic mutations lead to several and enough bad genetic diseases.

At our knowledge, the hybridization process of DNA has been detected by using Au NPs deposited on quartz surfaces only in one case (30), while has been widely studied by using colloid NPs in solution (35-37) or immobilized (not deposited) on surfaces (31-34).

The DNA hybridization process occurring at surfaces requires a number of delicate procedures: i) formation of single strand ssDNA SAM, ii) lateral spacing between the ssDNA in order to allow the hybridization process, iii) hybridization process by exposing the NPs surfaces functionalized by a ssDNA to the complementary strand to form the double strand DNA (dsDNA).

The formation of ssDNA SAMs requires a careful procedure to obtain a controlled architecture. Single strands of the DNA are much longer and more flexible than typical organic molecules forming SAMs; therefore, lateral spacing is length-dependent, and long-range lateral ordering is not observed in ssDNA monolayers (38).

The ssDNA functionalized by -SH group to form monolayers on the Au NPs does not presents neither a rigid backbone, nor strong lateral interactions, so that the SAMs results to be disordered by molecular fluctuation. In addition, the presence of bases containing nitrogen in

the nucleotides of the DNA, can lied to interaction with the metal surfaces and therefore to ssDNA laying on the surface (39).

Several studies have been done to optimize ssDNA SAMs architecture suitable for hybridization (40-49). A widely accepted procedure consists in forming a mixed SAMs of incorporating a ssDNA modified in 5' with an alkane chain of six carbons terminating thiol group ($HS(CH_2)_6$ -) and a spacer, the 6-mercapto-1-hexanol (MCH) (39). The spacer has several fundamental functions: minimize nonspecific adsorption of single stranded DNA (50), control the DNA up-right organization, and create a free space between the ssDNA allowing for nearly 100% hybridization activity (51).

In the present study, to test the sensitivity of the new plasmonic material to biorecognition, in particular to DNA hybridization processes, we have selected a DNA sequence of 19 base pair. The particular length has been selected by considering that: i) a longer DNA strand could generate a very disordered SAMs, ii) the number of bases is large enough to allow for stable hybridization, and iii) will allow for detect a basis mismatch test. We have used the modified oligonucleotide (5'-$HS(CH_2)_6$-CAG TGA GGC GTG GCC AGG G-3'), called *probe*, and the complementary strand (5'-CCC TGG CCA CGC CTC ACT G-3'), called *target*. A non complementary (5'-AAG TGC ATC GTG ATT CAT A-3') sequence was used to test the specificity of the sensor. In addition, in order to optimize the performance of our sensor, we have repeated the experiment by using shorter times for each incubation step.

## 4.2 Materials and Methods

### Materials

6-mercapto-1-hexanol was purchased from Sigma Aldrich (Germany) and phosphate-buffered saline (PBS) solutions from Lonza Walkersville Inc. (Walkersville, MD). The Bovine Serum Albumin (BSA) was kindly provided by Professor Roberto Gambari (Department of Biochemistry and Molecular Biology, University of Ferrara). The Fluorine Tin Oxide (FTO) (TEC 8) surfaces were purchased from Pilkington North America Inc. (Toledo, OH). The modified oligonucleotide (5'-HS$(CH_2)_6$-CAG TGA GGC GTG GCC AGG G-3'), the complementary (5'-CCC TGG CCA CGC CTC ACT G-3'), and the non complementary (5'-AAG TGC ATC GTG ATT CAT A-3') sequences were purchased from Eurofines MWG Operon (Ebersberg, Germany).

### Au NPs fabrication

The fluorine tin oxide surfaces was cleaned by a solution 1:1 of acetone and 2-propanol in ultrasounds bath for 15 minutes, then repeatedly rinsed with copious amounts of water MilliQ and lastly gently dried with a pure nitrogen stream. The gold nanoparticles were deposited on the FTO surfaces by thermal evaporation at a pressure of $10^{-6}$ mB and at deposition rate of 0.0016 nm $s^{-1}$. The deposition process of NPs is controlled by measuring a nominal thickness of 5nm with a built-in quartz balance. The samples were then annealed for 10 hours at to 200°C.

### Characterization

The UV-Vis measurements were carried out by using a Jasco V-570 UV-Vis-NIR spectrophotometer in transmittance mode by placing the samples into the spectrophotometer cavity (scan speed 200 nm/min, band width 1 nm). All the spectra were recorded in air and by using air as reference. A series of measurements performed by repetitive removing and replacing the same sample into the spectrophotometer cavity showed an error in $\lambda_{max}$ values of 1 nm.

### Bio-functionalization of Au NPs

The DNA hybridization was performed according to the literature protocols (39,40,50-51). In the present case, the samples have been incubated with a PBS buffer solution containing the 5'-HS$(CH_2)_6$-CAG TGA GGC GTG GCC AGG G-3'-oligonucleotide (ssDNA) for 16 hours at

room temperature. After incubation, the sample was rinsed with PBS buffer and MilliQ water, in order to take away residual thioled ssDNA sequences. Thus, the samples have been incubated for 1 hour in an aqueous solution of 6-mercapto-1-hexanol (MCH) according to the protocol (39). MCH is used as spacer between the ssDNA in order to minimize nonspecific adsorption of the ssDNA and to facilitate the hybridization (39). To perform the hybridization of the ssDNA, the samples have immersed into a PBS solution of the complementary sequence for 16 hours a room temperature. After incubation, the samples were rinsed with PBS buffer and MilliQ water, and dried with nitrogen stream. After each step, the T-LSPR spectra of the samples were recorded.

A control experiment was done by incubating for 16 hours the mixed SAM of ssDNA-MCH carrying samples in a PBS solution containing the not complementary strand 5'-AAG TGC ATC GTG ATT CAT A-3'. After incubation, the samples were rinsed with PBS and MilliQ water, and then dried with nitrogen.

The experiment performed to test a protein aspecific binding was done by incubation of the mixed SAM of dsDNA-MCH with the BSA protein for 1 hour in 10 mM PBS buffer. After incubation, the samples were rinsed with PBS and MilliQ water, and then dried with nitrogen.

## 4.3 Results and Discussion

The sensitivity of the Au NPs LSPR to biorecognition reactions occurring at their surfaces has been tested by measuring $\Delta\lambda_{max}$ upon DNA hybridization. In the present case, we have exploited the hybridization of 19 oligonucleotides bases in particular, a modified oligonucleotide (5'-HS$(CH_2)_6$-CAG TGA GGC GTG GCC AGG G-3') and the complementary strand (5'-CCC TGG CCA CGC CTC ACT G-3').

The NPs were functionalized following a standard procedure (50-51) which consists of several steps (see Materials and Methods). Figure 1 reports the LSPR bands recorded for each step.

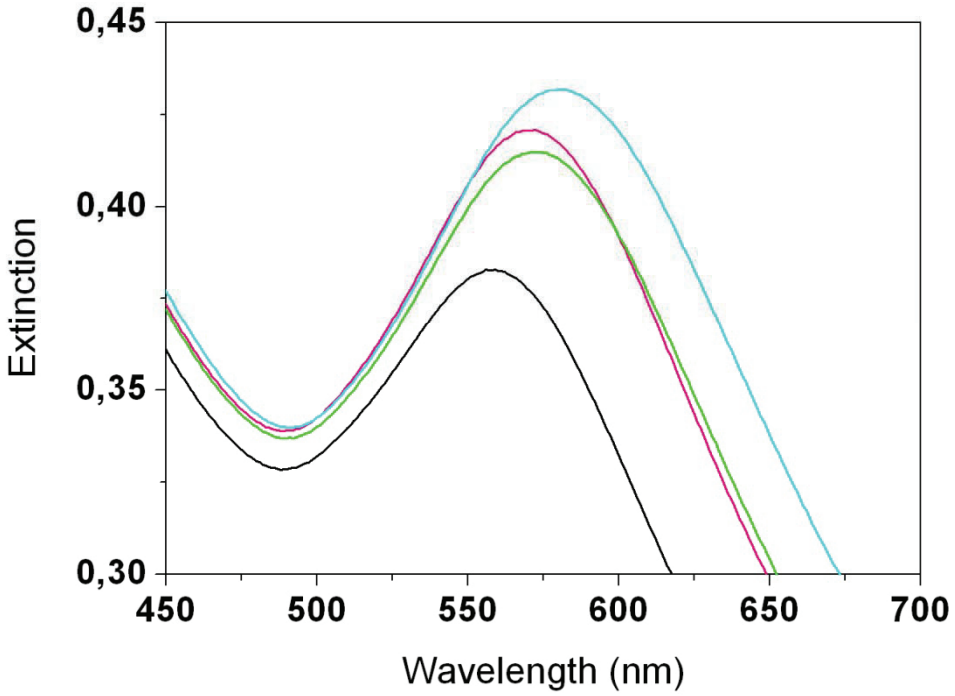


**Figure 1.** LSPR spectra recorded for Au NPs (*black*), after absorption of the thiolated ssDNA (*magenta*), after immersion in a water solution of MCH (*green*), and after hybridization with the complementary strand (*turquoise*).

We can observe that the $\lambda_{max}$ LSPR band recorded for bare Au NPs shifts of 11 nm after absorption of the ssDNA, remains almost constant under insertion of MCH, and shifts of further 11 nm upon hybridization. The results indicate that the Au NPs LSPR is sensitive to the

presence of monolayers of ssDNA and more significantly, that the hybridization process induces a shift towards the red region. Considering that this shift is the result of the hybridization of an ssDNA, which is diluted into a MCH SAMs, we can conclude that the LSPR of these NPs shows a good sensitivity toward the hybridization DNA.

We have also performed in parallel a blank experiment where we have incubated the sample with a non complementary DNA sequence (5'-AAG TGC ATC GTG ATT CAT A-3'), instead of the complementary strand of DNA.

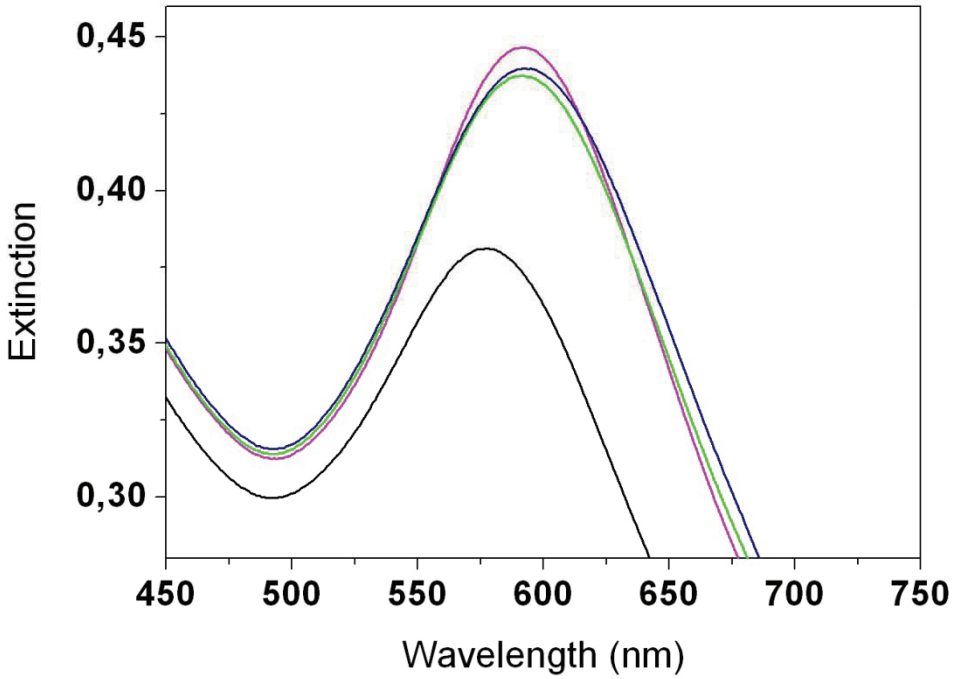


**Figure 2.** LSPR spectra recorded for Au NPs (*black*), after absorption of the thiolated ssDNA (*magenta*), after immersion in a water solution of MCH (*green*), and after incubation with the non complementary strand (*blue navy*).

Figure 2 reports the LSPR bands after the different steps of functionalization. The binding of ssDNA on the Au NPs surface generates a red shift of 14 nm. As shown in Figure 1, the insertion of MCH into the ssDNA SAM does not lead to any shift of the plasmon band. When the sample is incubated with a non complementary strand, the LSPR band exhibits a red shift of only 1 nanometer. These data show clearly that the biosensor could discern between a

complementary and not complementary strand of DNA, and prove the specificity of the sensor to the binding of complementary DNA strand. The results indicate that the sensor is suitable for the detection of DNA mismatches in the analysis of genetic mutations.

Herne and Tarlov (39) found by XPS analysis that the maximum coverage surface with ssDNA take place after 4 hours of incubation. In analogy, we exposed the Au NPs to the same time of incubation; in particular we have tested the sensor by the following procedure: 4 hours of incubation with the modified oligonucleotide (5'-HS($CH_2$)$_6$-CAG TGA GGC GTG GCC AGG G-3'), thirty minutes of incubation with the spacer MCH and 1 hour and thirty minutes with the complementary strand (5'-CCC TGG CCA CGC CTC ACT G-3'). The results are reported in Figure 3.

Figure 3 shows a red shift of the SP band for every step; in particular the shift value for the hybridization process is of 10 nm, in agreement with the previous results reported in Figure 1. Summarizing, we can obtain the same performances of the sensor by reducing the analysis time; this is an important goal in the field of biosensors.

The DNA test requires a complicated and expensive procedure of DNA extraction from the cell nucleus, of DNA amplification and purification. In the cell nuclear extract, a large number of biological components, as proteins of different nature, are present. It is possible to avoid the DNA amplification and purification processes and to use directly cell nuclear extract?

A first step for answer to this question is to test the response of the sensor to an aspecific binding of a protein, the ubiquitous Bovine Serum Albumin (BSA) protein. The BSA protein has been selected for its stability, its lack of effect in many biochemical reactions, and its low cost. Figure 4 shows that the LSPR band shifts towards the red only of 1 nm, after incubation with BSA. Significantly, these results indicate that most probably, the protein does not interact with the mixed SAM present on the Au NPs surface and then, the present sensor could be suitable for a genetic test by using *directly* the cell nuclear extracts.

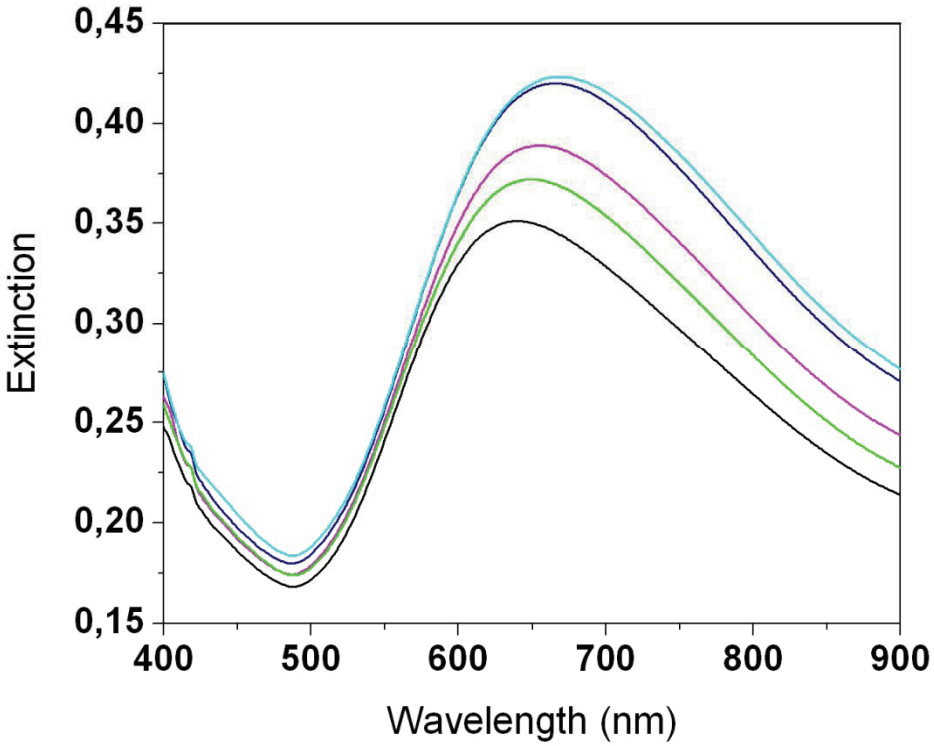


**Figure 3.** LSPR spectra recorded for Au NPs (*black*), after absorption of the thiolated ssDNA (*magenta*), after immersion in a water solution of MCH (*green*), after hybridization with the complementary strand (*blue navy*), and after incubation with BSA protein (*turquoise*).

## 4.4 Conclusions

In this part of our study we have proved that the new plasmonic material characterized as described in Chapter 2 and 3, is able to detect biorecognition processes as DNA hybridization.

The red shift of $\lambda_{max}$ of the LSPR band recorded under hybridization of DNA single strand anchored to Au NPs surface indicates that this plasmonic material is very sensitive to biomolecular interactions occurring at their surface. In addition, the sensor shows the same sensitivity even by reducing the preparation and analysis time.

The result of the blank experiment with the non complementary strand indicates that the LSPR biosensor shows good specificity. In addition the sensor functionalized with mixed SAMs of DNA and MCH does not show interaction with the aspecific protein BSA. This means that this sensor could be a start point for several kinds of medical and biological diagnostic.

Further experiments will be required to verify whether this approach is suitable to determine hybridization of single DNA strand of gene sequences generated by polymerase-chain reaction. These results encourage further studies aimed at determining whether this strategy is important to detect point mutations. Both these issues are relevant to possible application of this novel strategy to biomedicine.

## References


1. D. Shalon, S. J. Smith, P. O. Brown. A DNA microarray system for analyzing complex DNA samples using two-color fluorescent probe hybridization . *Genome Research*. **1996**, 6, 639-645.

2. E. Engvall, P. Perlmann. Enzyme-linked immunosorbent assay (ELISA) quantitative assay of immunoglobulin G. *Immunochemistry*. **1971**, 8(9), 871-874.

3. E.-H. Yoo, S.-Y. Lee. Glucose biosensors: an overview of use in clinical practice. *Sensors*. 2010, 10, 4558-4576.

4. M. Uttamchandani, J. Wang, S. Q. Yao. Protein and small molecule microarrays: powerful tools for high-throughput proteomics. *Molecular BioSystems*. **2006**, 2, 58-68.

5. J. Homola. Surface plasmone resonance based sensors. Berlin-Heidelberg-New York: Springer-*Verlag*, **2006**.

6. S. I. Stoeva, J.-S. Lee, C. S. Thaxton, C. A. Mirkin. Multiplexed DNA detection with biobarcoded nanoparticle probes. *Angewandte Chemie International Edition*. **2006**, 45, 3303-3306.

7. G. Wu, R. H. Datar, K. M. Hansen, T. Thundat, R. J. Cote, A. Majumdar. Bioassay of prostate-specific antigen (PSA) using microcantilevers. *Nature Biotechnology*. **2001**, 19, 856-860.

8. T. H. Rider, M. S. Petrovick, F. E. Nargi, J. D. Harper, E. D. Schwoebel, R. H. Mathews, D. J. Blanchard, L. T. Bortolin, A. M. Young, J. Chen, M. A. Hollis. A B cell-based sensor for rapid identification of pathogens. *Science*. **2003**, 301, 213-215.

9. M. Zhanga, B.-C. Yina, W. Tanb, B.-C. Ye. A versatile graphene-based fluorescence "on/off" switch for multiplex detection of various targets. *Biosensors and Bioelectronics*. **2011**, 26(7), 3260-3265.

10. C. R. Taitt, J. P. Golden, Y. S. Shubin, L. C. Shriver-Lake, K. E. Sapsford, A. Rasooly, F. S. Ligler. A portable array biosensor for detecting multiple analytes in complex samples. *Microbial Ecology*. **2003**, 47(2), 175-185.

11. T. G. Drummond, M. G Hill, J. K. Barton. Electrochemical DNA sensors. *Nature Biotechnology*. **2003**, 21, 1192-1199.

12. M. K. Wagner, F. Li, J. Li, X.-F. Li, X. C. Le. Use of quantum dots in the development of assays for cancer biomarkers. *Analytical and Bioanalytical Chemistry*. **2010**, 398(8), 3213-3224.

13. J. D. Newman, A. P. F. Turner. Home blood glucose biosensors: a commercial perspective. *Biosensors and Bioelectronics*. **2005**, 20(12), 2435-2453.

14. J. M. Bingham, K. A. Willets, N. C. Shah, D. Q. Andrews, R. P. Van Duyne. Localized surface plasmon resonance imaging: simultaneous single nanoparticle spectroscopy and diffusional dynamics. *The Journal of Physical Chemistry C*. **2009**, 113(9), 16839-16842.

15. U. Kreibig, M. Vollmer. Optical Properties of Metal Clusters. Berlin: *Springer*, **1995**.

16. K. L. Kelly, E. Coronado, L. L. Zhao, G. C. Schatz. The optical properties of metal nanoparticles: the influence of size, shape, and dielectric enviroment. *The Journal of Physical Chemistry B*. **2003**, 107, 668-677.

17. A. J. Haes, S. Zou, G. C. Schatz, R. P. Van Duyne. A nanoscale optical biosensor: the long range distance dependence of the localized surface plasmon resonance of nobel metal nanoparticles. *The Journal of Physical Chemistry B*. **2004**, 108, 109-116.

18. C. L. Haynes, R. P. Van Duyne. Nanosphere lithography: a versatile nanofabrication tool for studies of size-dependent nanoparticle optics. *The Journal of Physical Chemistry B*. **2001**, 105 (24), 5599-5611.

19. M. A. El-Sayed. Some interesting properties of metals confined in time and nanometer space of different shapes. *Accounts of Chemical Research*. **2001**, 34(4), 257-264.

20. M. D. Malinsky, K. L. Kelly, G. C. Schatz, R. P. Van Duyne. Chain length dependence and sensing capabilities of the localized surface plasmon resonance of silver nanoparticles chemically modified with alkanethiol self-assembled monolayers. *Journal of American Chemical Society*. **2001**, 123, 1471-1482.

21. S. J. Hurst, M. S. Han, A. K. R. Lytton-Jean, C. A. Mirkin. Screening the sequence selectivity of DNA-binding molecules using a gold nanoparticle-based colorimetric approach. *Analytical Chemistry*. **2007**, 79, 7201-7205.

22. J. K. Konstantou, P. C. Ioannou, T. K. Christopoulos. Dual-allele dipstick assay for genotyping single nucleotide polymorphisms by primer exstension reaction. *European Journal of Human Genetics*. **2009**, 17, 105-111.

23. X. Xu, D. G. Georganopoulou, H. D. Hill, C. A. Mirkin. Homogeneous detection of nucleic acids based upon the light scattering properties of silver-coated nanoparticle probes. *Analytical Chemistry*. **2007**, 79(17), 6650-6654.

24. R. Tanaka, T. Yuhi, N. Nagatani, T. Endo, K. Kerman, Y. Takamura, E. Tamiya. A novel enhancement assay for immunochromatographic test strips using gold nanoparticles . *Analytical and Bioanalytical Chemistry*. **2006**, 385(8), 1414-1420.

25. Y.-Y. Chena, C.-W. Tsenga, H.-Y. Changa, Y.-L. Hunga, C.-C. Huang. Gold nanoparticle-based colorimetric assays for coagulation-related proteins and their inhibition reactions. *Biosensors and Bioelectronics*. **2011**, 26(7), 3160-3166.

26. J. Zhang, L. Wang, D. Pan, S. Song, F. Y. C. Boey, H. Zhang, C. Fan. Visual Cocaine detection with gold nanoparticles and rationally engineered aptamer structures. *Small*. **2008**, 4(8), 1196-1200.

27. K. Ai, Y. Liu, L. Lu. Hydrogen-bonding recognition-induced color change of gold nanoparticles for visual detection of melamine in raw milk and infant formula. *Journal of the American Chemical Society*. **2009**, 131(27), 9496-9497.

28. J. Zhou, J. Ralston, R. Sedev, D. A. Beattie. Functionalized gold nanoparticles: synthesis, structure and colloid stability. *Journal of Colloid and Interface Science*. 2009, 331, 251-262.

29. M. Brust, M. Walker, D, Bethell, D. J. Schiffrin, R. Whyman. Synthesis of thiol-derivatised gold nanoparticles in a two-phase liquid-liquid system. *Journal of the Chemical Society, Chemical Communications*. 1994, 801-802.

30. E. Hutter, M.-P. Pileni. Detection of DNA hybridization by gold nanoparticle enhanced transmission surface plasmon resonance spectroscopy. *The Journal of Phical Chemistry B*. **2003**, 107(27), 6497-6499.

31. T. Endo, K. Kerman, N. Nagatani, E. Tamiya. Excitation of localized surface plasmon resonance using a core–shell structured nanoparticle layer substrate and its application for

label-free detection of biomolecular interactions. *Journal of Physics: Condensed Matter*. **2007**, 19(21), 215201.

32. T. Endo, K. Kerman, N. Nagatani, Y. Takamura, E. Tamiya. Label-free detection of Peptide Nucleic Acid−DNA hybridization using localized surface plasmon resonance based optical biosensor. *Analytical Chemistry*. **2005**, 77(21), 6976-6984.

33. T. Endo, D. Ikedaa, Y. Kawakami, Y. Yanagidaa, T. Hatsuzawa. Fabrication of core-shell structured nanoparticle layer substrate for excitation of localized surface plasmon resonance and its optical response for DNA in aqueous conditions. *Analytica Chimica Acta*. **2010**, 661, 200-205.

34. C. Sönnichsen, B. M. Reinhard, J. Liphardt, A. P. Alivisatos. A molecular ruler based on plasmon coupling of single gold and silver nanoparticles. *Nature Biotechnology*. **2005**, 23, 741-745.

35. J. E. Millstone, D. G. Georganopoulou, X. Xu, W. Wei, S. Li, C. A. Mirkin. DNA-gold triangular nanoprism conjugate. *Small*. **2008**, 4(12), 2176-2180.

36. Z. Li, R. Jin, C. A. Mirkin, R. L. Letsinger. Multiple thiol-anchor capped DNA-gold nanoparticle conjugates. *Nucleic Acids Research*. **2002**, 30(7), 1558-1562.

37. G. L. Liu, Y. Yin, S. Kunchakarra, B. Mukherjee, D. Gerion, S. D. Jett, D. G. Bear, J. W. Gray, A. P. Alivisatos, L. P. Lee, F. F. Chen. A nanoplasmonic molecular ruler for measuring nuclease activity and DNA footprinting. *Nature Nanotechnology*. **2006**, 1, 47-52.

38. D. Y. Petrovykh, V. Pérez-Dieste, A. Opdahl, H. Kimura-Suda, J. M. Sullivan, M. J. Tarlov, F. J. Himpsel, L. J. Whitman. Nucleobase orientation and ordering in films of single-stranded DNA on gold. *Journal of the American Chemical Society*. **2006**, 128(1), 2-3.

39. T. M. Tarlov, M. J. Herne. Characterization of DNA probes immobilized on gold surfaces. *Journal of the American Chemical Society*. **1997**, 119(38), 8916-8920.

40. A. W. Peterson, R. J. Heaton, R. M. Georgiadis. The effect of surface probe density on DNA hybridization. *Nucleic Acids Research*. **2001**, 29(24), 5163-5168.

41. F. Nakamura, M. Hara. The length e ect of probe DNA for hybridization using DNA self-assembled monolayer. *e-Journal of Surface Science and Nanotechnology*. **2005**, 3, 250-253.

42. Y. Sakaoa, F. Nakamura, N. Uenoa, M. Hara. Hybridization of oligonucleotide by using DNA self-assembled monolayer. *Colloids and Surfaces B: Biointerfaces*. **2005**, 40, 149-152.

43. R. Kaufmann, I. Averbukh, R. Naaman. Controlling the reactivity of adsorbed DNA on template surfaces. *Langmuir*. **2003**, 19, 10573.

44. D. Erts, B. Polyakov, H. Olin, E. Tuite. Spatial and mechanical properties of dilute DNA monolayers on gold imaged by AFM. *The Journal of Physical Chemistry B*. **2003**, 107(15), 3591-3597 .

45. C.-Y. Lee, P. Gong, G. M. Harbers, D. W. Grainger, D. G. Castner, L. J. Gamble. Surface coverage and structure of mixed DNA/alkylthiol monolayers on gold: characterization by XPS, NEXAFS, and fluorescence intensity measurements. *Analytical Chemistry*. **2006**, 78(10), 3316-3325.

46. R. Georgiadis, K. P. Peterlinz, A. W. Peterson. Quantitative Measurements and Modeling of Kinetics in Nucleic Acid Monolayer Films Using SPR Spectroscopy. *Journal of the American Chemical Society*. **2000**, 122(13), 3166-3173.

47. O. Taratula, E. Galoppini, R. Mendelsohn, P. I. Reyes, Z. Zhang, Z. Duan, J. Zhong, Y. Lu. Stepwise functionalization of ZnO nanotips with DNA. *Langmuir*. **2009**, 25(4), 2107-2113.

48. L. K. Wolf, Y. Gao, R. M. Georgiadis. Sequence-dependent DNA immobilization: specific versus nonspecific contributions. *Langmuir*. **2004**, 20(8), 3357-3361.

49. M. Gotoh, Y. Hasegawa, Y. Shinohara, M. Shimizu, M. Tosu. A new approach to determine the effect of mismatches on kinetic parameters in DNA hybridization using an optical biosensor. *DNA Research*. **1995**, 2, 285-293.

50. A. B. Steel, R. L. Levicky, T. M. Herne, M. J. Tarlov. Immobilization of nucleic acids at solid surfaces: effect of oligonucleotide length on layer assembly. *Biophysical Journal*. **2000**, 79(2), 975-981.

51. R. Levicky, T. M. Herne, M. J. Tarlov, S. K. Satija. Using self-assembly to control the structure of DNA monolayers on gold: a neutron reflectivity study. *Journal of the American Chemical Society*. **1998**, 120(38), 9787-9792.

# Acknowledgements

I would like to express gratitude to my supervisor, Prof. Maria Anita Rampi that allows me to study and to research in this wonderful field that are the nanobiotechnologies, thank you for having accepted me in your research group.

A very special acknowledgement goes to Prof. Richard Van Duyne who has welcomed me in its fantastic research group at the Northwestern University. He has placed his trust in me and in my research project. Thanks for having given me this big opportunity.

Thanks to all guys of the Van Duyne's group, especially to Julia Ruemmele, Paige Hall, Lauren Kreno and Anne-Isabelle Henry, very precious people that followed me in my first steps as a foreigner in a new country and in a new lab. I learnt so much from you.

Thanks to all my workmates: Felice Simeone, Barbara Branchi, Elisa Bono and, in particular, to Gaia Cesari that has introduced me in the chemistry world.

Special thanks to Stefano Caramori, my "mentor" in these years, for his help in clarifying some of my chemistry doubts; a great and generous person.

I am very grateful to all my department friends. Spending with you these years has made easier to me to pass over every sad and heavy moment. It was a great adventure.

Finally, my deepest gratitude goes to all my friends and to my family, present every day even at 8000 kilometers of distance. I love you.